A Portable Gas Chromatograph with Tunable Separation and Microsensor Array Detection: Design, Characterization, and Environmental Health Applications

by

Qiongyan Zhong

A dissertation submitted in partial fulfillment
of the requirements for the degree of
Doctor of Philosophy
(Industrial Health)
in The University of Michigan
2008

Doctoral Committee:

Professor Edward T. Zellers, Chair
Professor Mark E. Meyerhoff
Professor Stuart A. Batterman
Associate Research Scientist Sergei M. Chernyak

Dedication

This dissertation is dedicated to my parents in appreciation of their enduring support and encouragement.

Acknowledgements

I would like to thank my advisor Prof. Edward T. Zellers for his guidance and support. He not only taught me about the research, but also helped me to improve my scientific thinking, communication, and writing skills. I appreciate the opportunity he provided me in attending conferences, and learning to write grant proposals.

I would like to thank Prof. Stuart A. Batterman, who is both a member of my committee, and a collaborator in my research. He has given a lot of guidance to my research.

I would like to thank Prof. Mark E. Meyerhoff and Research Scientist Sergei M. Chernyak. I am grateful to have them in my committee. Their sharp questions during my preliminary and data meeting broadened my thinking.

I would like to thank Prof. Richard Sacks for his guidance in GC separation. He is missed.

I would like to thank Dr. Hank Wohltjen and Mr. Brent Busey of Microsensor Systems, Inc. for instrument construction. Thanks also go to Mr. Stephen J. Parus at the University of Michigan Department of Chemistry for revising the Labview code used in the instrument control and data acquisition.

I would like to thank all of my past and present peers in the Zellers' group. Chia-Jung (Vincent) Lu and William H. Steinecker taught me many things in instrumentation development, and provided technical training for my research upon my joining the group. Rebecca A. Veeneman worked with me on the portion of the project related to the determining of the markers in environmental tobacco smoke. Without her work in the preconcentrator development, the project could not have been completed. Sun Kyu Kim assisted me in the experiments for detecting breath biomarkers of lung cancer. Chunguang (Jerry) Jin provided assistance in chemometrics analysis. Michael P. Rowe synthesized all the nanoparticles for the chemiresistor sensors used in this research, and

help to coat sensor arrays. Chao Xu helped with the sensor array coating during a key step in the project. I would also like to thank Chunrong Jia and Jo-Yu Chin of Prof. Batterman's group for their assistance in field testing and GC-MS analysis. Friendship and support from all these peers is greatly appreciated.

I would like to thank the secretary staff in our department. They provide me great assistance in research item ordering, and other logistics.

I would like to acknowledge the support and friendship from Nancy Miller, Bian Liu, Yi-Hsuan Wu, Ke Li, Guangyu Zhang, Tingting Zhao, and Sing Liu. Their friendship is a very important part of my life in Michigan.

Especially I wish to express my great appreciation to Michael R. Remenak. Without his mental support, assistance in data processing with Excel, and proofreading of my dissertation, I could not have finished my writing in time.

Most importantly, I would like to thank my family. Yuexiang Qi, my aunt, has also given me tremendous support over the years. Lastly, my parents and brothers always support me, no matter wherever I go, and whatever I do.

Funding was provided by National Institute for Occupational Safety and Health, the American Legacy Foundation, and Intel Corporation. This work made use of Engineering Research Centers Shared Facilities supported by the National Science Foundation.

Table of Contents

List of Figures

List of Tables

List of Appendices

Abstract

The development of a prototype portable gas chromatograph (GC) with several novel design and operating features is described. Building on a previous design, this prototype incorporates modifications that enhance the capability for determining the components of complex mixtures of volatile organic compounds (VOCs). The instrument employs a miniature multi-adsorbent preconcentrator/injector (PCI), two series-coupled columns with fast, independent temperature-programming capabilities and junction-point pressure/flow control, and a thermostatted detector consisting of an array of microfabricated chemiresistor sensors coated with Au-thiolate monolayer-protected nanoparticles whose responses patterns can be used together with retention times to identify and quantify eluting VOCs. Scrubbed ambient air is employed as the carrier gas. The instrument was characterized, with a focus on the tradeoffs in performance associated with thermal and fluidic operating variables. The influences of flow rate and operating temperature on the responses from a microsensor array used as a GC detector are described for the first time. The determination of a 31-component mixture is achieved in a total analytical cycle time of 16 min, with projected limits of detection limit (LOD) in the parts-per-trillion range for many vapors, assuming a 1-L sample volume. Application of the instrument to the determination of vapor-phase markers of environmental tobacco smoke (ETS) and to breath biomarkers of lung cancer is illustrated. For the former application, an adsorbent pre-trap was developed to remove semi-volatile organic compounds from the sample stream. The two markers were successfully separated from the 34 most prominent co-contaminants found in smoking-permitted environments and detected at relevant concentrations. By combining the capabilities for retention-time tuning and chemometric vapor recognition it was possible to reduce the overall analytical cycle time by 16%. For the latter application, attempts were made to establish conditions necessary to analyze breath samples spiked with seven

biomarkers and 30 endogenous and exogenous interferences. Approaches to removing water vapor co-adsorbed onto the PCI during sampling were explored, and the sample volumes and separation conditions required for practical application were determined. These investigations demonstrate the potential for this novel technology to solve problems in environmental health that demand on-site analysis of complex VOC mixtures.

Chapter 1

Introduction

1.1 Dissertation Overview

Human exposure to toxic chemicals is one of the most important issues of public health. Many such chemicals can be classified collectively as volatile organic compounds (VOCs). Quantitative exposure assessment relies critically on technological and methodological innovations. This dissertation research focuses on the development of a portable analytical system with several novel design and operating features for near-real-time determinations of complex VOC mixtures commonly found in residential, occupational, and ambient environmental settings. This work represents an extension of an earlier effort in Professor Zellers' group that produced a first-generation prototype portable gas chromatograph (GC) capable of determining mixtures of 30 or more VOCs and semi-VOCs (SVOC) in a 10-min cycle time, with detection limits for many vapors in the part-per-trillion (ppt) concentration range.[1,2] Although that prototype was used to demonstrate the value of combining on-board preconcentration, tunable retention, and sensor-array detection for applications such as indoor air quality monitoring, a number of features required improvement. Such improvements were incorporated into a second-generation instrument, which is the topic of this dissertation.

The research described herein focuses on the development and implementation of the second-generation portable GC for trace-level determination of complex VOC mixture components. This chapter (Chapter 1) provides the background and significance of the work as they relate to the application of the prototype to problems in indoor air quality (IAQ) and breath analysis. An overview of the first-generation prototype instruments, with some basic discussion of sample preconcentration, separation tuning, and sensor array detection, is also provided. Chapter 2 contains a detailed

characterization study that evaluates the performance of the second-generation instrument, with a focus on the tradeoffs associated with thermal and fluidic operational variables. The improved performance of this instrument is illustrated by the analysis of a synthetic mixture containing 31 common indoor and outdoor VOCs. After some modifications, most of what is presented in Chapter 2 will be submitted for publication in the peer-reviewed literature. Chapter 3 explores the application of the instrument to the determination of vapor-phase environmental tobacco (ETS) markers. The content of Chapter 3 has been published, with minor modifications, in the Journal of Environmental Monitoring.[3] Chapter 4 explores the adaptation of the instrument to the determination of breath biomarkers of lung cancer. Although not completely successful, this work has made significant progress toward the goal of lung-cancer biomarker determinations and has set the stage for follow-work by another student in the Zellers group. Chapter 5 summarizes the key findings and major contribution of this dissertation research and provides avenues for future studies.

1.2 Background and Significance

1.2.1 Indoor VOCs and Monitoring Methods

VOCs are defined as organic compounds having vapor pressures of > 0.1 torr at 25 ºC.[4] Those with vapor pressures lower than this value are regarded as semi-volatile organic compounds (SVOCs). Health problems associated with exposure to indoor VOCs and SVOCs have become a growing public health concern. This can be mainly attributed to two major factors, one being that the majority of the population spends greater than 90% of their time indoors,[5] and the other one being that indoor VOC concentrations are generally higher than those outdoors.[6] The main sources of indoor VOCs are: 1) emissions from building materials;[7] 2) infiltration from outdoor air;[8] 3) human activities;[9] 4) microorganisms;[10] and 5) reaction products of existing VOCs.[11] Results from numerous investigations have found strong positive correlations between exposure to indoor VOCs and sick building syndrome (SBS), as well as other health effects.[12] The established investigations show that indoor VOC concentrations are typically below 10 $\mu g/m^3$, and the most abundant VOCs are aliphatic and aromatic hydrocarbons, such as alkanes and BTEX (benzene, toluene, ethylbenzene, and xylenes).[13-16]

Although the role of VOCs in indoor health problems is recognized, no indoor air quality (IAQ) standard specifies the measurement of individual VOCs. The most often used standard for controlling IAQ is the American Society of Heating, Refrigerating and Air Conditioning Engineers (ASHRAE) Standard 62.1-2007 entitled "Ventilation for Acceptable Indoor Air Quality."[17] This standard sets minimum ventilation rates for commercial and institutional buildings, uses CO_2 as a surrogate measure of IAQ. Total VOC (TVOC) is also often used as an IAQ indicator.[18] However, TVOC cannot specify the presence of individual compounds, and is therefore not considered very useful in correlating exposure to VOCs with health effects .[19,20] The lack of VOC standards is partly due to the fact that inadequate or insufficient exposure data are available.

To date, virtually all investigations of VOCs indoors have utilized separate sample collection and laboratory analytical steps. They rely on conventional adsorbent-tube samplers followed by gas-chromatography/mass-spectrometry (GC-MS)[6,21-24] or GC-flame-ionization-detector (GC-FID).[16,25] While reliable, due to the cost and delay between sampling and analysis, these methods inherently limit the quality, quantity and frequency of data collected in field investigations. Also, these conventional methods do not permit characterization of concentration profiles with respect to spatial and temporal variations.

1.2.2 Environmental Tobacco Smoke (ETS) and Determination of Its Airborne Markers

Environmental tobacco smoke (ETS), also called secondhand tobacco smoke,[26] is a mixture of the smoke given off by the burning end of tobacco products and the smoke exhaled by smokers. Burning tobacco smoke is referred to as sidestream smoke, and exhaled smoke is called mainstream smoke. These are the primary and the secondary contributors to ETS, respectively. The International Agency for Research on Cancer (IARC) classifies ETS as a Group 1 (i.e. carcinogenic) substance.[27] Sufficient evidence has shown that ETS can cause lung cancer, heart disease and other health effects. An estimated 3,400 lung cancer deaths and 23-70,000 heart disease deaths occur annually among adult nonsmokers in the US as a result of exposure to ETS.[26] People can be exposed to ETS in smoking-permitted environments, such as the home, public places (i.e., restaurant, bar, bowling alley, etc.), at work, and in the car. Due to these public

health concerns, a great deal of research has been conducted in an effort to accurately assess ETS exposure.

ETS contains a complex mixture of more than 4,000 specific chemicals,[28] among which more than 50 have been shown to individually cause cancer.[26] These chemicals are components of exhaled mainstream smoke, sidestream smoke, and their aged reaction products. The complexity of ETS and the presence of confounding sources make determinations of airborne ETS difficult, prompting the use of marker compounds as surrogates for ETS detection. Among the airborne marker compounds that have been explored, vapor-phase nicotine (VPN) and 3-ethenylpyridine (3-EP) are mostly used.[28] 2,5-Dimethylfuran (2,5-DMF) has also been used as a biomarker of ETS.[29]

Nicotine is unique to tobacco. It meets three of the four primary criteria for a good marker as defined by the National Research Council.[30] VPN is approximately 95% of total ETS nicotine. The existence of nicotine is a strong indication that smoking has occurred. However, its adsorptive tendencies and unpredictable decay rate make it a less-than-ideal marker. 3-EP, a pyrolysis product of nicotine degradation during smoking, is a far better gas-phase marker of ETS.[31] When used as an ETS marker, 3-EP has several advantages over VPN: 1) its concentration correlates well with ETS particle concentrations and other gas-phase ETS components; 2) it is found exclusively in the gas phase; 3) it follows nearly first-order reaction kinetics, and thus its decay can be well predicted; and 4) its concentration increases linearly with the number of cigarettes smoked.[31] Data from several large-scale studies indicate that the mean concentrations of 3-EP in smoking offices, homes, and restaurants fall within the range of 0.8-6.3 $\mu g/m^3$ (0.18-1.5 ppb), with generally lower average personal exposure levels (0.4-0.7 ppb).[32-37]

2,5-dimethylfuran (2,5-DMF) has also been identified as a gas-phase marker of ETS.[29,38,39] In tests designed to simulate ETS levels in an office environment, 2,5-DMF concentrations were found to range from 2.4–30 $\mu g/m^3$ (0.6-7.5 ppb).[29,39] Concentrations of 2,5-DMF in the breath of passively exposed non-smokers averaged 6.8 ppb, those in the breath of smokers averaged 94 ppb immediately after smoking.[39] The major co-contaminants are the other gas-phase components of ETS and common indoor air contaminants (e.g., aromatic and aliphatic hydrocarbons, Cl- and N-substituted hydrocarbons, aldehydes, ketones).[29,40]

The current American Society for Testing and Materials (ASTM) standard method for monitoring 3-EP and nicotine in indoor air, ASTM D5075-01, is to collect an air sample on a tube packed with XAD-4 resin and extract the sample with a solvent, followed by GC-MS analysis.[41] Thermally-desorbed Tenax adsorbent tubes are also often used for ETS sample collection.[29,38] In addition to GC-MS,[42-54] GC-FID[55-57] and GC with a nitrogen-phosphorus detector (NPD)[32,33,36,42-48] are commonly used for analysis.

However, these conventional methods have many disadvantages: they are labor and capital-intensive, and provide less effective intervention feedback for affected individuals. Although Gordon et al. have described a field portable breath analyzer,[29] there are no published reports on the determination of ambient concentrations of vapor-phase ETS markers with portable direct-reading instrumentation.

1.2.3 Breath VOC Analysis and the Determination of Lung Cancer Biomarkers

Analysis of VOCs in breath can provide information about metabolic disorders or environmental and occupational exposure.[49,50] This is due to the rapid equilibration between the pulmonary blood and alveolar air. The non-invasive nature of this bio-monitoring method makes it more attractive than blood analysis. Breath is a very complex mixture. Among the major components of carbon dioxide, oxygen, water, and inert gases are numerous trace-level VOC components with concentrations in part-per-million (ppm) to ppt range.[53] Although large variations in component species and concentrations occur among tested human subjects,[51] as many as 150-200 VOCs have been measured in the breath of a single subject.[52]

The major VOCs in the breath of healthy individuals are isoprene, acetone, and alcohols.[53] Breath VOCs come from either endogenous or exogenous sources. Measured exogenous VOCs indicates recent exposure to environmental contaminants,[50] and testing of endogenous VOCs can provide information on health status. Although links between breath substances and diseases have not been well established,[49] some of the VOCs in breath may serve as biomarkers for screening purposes for specific health disorders or diseases.[49,54]

Deaths occur from lung cancer more than any other cancer.[26] Worldwide, lung cancer is also the most prevalent associated with occupational exposure to chemicals. Occupational exposure to a variety of agents (e.g., asbestos, As, Be, Cd, Ni, silica, and

diesel exhaust) occurs across numerous sectors and accounts for an estimated 10% of lung cancers.[58] Detection and surgical treatment at an early stage can dramatically increase the 5-year survival rate.[59] Breath biomarker analysis has recently been cited as a promising lung cancer screening method.[60] The study of breath VOCs as a screening method for lung cancer can be traced back two decades.[61] Although it is generally acknowledged that no single VOC from breath can serve as a unique breath biomarker of lung cancer, certain VOCs have been found to be associated with this disease. These are mainly alkanes and aromatic compounds.[60,62-64] Alkanes are the products of lipid peroxidation of polyunsaturated fatty acids in cell membranes.[65] Aromatic compounds are mostly related to environmental exposure or personal behaviors, such as tobacco smoke.[62] Patterns of a set of VOCs can be used to develop multivariate statistical models to differentiate/predict lung cancer.[62]

To use breath analysis as a routine clinical diagnostic tool, advancement is required in the determination of biomarkers for specific diseases.[54,66,67] Since the first reports on breath VOCs, analytical technologies have been greatly improved. However, standards for breath collection and analysis have not been established yet, making it difficult to compare or interpret the results from different studies.[49,54] The lack of standardization of sampling procedures is one of the reasons that breath analysis has not been introduced into clinical practice.[54]

There are several significant challenges in breath biomarker analysis. First, sample collection requires large volumes, and preconcentration is normally required. Most of the VOCs are found at sub-ppb levels, with some exceptions which are found at high ppb or low ppm level.[53] Required sample volumes depend on the sensitivity of the analytical system for the target compounds. In the past, samples as large as 30 L were necessary.[51,52,61,68-71] With improved analytical methods, required sample volumes have been reduced to ~1 L for GC-FID or MS analysis.[72-75] Single or multi-stage adsorbent traps and solid-phase microextraction (SPME) are the preconcentration devices most often reported for capturing VOCs from breath. SPME can be used to extract vapors directly from the mouth of a subject,[76] or from a commercial sampling device,[62] with an extraction time ranging from 30 s to 30 min. SPME has less adsorption capacity than multi-stage adsorbent trap,[62] which may result in detection of less VOCs. A GC equipped

with a low-temperature glassy carbon-coated SPME microfiber showed to have lower LODs than those equipped with conventional SPME fibers, in low- to sub-picomolar range for alkanes and aromatic compounds tested.[77] Therefore, most studies using SPME are confined to those looking at a small number of target VOCs. Where complex mixture analysis was desired, multi-stage adsorbent traps are generally used.[52,70,72,73,79]

A second major challenge is to obtain a complete 'spectrum' of breath VOCs. Breath VOCs are generally subject to large intra- and inter-subject variations. Although as many as 150-200 VOCs can be obtained from a healthy human subject,[52] one study has shown that as many as 3481 VOCs could be detected at least once from 50 subjects.[51] Notably, however, only 27 detected compounds were common for all these subjects. In addition the breath VOC composition is subject to changes due to the environment where the subjects spend time, where the samples were collected, and the diet of the individuals.

Third, the high concentrations of water vapor in breath samples poses several problems, including competition for sites on the preconcentrator adsorbent, possible changes in retention time on the GC column, and interference with responses to early-eluting VOCs due to overlap with water peaks. Therefore, it is generally necessary to reduce the amount of water vapor transferred into the analytical system. One simple option is to place a water trap in series with adsorbent trap.[70] However, some of the polar compounds can be lost at the same time. Another simple method is to heat the adsorbent trap to 40 °C during sampling.[52] However heating can cause the loss of volatile compounds and/or decrease the adsorption capacity of the trap. To avoid the use of carbon molecular sieves which has very high surface area and have high affinity for water vapor in the adsorbent trap has been proposed. Unfortunately carbon molecular sieves have still been the best adsorbent when very volatile compounds are sampled. One favorable method is dry-air purge. Dry-air purge of the adsorbent prior to thermal desorption can remove as much as 98% of the water from the adsorbent with minimum loss of adsorbed VOCs.[79] It is clear that more research is needed to seek effective approaches to reduce water vapor from breath samples.

Despite the advantages of GC-MS, which include fairly high sensitivity and the ability to identify compounds on the basis of their fragmentation spectra, the expense of the system and need for expertise in operation make it difficult to be used routinely in

field settings.[80] Two-dimensional (2-D) GC-FID has also been used to determine breath VOCs.[73] However, the complicated system design and data analysis associated with 2-D GC precludes its use in fielded systems at this point in time. Attempts to apply electronic nose technologies comprising stand-alone sensor arrays to differentiate lung cancer patients from healthy controls have been partially successful,[63,80,81] but have been criticized for their low sensitivity and inability to identify specific VOCs.[82] To make these results more reliable, sensors should be operated in parallel with other analytical methods.

1.2.4 Portable GC for VOC Mixture Analysis

Very few portable instruments have the capability to analyze the components of complex VOC mixtures. These include Fourier Transform Infrared Spectrophotometers (FTIR),[83-85] hand-held ion mobility spectrometers (IMS),[86,87] hand-held mass spectrometers (MS),[88] and portable GCs with various detectors. Among these, portable GCs are the most popular for on-site VOC monitoring due to the versatility associated with the ability to separate components prior to detection, and to their compatibility with different types of detectors.

On-site VOC monitoring with portable GCs has been practiced since the 1980's,[88,90] and numerous field portable GC are commercially available.[91,92-96] Development efforts related to portable GC focus on the three key analytical components: sampler/injector, column and the heating module, and detector. Thermal desorbed single-stage[25,,97-99] or multi-stage micro-adsorbent trap[1] and solid phase micro extraction (SPME)[1001,101] are the most popular samplers used in portable GCs. Micro-sampling loop/chip has also been used.[102] Column lengths used in portable GCs differ much, ranging from a few meters[1] to 30 m.[101,103] Basically there are two different heating methods: at-column heater (this column module is called Low-Thermal-Mass column module,[1,100,104] such as RVM columns), and heating oven.[99] A variety of detectors are employed in research portable GC prototypes. These include micro-FID,[25,99] PID,[105,106] IMS,[86] micro-flame photometric detector (μFPD),[100] micro-counter-flow FID,[100] argon-doped helium ionization detector (HID),[103] electron capture detector (ECD),[103] micro-machined thermal conductivity detector (TCD),[102] MS,[97,100,101,104] single surface acoustic wave (SAW) sensor,[107] SAW sensor array,[1,98,108] and chemiresistor (CR) sensor array.[109]

However, only a few of these detectors have been equipped in commercial units, for example IMS,[87] MS,[91,110] and SAW.[111] With the exception of MS, IMS and sensor array, vapor identification with all other detectors rely solely on the retention time. Some of them lack selectivity (FID, PID), and others are limited by sensitivity.

Many advances have been made in the development of portable GC, especially in the aspect of detection technology. However, most of the commercial portable GC units have still rely on MS as their detectors. The complexity and high cost of these instruments may limit their use for routine monitoring. A survey of the archival literature on portable GC technologies revealed that VOC mixtures that can be analyzed is generally limited to < 20 compounds.[102,112-114]

1.2.5 Chemiresistor Sensor Array for VOC Detection

A chemical sensor consists of a chemically selective layer which interacts with incoming VOCs, causing changes of one of the physical properties, and a transducer which transforms this change into another signal.[115] Chemical sensors for VOC detection have been developing rapidly and have become popular in recent years. One of the driving forces is the need for portable instruments in applications such as environmental monitoring, industrial hygiene, and homeland security.[116] Compared with conventional detectors which are used in portable instruments, chemical sensors offer many advantages: low-cost of production, small size, simplicity, low power operation, minimal maintenance, etc.[117] For VOC mixture detection, using an array of sensors of different functionalities, partial selectivity can be obtained. Like a characteristic ‘fingerprint’ of each analyte, response patterns can be used to identify vapors.

A comprehensive study of vapor recognition with arrays of polymer-coated surface acoustic wave (SAW) sensors showed that binary mixtures could generally be recognized by an array of only two or three SAW sensors.[127] The recognition of ternary mixture with a sensor array was also possible if the functional groups of the components were very different. Low recognition rates were generally observed for more complex mixtures or mixtures of structurally homologous compounds. Increasing the number of sensors in the array did not necessarily improve the recognition. However, if a sensor array is employed as the detector of a portable GC, significant advantages can be achieved from the combination of column separation and sensor array detection. The

response patterns can be used with retention times to identify target VOCs among a complex mixture. Promising results have demonstrated these advantages.[1,109,118]

Chemical sensors are classified by their transduction mechanisms. Several types of sensors have been shown to be useful as VOC detectors. These include metal-oxide semiconductor,[119] optical,[120] piezoelectric (e.g. SAW sensors),[1,121] and chemiresistor (CR) sensors.[122,123] CR sensors are the most marketed sensors due to their easy and inexpensive fabrication.[124] CR sensors require simpler measurement/driving circuitry and physical system than other sensors. Figure 1-1 shows a typical CR device, which includes pairs of electrodes, an electrically insulated substrate to support the electrodes, and chemically sensitive interface film deposited on the electrodes.

Electrically conductive polymers and carbon-doped polymers have been widely used as interfaces of CR sensors.[124-127] Providing lower detection limits and requiring simpler electrical circuitry and physical system, gold-thiolate monolayer-protected nanoparticles (MPNs) have emerged as a new class of CR interface.[123,128,129] The structure of MPNs is a gold core of nano-dimensions, surrounded by a monolayer of self-assembled thiolate which provides stability for the formation of the thermodynamically unfavorable gold cores.[130] Polymer- or MPN-CR sensors rely on the reversibly vapor sorption on the interfacial films. When a sorption-dependent sensor is exposed to a certain concentration of vapor (C_a), the steady-state absorbed concentration (C_s) inside the interfacial film will reach thermodynamic equilibrium:

$$K = \frac{C_s}{C_a} \tag{1}$$

where K is the partition coefficient, which is affected by the strength of the non-bonding interaction between the vapor and interfacial. K is temperature dependent. The Arrhenius-type relationship can be used to describe the temperature dependence of partition coefficient for low vapor concentrations at a finite temperature ranges:[131]

$$K = K_0 e^{-\Delta H_s / RT} = K_0 e^{-(\Delta H_c + \Delta H_m)/RT} = K_0 e^{(\Delta H_v - \Delta H_m)/RT} \tag{2}$$

where K_0 is the pre-exponential term that includes the sorption entropy, ΔH_s is the heat of sorption, ΔH_c is the molar heat of condensation and equal to heat of vaporization ΔH_v, ΔH_m is the partial molar heat of mixing, and is always smaller than the molar heat of condensation. In an ideal case, $\Delta H_m = 0$. The relationship of vapor pressure and heat of

vaporization can be described by the Young's Equation, an alternative form of the Clausius Clapeyron Equation:

$$p_v^0 = Ae^{\Delta H_v / RT} \tag{3}$$

where p_v^0 is the saturated vapor pressure of the pure liquid form of the analyte, A is a constant. Combining Equations 2 and 3, and defining $\Delta H_m = 0$ for ideal cases, an inversely proportional relationship between K and vapor pressure can be obtained:

$$K(ideal) = (const.)(\frac{1}{p_v^0}) \tag{4}$$

Deviations from this relationship can be found in cases where heat of mixing is significant, which occurs when the functional groups of the vapor and interfacial material are different.

For MPN-CRs, it is generally recognized that vapors partitioning into the MPN film cause it to swell, which changes the electron tunneling barrier and thereby the film resistance.[109,118,123, 128,132] CR response is obtained by measuring the resistance changes ($\Delta R/R$). However, the transduction mechanism has not been fully established. Recently, Steinecker et al. have proposed a model to predict responses of MPN-CRs from vapor-film partition coefficient, and analyte density and dielectric constants.[133] This model also indicates that the sensitivity of the MPN-CR sensors is only dependent on vapor concentration, regardless of electrode geometry and film thickness. Therefore, miniaturization of MPN-CRs is possible, providing bases of the usage of these devices in a microsystem.

1.3 The First-Generation Prototype

1.3.1 Overview of Primary Components

Figures 1-2 shows the layout of the analytical sub-system and a photo of the first-generation instrument.[1] The instrument had a footprint about the size a laptop computer, measuring 30 cm (l) x 30 cm (w) x 10 cm (h). The key features of the first-generation prototypes were a mini multi-stage adsorbent preconcentrator/injector (PCI), two series-coupled 4.5-m-long low-thermal-mass separation columns with pressure and temperature tunable retention control, and a detector comprising an integrated array of polymer-

coated SAW sensors whose responses patterns could be treated as digital 'spectra' of eluting vapors and used together with retention times for peak identification. Scrubbed air is used as the carrier gas. The performance of the systems relies on the functional integration of these components.

The PCI was designed to function both as a sample preconcentrator and a focused injector. By capturing VOCs from a large volume of ambient air and desorbing them into a sharp injection plug, it permited detection of mixtures of VOCs at low (i.e., part-per-billion to part-per-trillion) concentrations, which are the prevalent concentrations encountered in residential, occupational, and ambient environmental settings,[6] and are generally too low for direct measurement by most current detectors or the sensors employed in the instrument. A typical PCI consisted of a metal capillary tube filled with a series of carbon-based granular adsorbent materials having graded specific surface areas. The adsorbents were in order of from weakest to strongest in sampling flow direction. Once a sample of vapor was captured a resistive heater is activated and the flow was reversed in order to backflush and desorb trapped vapors for injection into the separation module. Depending on the analytes and sampling conditions, the adsorbents and bed masses of the PCI could be changed.

Figure 1-3 shows the distribution of 43 vapors in a three-stage PCI containing contains 8 mg of Carbopack B, 2.5 mg of Carbopack X, and 1.8 mg of Carboxen 1000.[134] This PCI has sufficient capacity for quantitatively capturing mixtures of up to 43 compounds at 100 ppb from a 1-L air sample and efficiently desorbing them at 300 °C. Carboxen 1000 is a carbon molecular sieve adsorbent with very high specific surface area (1200 m^2/g) and is included in order to capture (and thermally desorb) highly volatile compounds. Carbopack X is a graphitized carbon adsorbent with moderate surface area (250 m^2/g) and effectively captures (and desorbs) moderately volatile compounds. Carbopack B is also a graphitized carbon adsorbent with relatively low surface area of 100 m^2/g and can effectively capture (desorb) less volatile compounds.

The prototype employed a dual-column ensemble consisting of two-low-thermal mass capillary columns 4.5 m long (0.25 mm i.d.). The first column had a nonpolar stationary phase and the second column had a moderately polar stationary phase. With air as carrier gas, the stationary phases are stable as long as the column temperature is

maintained ≤ 200 °C.[135] Each column has an "at-column heating" configuration, and can be heated independently at a very high rate. The midpoint-tuning valve connected to the junction point of the two columns can be opened for short periods of time during an analysis causes the flow in the first column to cease, while accelerating flow in the second column, which can be used to enhance separation. The combination of pressure tuning and fast independent temperature programming of each column improves the separation of compounds that would otherwise co-elute from the columns.

Figure 1-4 presents a so-called band trajectory plot that illustrates how separation tuning works.[136] The y-axis of the plot shows the position of analytes along the dual column ensemble as a function of retention time (x-axis). Under an initial set of operating conditions certain analytes are separated and others co-elute (top row of the plot). The goal is to maximize separation. In the case of compounds A and B, there is separation after passing through the 1st column but fortuitous merging and co-elution by the time they reach the end of the 2nd column. This pair is amenable to pressured tuned separation. If the junction-point tuning valve is closed for a few seconds just after compound A passes the dual column junction point (while compound B is still in the 1st column), compound A will be accelerated through the second column and will be separated from compound B at the end of the 2nd column. In the case of C and D, pressure tuning could also be used, however, if the 2nd column heating rate is increased both C and D elute faster than at the initial condition, but C is more sensitive to the effects of column temperature and C and D are separated.

The detector used in this instrument was an integrated array of four SAW sensors. One of the sensors was uncoated and served as the reference. The other three were coated with different polymers, and thus named: polyisobutylene (PIB), ethyl cellulose (ECEL), and polydimethylsiloxane with hexafluorobisphenol A moieties incorporated along its backbone (BSP3). PIB has a non-polar structure, ECEL has moderate polar and hydrogen bonding properties, and BSP3 has a special fluorinated structure incorporated with hydrogen bonding acidity. When vapor is absorbed by the polymer, the change in mass and mechanical properties change the frequency of the propagating wave on the sensor. Sensor response is obtained measuring the frequency change.

Since the structure of the polymer differs for each sensor, the affinity for a given vapor differs among the films and the array of SAW produces a set of responses for each vapor eluting from the separation columns. It is possible to determine the contribution of the composite response pattern they produce, certain coelutions of simple mixtures can be tolerated, and peaks can be identified and quantified. Coeluting peaks are integrated, and the resulting responses are analyzed by extended disjoint principal components regression (EDPCR).[137] The approach of this analysis is based on the assumption that responses to multiple vapors are additive, which has been found true for a lot of polymer coated SAW-sensors.[138,139] Expected recognition rates for the components are estimated by combining Monte-Carlo simulations with EDPCR.[117,139] The Monte-Carlo simulations superimpose random error on calibrated sensor-array response patterns, which are then analyzed by EDPCR to determine if the components giving rise to the composite response pattern can be determined with low error.[117] Iterative analysis (n=500) over a range of concentrations yields statistical estimates of recognition.

1.3.2 Instrument Performance and Limitations

The first-generation prototype had successfully demonstrated its high performance obtained from the functional integration of multi-adsorbent PCI, tuned separation, and SAW-sensor array response by the determination of a 30-vapor mixture of common indoor contaminants in < 10 min, with detection limits (LODs) of many vapors in the ppt concentration levels, assuming a 1-L sample.[1] However, the sensitivities of the SAW sensors for certain more volatile vapors were relatively low, resulting in difficulty in obtaining useful response patterns at low concentrations. Batch to batch variation in performance with these sensors were somewhat high. This has led to the consideration of an alternative sensor technology and approach, involving the use of an array of CR sensors coated with Au-thiolate monolayer-protected nanoparticles (MPNs). These CR sensors have been shown to provide lower LODs than SAW sensors.[8] Indeed, a preliminary test showed that LODs were improved by 4 to 33 folds when the SAW array was replace by a MPN-CR array in the first-generation instrument under the similar GC conditions.[140]

IAQ field testing showed the potential of the portable instrument. However, laboratory and field testing also exposed needed improvements to this instrument in a lot

of aspects. The most serious problem is retention time (+) shift caused by a decrease in both flow rate and column temperature with the instrument continuously running. These problems were caused by the drift in the instrument reference voltages were used to set the target inlet pressure and column temperature. The voltage drift was caused by an increasing instrument temperature during long periods of operation. This behavior was an inherent electronic problem with the instrument's built-in microprocessor control. Some other design features of this prototype were observed to hinder the performance. These led to the development of the second-generation instrument.

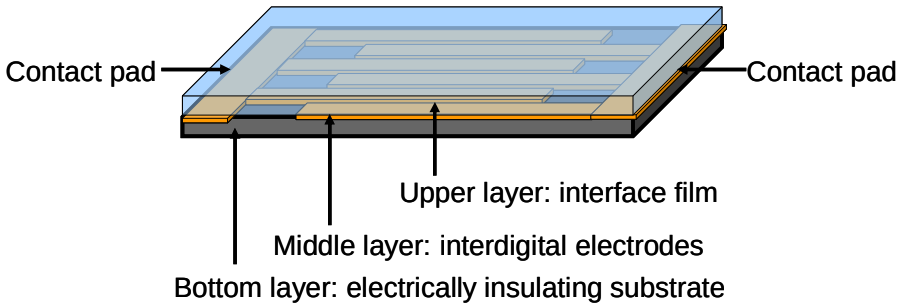

Figure 1-1. Schematic diagrams of a chemiresistor sensor.

(a)

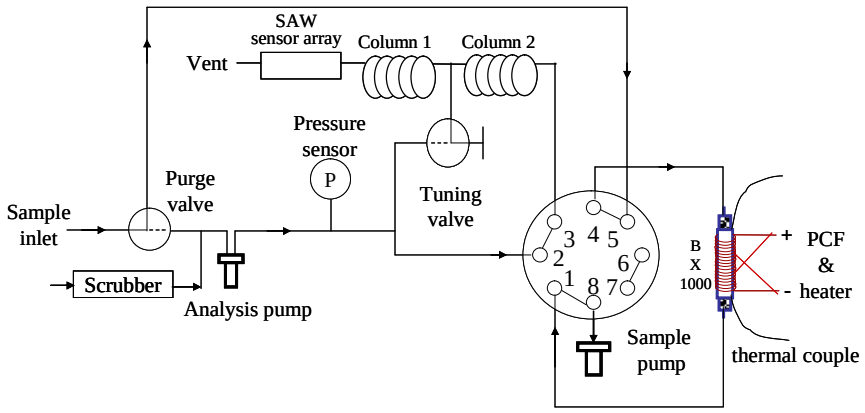

(b)

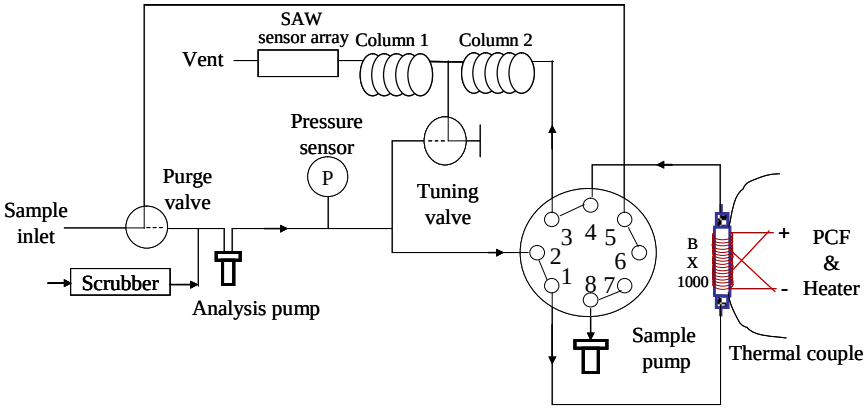

(c)

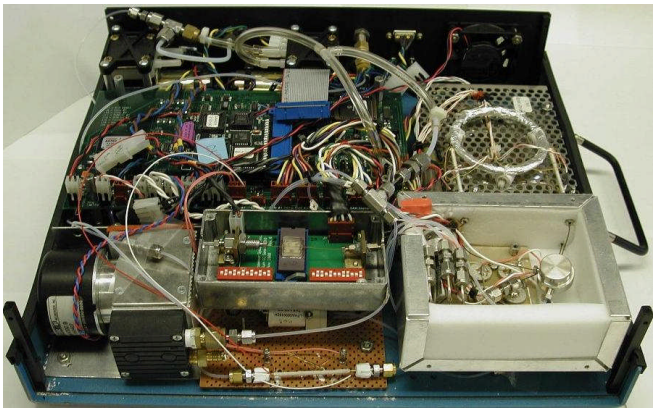

Figure 1-2. Block diagram and photos of the instrument: (a) flow direction during sampling, (b) flow direction during analysis, (c) photo of the instrument, (d) assembled PCI with heater and k-type thermocouple, (e) column wrapped with heater wire and thermocouples, (f) integrated SAW sensor array with inlet/outlet capillary tubing.

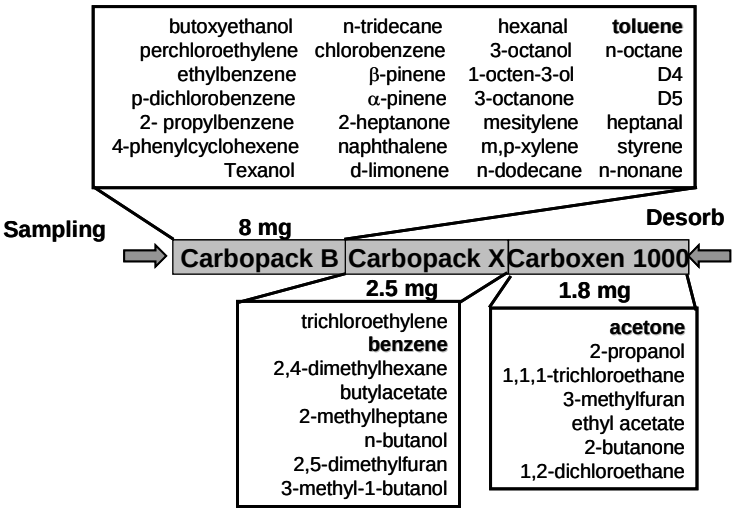

Figure 1-3. Distribution of 43 vapors ranging over four orders of magnitude in vapor pressure among the three adsorbent beds in the 3-stage PCI (adapted from Ref. 134).

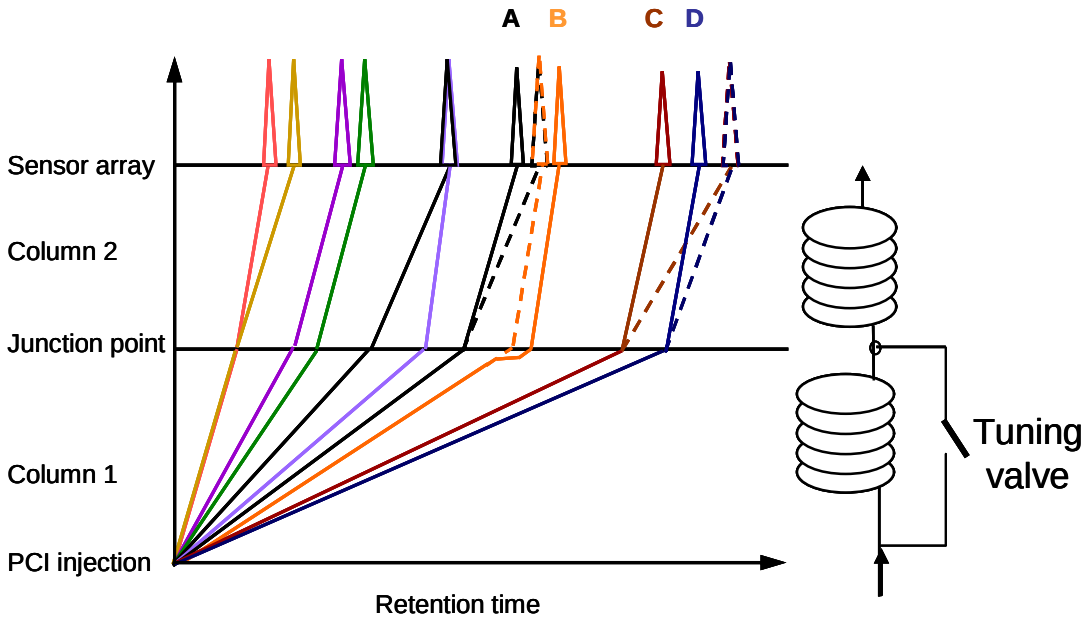

Figure 1-4. Band trajectory plot showing tuned separations. Under initial GC conditions, there are co-eluting pairs of interest: A+B and C+D (dash lines). Pressure tuning results in separation of A and B and independent column temperature programming results in separation of C and D.

1.4 References

1. Lu, C. J.; Whiting, J.; Sacks, R. D.; Zellers, E. T. *Anal. Chem*. **2003**, 75(6), 1400-1409.
2. Lu, C. J.; Jin, C.; Zellers, E. T. *J. Environ. Monit.* **2006**, *8*(2), 270-278.
3. Zhong, Q.; Veeneman, R. A.; Steinecker, W. H.; Jia, C.; Batterman, S. A.; Zellers, E. T. *J. Environ. Monit.* **2007**, *9*, 440-448.
4. U.S. Environmental Protection Agency. *Compendium Method TO-15, Determination of Volatile Organic Compounds (VOCs) in Air Collected in Specially-Prepared Canisters and Analyzed by Gas Chromatograpy/Mass Spectrometry (GUMS).* EPN6251R-96/010b, Cincinnati,OH, 1999.
5. US Environmental Protection Agency, *Exposure Factors Handbook*, Page 15-25, 1996.
6. Jia C.R.; Batterman S.; Godwin C. *Atmos. Environ*. **2008**, 42(9), 2083-2100.
7. Lee, C. S.; Haghighat, F.; Ghaly, W. S. *Indoor Air* **2005**, *15*(3), 183-196.
8. Srivastava, A.; Joseph, A. E.; Wachasunder, S. D. *Environ. Monit. Assess.* **2004**, *96*(1-3), 263-271.
9. Wolkoff, P.; Schneider, T.; Kildeso, J. et al. *Sci. Total Environ.* **1998**, *215*(1-2), 135-156.
10. Fischer, G.; Dott, W. *Arch. Microbiol.* **2003**, *179*(2), 75-82.
11. Fick, J.; Nilsson ,C.; Andersson, B. *Atmos. Environ.* **2004**, *38*(35), 5895-5899.
12. Takigawa, T.; Horike, T.; Ohashi, Y.; et al. *Environ. Toxicol.* **2004**, *19*(4), 280-290.
13. Pommer, L.; Fick, J.; Sundell, J.; et al. *Indoor Air* **2004**, *14*(1), 16-23.
14. Tham, K.W.; Zuraimi, M. S.; Sekhar, S. C. *Environ. International* **2004**, *30*(8), 1075-1088.
15. Grows, W. A.; Reynolds. *Applied Occupational Environ. Hygiene* **2003**, *18*(5), 1-9.
16. Hodgson, A.T.; Faulkner, D.; Sullivan, D. P.; et al. *Atmos. Environ.* **2003**, *37*(39-40), 5517-5527.
17. ASHRAE, ASHRAE Standard 62.1-2004 – Ventilation for Acceptable Indoor Air Quality, ASHRAE Publisher: Atlanta, 2007
18. Molhave, L.; Clausen, G.; Berglund, B.; et al. *Indoor Air* **1997**, *7*(4), 225-240.
19. Sundell, J.; Andersson, B.; Andersson, K.; Lindvall, T. *Indoor Air* **1993**, *3*, 82–93.
20. Skov, P.; Valbjorn, O.; Pedersen, B.V.; DICS Group. *Scand. J. Work Environ. Health* **1990**, *16*, 363–371.
21. Posniak, M.; Makhniashvili, I.; Koziel, E. *Indoor and Built Environ.* **2005**, *14*(3-4), 269-275.
22. Reynolds, S. J.; Black, D. W.; Borin,S. S.; Breuer, G.; Burmeister, L. F.; Fuortes, L. J.; Smith, T. F.; Stein, M. A.; Subramanian, P.; Thorne, P. S.; Whitten, P. *Applied Occupational Environ. Hygiene* **2001**, *16*(11), 1065-77.
23. Brickus, L. S. R.; Cardoso, J. N.; De Aquino Neto, F. R. *Environ. Sci. Technol.* **1998**, *32*(22), 3485-3490.
24. Wieslander, G.; Norback, D.; Walinder, R.; Erwall, C.; Venge, P. *International Arch. Occupational and Environ. Health* **1999**, *72*(8), 507-15.

25. Persily, A.; Howard-Reed, C.; Nabinger, S. J. *Atmos. Environ.* **2003**, *37*(39-40), 5505-5516.
26. US Center of Disease Control and Prevention Homepage, http://www.cdc.gov (accessed May 2008).
27. International Agency for Research on Cancer Homepage, http://www-cie.iarc.fr/htdocs/monographs/vol83/02-involuntary.html (accessed May 2008).
28. Jenkins, R. A.; Guerin, M. R.; Tomkins, B. A. *The Chemistry of Environmental Tobacco Smoke: Composition and Measurement, 2nd edition*, Lewis publishers: New York, Chapter 3, 2000.
29. Gordon, S. M.; Wallace, L.A.; Brinkman, M. C.; et al. *Environ. Health Perspect.* **2002**, *110*(7), 689-698.
30. National Research Council, *Environmental Tobacco Smoke – Measuring Exposures and Assessing Health Effects*, National Academy Press: Washington DC, Page 70, 1986.
31. Vainiotalo, S.; Vaaranrinta, R.; Tornaeus, J.; Aremo, N.; Hase, T.; Peltonen, K. *Environ. Sci. Technol.* **2001**, *35*, 1818-22.
32. Maskarinec, M. P.; Jenkins, R. A.; Counts, R. W.; Dindal, A. B. *J. Exposure Anal. Environ. Epidemiol.* **2000**, *10*(1), 36-49.
33. Bohanan, H. R.; Piade, J. J.; Schorp, M. K.; Saint-Jalm, Y. *J. Exposure Anal. Environ. Epidemiol.* **2003**, *13*(5), 378-392.
34. Hyvarinen, M. J.; Rothberg, M.; Kahkonen, E.; Mielo, T.; Reijula, K. *Indoor Air-Int J. Indoor Air Qual and Climate* **2000**, *10*(2), 121-125.
35. Jenkins, R. A.; Finn, D.; Tomkins, B. A.; Maskarinec, M. P. *Regul. Toxicol. Pharm.* **2001**, *34*(3), 213-220.
36. Jenkins, R. A.; Maskarinec, M. P.; Counts, R. W.; Caton, J. E.; Tomkins, B. A.; Ilgner, R. H. *J. Exposure Anal. Environ. Epidemiol.* **2001**, *11*, 369-380.
37. Kim, Y. M.; Harrad, S.; Harrison, R. M. *Environ. Sci. Technol.* **2001**, *35*(6), 997-1004.
38. Xie, J. X.; Wang, X. M.; Sheng, G. Y.; Bi, X. H.; Fu, J. M. *Atmos. Environ.*, **2003**, *37*, 3365-3374.
39. Charles, S. M.; Jia, C. R.; Batterman, S. A.; Godwin, C. *Environ. Sci. Technol.* **2008**, *42*(4), 1324-1331.
40. Singer, B. C.; Hodgson, A. T.; Guevarra, K. S.; Hawley, E. L.; Nazaroff, W. W. *Environ. Sci. Technol.* **2002**, *36*(5), 846-853.
41. ASTM International, ASTM D5075-01, Standard Test Method for Nicotine & 3-Ethenylpyridine in Indoor Air, West Conshohocken, PA, 2001.
42. Baek, S. O.; Jenkins, R. A. *Indoor and Built Environ.* **2001**, *10*(3-4), 200-208.
43. Jenkins, R. A.; Palausky, A.; Counts, R. W.; Bayne, C. K.; Dindal, A. B.; Guerin, M. R. *J. Exposure Anal. Environ. Epidemiol.* **1996**, *6*(4), 473-502.
44. Phillips, K.; Bentley, M. C. *Environ. Int.* **2001**, *27*(1), 69-85.
45. Phillips, K.; Howard, D. A.; Bentley, M. C.; Alvan, G. *Atmos. Environ.* **1999**, *33*(12), 1889-1904.
46. O'Connor T. Z.; Holford T. R.; Leaderer, B. P.; Hammond, S. K.; et al. *Am. J. Epidemiol.* **1995**., *142*(12), 1315-1321.
47. Eisner, M. D.; Katz, P. P.; Yelin, E. H.; Hammond, S. K. et al. *Environ. Health Persp.* **2001**, *109*(8), 809-814.

48. Hammond, S. K.; Sorensen, G.; Youngstrom, R. et al. *JAMA-J A. Med. Assoc.* **1995**, *274*(12), 956-960.
49. Cao, W. Q.; Duan, Y. X. *Clin. Chem.* **2006**, *52*(5), 800-11.
50. Wallace, L.; Buckley, T.; Pellizzari, E.; Gordon, S. *Environ. Health Perspect.* **1996**, *104*, 861-69.
51. Phillips, M.; Gleeson, K.; Hughes, J. M. B.; Greenberg, J.; Cataneo, R. N.; Baker, L.; Mcvay, W. P. *Lancet* **1999**, *353*, 1930-33.
52. Phillips, M. *Anal. Biochem.* **1997**, *247*, 272-78.
53. Fenske, J. D.; Paulson, S. E. *J. Air Waste Manage. Assoc.* **1999**, *49*, 594-98.
54. Miekisch, W.; Schubert, J. K.; Noeldge-Schomburg, G. F. E. *Clin. Chim. Acta* **2004**, *347*, 25-39
55. Ogden, M. W.; Martin, P. *Environ. Int.* **1997**, *23*(1), 123-138.
56. Ogden. M. W.; Heavner, D. L.; Foster, T. L.; et al. *Environ. Technol*. **1996**, *17*(3), 239-250.
57. Nelson, P. R.; Henvner. D. L.; Collie, B. B.; et al. *Environ. Sci. Technol*. **1992**, *26*(10), 1909-1915.
58. World Health Organization, World Health Report 2002.
59. CancerCare, www.lungcancer.org
60. Mcwilliams, A.; Lam, S. *Curr. Opin. Pulmonary Med.* **2005**, *11*, 272-77.
61. Gordon, S. M.; Szidon, J. P.; Krotoszynski, B. K.; Gibbons, R. D.; Oneill, H. J. *Clin. Chem.* **1985**, *31*, 1278-82.
62. Poli, D.; Carbognani, P.; Corradi, M.; Goldoni, M.; Acampa, O.; Balbi, B.; Bianchi, L.; Rusca, M.; Mutti, A. *Resp. Res.* **2005**, *6*.
63. Machado, R. F.; Laskowski, D.; Deffenderfer, O.; Burch, T.; Zheng, S.; Mazzone, P. J.; Mekhail, T.; Jennings, C.; Stoller, J. K.; Pyle, J.; Duncan, J.; Dweik, R. A.; Erzurum, S. C. *Am. J. Respir. and Crit. Care Med.* **2005**, *171*, 1286-91.
64. Chanin, T. D.; Merrick, D. T.; Franklin, W. A.; Hirsch, F. R. *Curr. Opin. Pulmonary Med.* **2004**, *10*, 242-47.
65. Ost, D.; Shah, R. D.; Fein, D.; Fein, A. M. *Chest* **2003**, *123*, 1788-92.
66. Di Francesco, F.; Fuoco, R.; Trivella, M. G.; Ceccarini, A. *Microchem. J.* **2005**, *79*, 405-10.
67. Miekisch, W.; Schubert, J. K. *TrAC, Trends Anal. Chem.* **2006**, *25*, 665-73.
68. Conkle, J. P.; Camp, B. J.; Welch, B. E. *Arch. Environ. Health* **1975**, *30*, 290-95.
69. O'neill, H. J.; Gordon, S. M.; Oneill, M. H.; Gibbons, R. D.; Szidon, J. P. *Clin. Chem.* **1988**, *34*, 1613-18.
70. Phillips, M.; Greenberg, J. *J. Chromatogr. Biomed. Appl.* **1991**, *564*, 242-49.
71. Liu, Y. M.; Dueker, S. R.; Jones, A. D.; Ebeler, S. E.; Clifford, A. J. *Clin. Chem.* **1995**, *41*, 1028-32.
72. Sanchez, J. M.; Sacks, R. D. *Anal. Chem.* **2003**, *75*, 2231-36.
73. Libardoni, M.; Stevens, P. T.; Waite, J. H.; Sacks, R. *J. Chromatogr. B-Anal. Technol. Biomed. Life Sci.* **2006**, *842*, 13-21.
74. Phillips, M.; Cataneo, R. N.; Cummin, A. R. C.; Gagliardi, A. J.; Gleeson, K.; Greenberg, J.; Maxfield, R. A.; Rom, W. N. *Chest* **2003**, *123*, 2115-23.
75. Phillips, M.; Cataneo, R. N.; Ditkoff, B. A.; Fisher, P.; Greenberg, J.; Gunawardena, R.; Kwon, C. S.; Tietje, O.; Wong, C. *Breast Cancer Res. Treat.* **2006**, *99*, 19-21.

76. Grote, C.; Pawliszyn, J. *Anal. Chem.* **1997**, *69*, 587-96.
77. Giardina, M.; Olesik, S. V. *Anal. Chem.* **2003**, *75*, 1604-14.
78. Phillips, M.; Herrera, J.; Krishnan, S.; Zain, M.; Greenberg, J.; Cataneo, R. N. *J. Chromatogr. B* **1999**, *729*, 75-88.
79. Groves, W. A.; Zellers, E. T. *Am. Ind. Hyg. Assoc. J.* **1996**, *57*, 257-63.
80. Mazzone, P. J.; Hammel, J.; Dweik, R.; Na, J.; Czich, C.; Laskowski, D.; Mekhail, T. *Thorax* **2007**, doi: 10.1136/thx.2006.072892.
81. Di Natale, C.; Macagnano, A.; Martinelli, E.; Paolesse, R.; D'arcangelo, G.; Roscioni, C.; Finazzi-Agro, A.; D'amico, A. *Biosens. Bioelectron.* **2003**, *18*, 1209-18.
82. Phillips, M. *Am. J. Respir. Crit. Care Med.* **2005**, *172*, 1060.
83. Drescher, A. C.; Park, D. Y.; Yost, M. G.; Gadgil, A. J.; Levine, S. P.; Nazaroff, W. W. *Atmos. Environ.* **1997**, *31*, 727-740.
84. Tsai, M.Y.; Yost, M.G.; Wu, C.F. Hashmonay, R.A., Larson, T.V. *Atmos. Environ.* **2001**, *35*, 4791-4799.
85. Goldthorp, M. D.; Lambert, P. *J. Hazard. Mater.* **2001**, *83* (1-2), 135-152.
86. Arnold, N. S.; Dworzanski, J. P.; Sheya, S. A.; et al. *Field Anal. Chem. Technol.* **2000**, *4*(5), 219-238.
87. Femtoscan Corporation, http://femtoscan.com (assessed Feb 2008).
88. Keil, A.; Hernandez-Soto, H.; Noll, R. J.; Fico, M.; Gao, L.; Ouyan, Z.; Cooks, R. G. *Anal. Chem.* **2008**, *80*(3), 734,741.
89. Miller, D. L.; Woods, J. S.; Grubaugh, K. W.; Jordon, L. M. *Environmental Science & Technology* **1980**, *14*(1), 97-100
90. Barker, N. J.; Leveson, R. C. *American Laboratory* **1980**, *12*(12), 76.
91. Inficon Corporate, http://www.inficon.com (accessed June 2006).
92. Photovac, Inc., http://www.photovac.com (accessed Feb. 2008).
93. SRI Instruments, http://www.srigc.com (accessed Feb. 2008).
94. Analytical Specialists, Inc., http://www.microfastgc.com (accessed Feb. 2008).
95. Varian, Inc., http://www.varianinc.com (accessed Feb. 2008).
96. Agilent Technologies, http://www.home.agilent.com (accessed Feb. 2008).
97. Eckenrode, B. A. *J. Am. Soc. Mass. Spectrom.* **2001**, *12*(6), 683-693.
98. Groves, W. A.; Achutan, C. *J. Occupational Environ. Hyg.* **2004**, *1*(12), 779-788.
99. Liu, X. Y.; Pawliszyn, R.; Wang, L. M.; et al. *Analyst* **2004**, *129*(1), 55-62.
100. Thurbide, K. B.; Hayward, T. C. *Anal. Chim. Acta* **2004**, *519*(1), 121-128.
101. Smith, P. A.; Kluchinsky, T. A.; Savage, P. B.; et al. *AIHA J.* **2002**, *63*(3), 284-292.
102. Dziuban, J. A.; Mroz, J.; Szczygielska, M.; Malachowski, M.; Gorecka-Drzazga, A.; Walczak, R.; Bula, W.; Zalewski, D.; Nieradko, L.; Lysko, J.; Koszur, J.; Kowalski, P. *Sens. Actuators, A*, **2004**, *115*, 318-330.
103. Whalley, L. K.; Lewis, A. C.; McQuaid, J. B.; et al. *J. Environ. Monit* **2004**, *6*(3), 234-241.
104. Sloan K. M.; Mustacich R. V.; Eckenrode B. A.; *Field Anal. Chem. Technol.* **2001**, *5*(6), 288-301.
105. Durana, N.; Navazo, M.; Alonso, L.; et al. *J. Air Waste Manage. Assoc.* **2002**, *52*(10), 1176-1185.

106. Jia, M. Y.; Koziel, J.; Pawliszyn, J. *Field Anal. Chem. Technol.* **2000**, *4*(2-3), 73-84.
107. Wohltjen, H. *196th Meeting of the Electrochemical Society, Meeting Abstracts*, Phoenix, AZ, October 9-14, 1994, ECS Inc.: Pennington, N. J., Abstract No. 640.
108. Whiting, J. J.; Lu ,C. J.; Zellers, E. T.; et al. *Anal. Chem.* **2001**, *73*(19), 4668-4675.
109. Lu, C. J.; Steinecker, W. H, Tian, W. C.; Agah, M.; Potkay, J. M.; Oborny, M. C.; Nichols, J.; Chan, H.; Driscoll, J.; Sacks, R. D.; Pang, S. W.; Wise, K. D.; Zellers, E. T. *Lab On A Chip* **2005**, *5*, 1123-1131.
110. Griffin Analytical technologies, http://www.griffinanalytical.com (accessed Feb. 2008).
111. Microsensor System Inc. http://microsensorsystems.com (accessed, March, 2008).
112. Sanchez, J. M.; Sacks, R. D. *J. Sep. Sci.* **2007**, *30*(7), 1052-1060.
113. Liu, X.; Pawliszyn, J. *Int. J. Environ. Anal. Chem.*, **2005**, *85*(15), 1189-1200.
114. Ji, J.; Deng, C. H.; Shen, W. W.; Zhang, X. M. *Talanta* **2006**, *69*(4), 894-899.
115. Payne P. A. *J. Phys. E. Sci. Instrum.* **1983**, *16*, 947-951.
116. Lieberzeit, P. A.; Dickert, F. L. *Anal. Bioanal Chem.* **2007**, *387*, 237-247.
117. Park, J.; Groves, W. A.; Zellers, E. T. *Anal. Chem.*, **1999**, *71*, 3877-3886.
118. Evan, S. D.; Johnson, S. R.; Cheng, Y. L.; Shen, T. *J. Mater. Chem.* **2000**, *10*(1), 183-188.
119. Zampolli, S.; Elmi, I.; Cardinali, G. C.; Betti, P.; Dalcanale, E. IEEE SENSORS 2006, VOLS 1-3, 1179-1182.
120. Elosua, C.; Matias, I. R.; Bariain, C.; Arregui, F. J. SENSORS **2006**, *6*(11), 1440-1465.
121. Grate, J. W. *Chemical Reviews* **2000**, *100*(7), 2627-2647.
122. Shields, H.C.; Fleischer, D.M.; Weschler, C. J. *Indoor Air-Int. J. Indoor Air Qual. Climate* **1996**, *6*(1), 2-17.
123. Wohltjen, H.; Snow, A. W. *Anal. Chem.* **1998**, *70*(14), 2856-2859.
124. Janata, J. *Proceddings of the IEEE* 2003, *91*(6), 864-869.
125. Severin, E. J.; Lewis, N. S. *Anal. Chem.* **2000**, *72*(9), 2008-2015.
126. Briglin, S. M.; Lewis, N. S. *J. Phys. Chem. B* **2003**, *107*, 11031-11042.
127. Rivera, D. R.; Alam, M. K.; Davis, C. E.; Ho, C. K. *Sens. Actuators, B* **2003**, *92*, 110-120.
128. Cai, Q. Y.; Zellers, E. T. *Anal. Chem.* **2002**, *74*, 3533-3539.
129. Grate, J. W.; Nelson, D. A.: Skaggs, R. *Anal. Chem.* **2003**, *75*, 1868-1879.
130. Rowe, M. P.; Plass, K. E.; Kim, K.; Kurdak, C.; Zellers, E. T.; Matzger, A. J. *Chem. Mater.* **2004**, *16*, 3513–3517.
131. Littlewood, A. B. *Gas Chromatography*, Academic press: New York, 1970.
132. Krasteva, N.; Fogel, Y.; Bauer, R. E.; Mullen, K.; Joseph, Y.; Matsuzawa, N.; Yasuda, A.; Vossmeyer, T. *Adv. Funct. Mater.* **2007**, *17*, 881-888.
133. Steinecker, W. H.; Rowe, M. P.; Zellers, E. T. *Anal Chem.* **2007**, *79*, 4977-4986.
134. Lu. C.J. and Zellers E.T. *Analyst* **2002**, *127*, 1061-1068.
135. Grall, A. J.; Zellers, E. T.; Sacks, R. D. *Environ. Sci. Technol.* **2001**, *35*, 163-169.
136. Veriotti, T.; Sacks, R. D. *Anal. Chem.* **2001**, 73, 813-819.
137. Skoog, D. A.; Holler, F. J.; Nieman, T. A. *Principles of Instrument Analysis*, Harcout Brace College Publication, San Francisco, 1998.

138. Patrash, S.; Zellers, E. T. *Anal. Chem*., **1993**, *65*, 2055-2066.
139. Zellers, E. T.; Batterman, S. A.; Han, M.; Patrash, S. J. *Anal. Chem*., **1995**, *67*, 1092-1106.
140. Zhong, Q.; Steinecker, W. H.; Zellers, E. T. *Rare Metal Materials and Engin.*, **2006**, *35*(suppl. 3), 61-64.

Chapter 2

Improved Portable Gas Chromatograph with Tunable Retention and Sensor-Array Detection for the Determination of Complex VOC Mixtures

Abstract

The laboratory characterization of a novel, second-generation portable gas chromatograph (GC) prototype designed for trace-level determinations of complex mixtures of volatile organic compounds (VOC) is described. The instrument incorporates a small, multi-stage adsorbent preconcentrator/injector (PCI), two series-coupled separation columns with fast, independent temperature-programming capabilities and junction-point pressure/flow control, and a detector consisting of an array of microfabricated chemiresistor sensors coated with thiolate-monolayer-protected gold nanoparticle films. Response patterns from the CR array are used in conjunction with chromatographic retention times to identify eluting mixture components. Scrubbed ambient air is used as the carrier gas. Improvements in design relative to a previously reported first-generation prototype instrument have led to performance enhancements, which are highlighted. A focus is placed on the tradeoffs in sensor array performance associated with thermal and fluidic operating variables. The separation of a preconcentrated mixture of 31 VOCs in < 420 seconds is demonstrated. Projected detection limits are in the ppt range for most compounds, assuming a 1 L sample volume.

2.1 Introduction

Characterizing the spatial and temporal variations in airborne volatile organic compounds (VOC) concentrations can be critical to the assessment of human exposure levels, emission-source locations and intensities, building ventilation effectiveness, and ambient environmental contaminant distributions. Where speciation of VOC mixture components is required, portable gas chromatographic (GC) instruments offer numerous potential advantages.[1]

On-site VOC monitoring with field-portable GCs has been practiced for nearly 30 years[2,3] and numerous manufacturers currently market compact instruments suitable for field deployment..[4-10] Increasingly, conventional approaches to separation and detection have given way to new approaches made possible by advanced technologies. For example, the use of low-thermal-mass column modules with embedded heaters and temperature sensors now permits faster temperature programming of capillary columns at lower power than with conventional ovens.[11,12] An increasing number of commercial GCs are incorporating microfabricated components for injection,[7,8] separation,[13,14] and detection[6,8,10] and several reports on prototype micro-GCs have appeared recently.[15,16]

Published reports on portable GC applications are generally limited to determinations of VOC mixtures of < 20 compounds.[17-20] Although this does not represent any sort of fundamental limit on the complexity of mixtures that can be analyzed, it does provide a benchmark value. Where single-channel detectors are used, speciation relies on retention times, which are subject to shifts in field settings. Continued progress is being made toward smaller and more rugged portable GC detectors based on mass-[9,21,22] and ion-mobility-[23-25] spectrometry, which provide an added dimension to the analysis that reduces reliance on retention time for qualitative information about eluting species. This is an invaluable feature for portable instruments.

The limited sensitivity of most detectors precludes their use for direct monitoring VOCs in many applications of interest (e.g., indoor air quality, breath biomarker analysis, ambient air monitoring), where concentrations in the low parts-per-billion (ppb) range are common.[26-28] The latter problem has led to increasing use of SPME[29] or similar extrinsic preconcentration methods[10] prior to injection. On-board preconcentration is apparently available as a standard component in only one commercial portable GC.[9]

Several years ago, we reported on a first-generation portable GC prototype that incorporated a miniature, multi-stage adsorbent preconcentrator/injector (PCI) with a tandem-column separation module and a detector consisting of an array of polymer coated surface-acoustic-wave (SAW) microsensors.[30] That prototype was capable of quantitatively analyzing 30 VOCs at low- and sub-part-per-billion levels in a period of 10 minutes.[30] The PCI was designed to increase the effective concentrations of trapped vapors spanning a wide range of vapor pressures and to inject samples by thermal desorption directly onto the first column. By carefully determining the minimum quantities of adsorbents required, it was possible to avoid loss of any vapors due to breakthrough of the adsorbent beds, while also avoiding the need for downstream focusing prior to injection into the separation module.[31,32] Two columns in series, each with a different stationary phase, independent at-column temperature programming, and a pressure equalization bypass at their juncture for flow control, imparted the capability for 'tuning' the retention of eluting species thermally and pneumatically. Response patterns derived from the array of SAW sensors, coupled with retention times, facilitated the determination of the identities of eluting species, even where full chromatographic resolution was not achieved. The first-generation instrument was also successfully tested in a chamber study.[33]

Although these previous efforts established an unprecedented capability for trace-level determinations of fairly complex VOC mixtures with a portable GC, and confirmed the value of coupling tunable retention with sensor-array pattern recognition, there were several features of the instrument that limited its use in practical applications. The instrument described here retains the use of scrubbed ambient air as the carrier gas, and the same multi-stage PCI and dual-column separation modules. An alternative sensor technology is employed, however, comprising an array of chemiresistors (CR) coated with thiolate-monolayer-protected gold nanoparticles (MPNs) as interface layers, which provides higher sensitivity.[15,28,34] Other enhancements in design include a thermoelectrically (TE) cooled sensor array, split-flow injection, an on-board calibration-vapor generator, instrument control via a LabVIEW program run from a laptop computer, and a wireless link for operating the instrument remotely. In a recent preliminary study, this second-generation instrument was used to determine two environmental tobacco

smoke (ETS) markers at sub-ppb concentrations in the presence of >30 common indoor-air co-contaminants.[28]

This chapter provides a complete characterization of the second-generation instrument. An emphasis is placed on the influence of changes in flow rate and temperature on sensor-array performance and on overall system performance. Integration of the unique components and functions of this prototype to effect multi-vapor determinations by use of retention times and sensor-array pattern recognition is illustrated.

2.2 Prototype Description and Experimental Methods

2.2.1 Instrument Features and Operating Modes

Figure 2-1 presents photographs of the interior and exterior of the instrument and diagrams of the analytical train in two of its four operating modes. It operates on AC power and has two on-board AC/DC converters (12-V and 6-V) for driving all components. The sequencing of all functions is controlled by a laptop computer running routines written in LabVIEW 7.1 (National Instruments, Austin, TX). Air flow is provided by one of two small diaphragm pumps (UN86KTDC, KNF Neuberger Inc., Trenton, NJ) and is directed by four low-dead-volume solenoid-actuated diaphragm valves (NResearch Inc., West Caldwell, NJ). All exposed valve surfaces are Teflon-coated. Five miniature axial fans were added to dissipate heat generated within the instrument during normal operation.

The instrument proceeds through a sequence of up to four user-programmable operating modes. In Sampling Mode (Figure 2-1a), air is drawn by the on-board sampling pump through an externally mounted polymer-membrane particulate filter and then through the PCI at an adjustable flow rate of up to 0.16 L/min. Vapors are captured on the three PCI adsorbents contained in an insulated, thin-walled Inconel 600® tube (1.35 mm i.d., 5-cm long) (Accu-tube Corp., Englewood, CO). For the tests performed in this study, the PCI tube was packed, in order, with 8 mg of 40/60-mesh Carbopack B, 2.5 mg of 40/60-mesh Carbopack X, and 1.8 mg of 45/60-mesh Carboxen 1000 (separated by glass woo1), which have specific surface areas of 100, 250, and 1200 m^2/g, respectively (Supelco, Bellefonte, PA).[32] Thus, incoming vapors pass through the lowest surface area

adsorbent first and the least volatile vapors are trapped on this adsorbent, with progressively more volatile vapors trapped by the progressively higher surface area adsorbent materials downstream. The adsorbent masses used here were determined on the basis of a previous breakthrough study and have sufficient capacity for 1-L sample containing over 40 compounds, each at 100 ppb.[32]

An on-board calibration-vapor generator was installed as a quality control measure to assist in diagnosing uncompensated changes in ambient temperature or pressure, drift in flow rates or temperatures, leaks, and malfunctions in system components. The generator consists of a small vial packed with glass wool that is connected at one end to the inlet flow path through a 2-way solenoid valve (Figure 2-1a) and at the other end to the exhaust port of a dedicated mini-diaphragm pump. A small volume of liquid calibrant (user selectable) is injected onto the glass wool and the vial is sealed to produce a saturated atmosphere. Brief actuation of the valve and pump dispense~~s~~ a small amount of the headspace vapor into the inlet flow stream for capture by the downstream PCI.

After sampling a pre-set air volume, the sampling pump is turned off and isolated from the system by an upstream valve. An optional dry-air purge (Purge Mode) can then be performed in which the analysis pump draws ambient air in through a second inlet port and passes it through a scrubber cartridge located inside the instrument. The scrubber is packed with charcoal and 4A molecular sieves to remove VOCs and water vapor, respectively. The purified air is directed through the PCI and out through the sample inlet port, and serves to remove a portion of the water from the PCI adsorbents and to backflush residual VOCs from the fore line. In a typical sequence, the Purge Mode duration is about 60 sec, resulting in 0.16 L being passed through the PCI, which has been shown in previous work to remove the majority of adsorbed water while not removing significant quantities of adsorbed VOCs.[30,32]

In Analysis Mode (Figure 2-1b), the inlet valve is closed and ambient air is drawn into the system by the analysis pump is scrubbed and then directed through the PCI, the separation columns, and the detector cell prior to being exhausted from the instrument. After a 40-sec pressure stabilization period, the PCI is heated with an insulated Cu-wire coil to 300 °C in < 2 sec and maintained at this temperature for up to 90 sec. A fine-wire

type-K thermocouple, insulated from the metal wall of the PCI by a thin sheath of polyimide tape and held against the PCI wall by the Cu wire, was used for temperature feedback. The captured vapors are thereby thermally desorbed and injected into the first of the two separation columns. A split injection capability was incorporated to reduce injection band broadening by venting a portion of the desorbed flow stream.[15,35] The split ratio is determined by the relative resistances of the analytical and vent flow paths.

The first separation column (4.5-m long, 0.25-mm i.d.) contains a wall-bonded polydimethylsiloxane stationary phase (DB-1, 0.5-μm thickness, Agilent, Wilmington, DE) and the second column, which has the same dimensions as the first, contains a wall-bonded polytrifluoropropylmethylsiloxane phase (RTX-200, 0.25-μm thickness, Restek, Bellefonte, PA). The moderately polar nature of the RTX-200 provides retention properties that complement those of the non-polar DB-1 phase.[36] It has been reported to be stable in air at a column temperature of 200°C.[37] The columns are heated independently at rates of up to 1000 °C /min using coiled 'at-column' heaters,[11,30] (note: the dual-column assembly was provided for this project by RVM Scientific Inc., Santa Barbara, CA). A bypass line shunts flow around the first column when the junction-point tuning valve is open, which stops the flow in the first column while accelerating the flow through the second column. This valve can be opened for short periods of time during an analysis to separate compounds that are resolved on the first column but would otherwise converge and co-elute from the second column.[30]

Eluting vapors are recognized and quantified by the CR array, which consists of four sets of interdigital Au/Cr electrodes patterned on a single oxide-coated Si substrate. Each CR device contains 20 pairs of electrodes 0.40-μm thick, and 15 μm wide with a 15 μm spacing and a 1.4 mm overlap. Header pins bent at a 90º angle were soldered to the gold bonding pads and inserted into header sockets on a custom printed-circuit board (PCB) with multiple analog circuit trains for measuring resistance. A TE cooler and RTD temperature sensor were fixed to the lid of the detector cell with thermally conductive epoxy for control of the array temperature via a simple, manually set, feedback controller (MPT-5000, Wavelength Electronics, Inc, Bozeman, MT).

Each CR sensor is coated with a different solvent-cast film of a gold-thiolate monolayer protected nanoparticle (MPN).[15,34,38] Film thicknesses were estimated to be

~200 nm, assuming 3 g/mL density.[38] The coated array is capped with a Macor® lid (cell volume ~ 3 μL) and fitted with inlet and outlet capillaries for fluidic interconnections. The cap is held in place with a patterned rectangular gasket of double-sided tape that is 120-microns thick (UHB tape, 0.005 inch thickness, 3M, St. Paul, MN). MPNs derived from the following thiols were used in this study: n-octanethiol (C8), 1-mercapto-6-phenoxyhexane (OPH), 7-mercaptoheptanitrile (CCN), methyl 6-mercaptohexanoate (HME), and 4-mercaptodiphenylacetylene (DPA).[28,39]

A constant dc bias is applied to each sensor and the current is converted to a voltage, baseline corrected, amplified, and transmitted to a D/A card on a laptop computer. Baseline drift compensation is achieved by dividing the sensor output signal and passing one branch of the circuit through an RC filter with a long time constant (low-pass filter) that essentially removes the response. The two branches are then passed through a differential operational amplifier to obtain the difference signal. A two-stage amplification circuit was used, which converts the normalized resistance change due to vapor sorption, $\Delta R/R$, into a voltage, V_{out}, according to the following relationship: $V_{out} = 50(V_i)\Delta R/R$, where V_i is the absolute value of the voltage after the first stage of amplification.

In the CR array, vapors reversibly partition into each MPN film and cause it to swell, which changes the electron tunneling barrier and thereby the film resistance.[38,40] Since the structures of the MPN ligands differ on each sensor, the affinities for a given vapor differ as well, and the array of CRs produces a different set of responses for each vapor. The pattern of responses can then be combined with the retention time to identify each vapor, and the magnitudes of the responses from the sensors can be used collectively to quantify the vapor concentrations.[15,28,33] Over the course of this study, several different arrays were installed in the instrument, depending on the particular issue being examined and due to some electronic and fluidic mishaps. Baseline noise levels varied with the MPN film and were generally lowest for CRs coated with C8 MPN and highest for CCN MPN films. Some typical RMS noise levels are as follows: 10 mV, 13 mV, 18 mV, 20 mV, and 47 mV for C8, OPH, HME, DPA, and CCN, respectively. Only ~1 mV could be ascribed to the supporting electronic hardware.

Following detection, the PCI is re-conditioned by sequentially heating and purging with scrubbed air and then cooling actively with on-board fans prior to collecting the next sample. During re-conditioning the analysis pump remains on, the PCI heater is actuated to 300ºC, the inlet valve is open, and scrubbed air is swept through the heated PCI. The PCI is normally heated for 60 sec and then cooled. Assuming a 1-L sample volume and a 5-min separation, an entire analytical cycle (including post-sample PCI purge and cooling) can be completed in 16 min.

Software written in house is run from a laptop computer and used to control the instrument and process the sensor output signals through separate 12 bit and 16 bit D/A data acquisition cards (Measurement Computing Corp., Middleboro, MA) at a rate of ≥ 50 Hz. There are four main panels on the laptop screen. Panel 1 is for inputting operating parameters, Panels 2 and 3 display real-time traces of sensor responses and the FID (for calibration only), respectively, and Panel 4 is for setting the sampling rate and for file manipulations. There are eight temperature-programming intervals possible for each column, and all other actuated components can be scheduled at 0.1 second intervals. A wireless network card in the laptop computer permits remote access and control of the instrument.

The output voltage from this circuitry is recorded by the LabVIEW program in a two-column (time and voltage) text file. The text files are converted to chromatogram format with Grams 32 software (Thermogalactics, Inc., Salem, NH). Peaks were integrated with Grams following smoothing using 40-point running average.

2.2.2 Materials and Test Atmosphere Generation

All test compounds were obtained from Aldrich (Milwaulkee, WI) Acros/Fisher (Pittsburgh, PA), or Lancaster (Windham, NH) at ≥ 98% purity and used as received. Test atmospheres of the vapors were generated by injecting small volumes of the liquids into 12-L Tedlar® bags (SKC, Eighty-Four, PA) prefilled with a known volume of clean, dry air from a compressed-air cylinder. Concentrations were confirmed via GC-FID by comparison with injected masses of CS_2 solutions of the same compounds. For compounds with very low vapor pressures, a saturated test atmosphere was created in a 1-L Tedlar bag and aliquots were transferred by gas-tight syringe to a series of other bags

or injected directly into the inlet of the instrument. Methane from the house supply was used for testing hold-up times in the separation module.

2.2.3 Instrument Calibration and Chemometrics

Conditions required to separate a 31-component mixture in a minimum amount of time were established using external sample loops with volumes ranging from 0.01-1 mL to cover the desired range of injected masses. Effective (mass-equivalent) vapor concentrations were calculated according to the ratio of injection and sample volumes. For example, an aliquot of 1 mL from a sample loop containing 10 ppm of vapor is equivalent to 10 ppb in a 1-L sample volume. Mass-equivalent calibration concentrations ranged from 0.15 - 150 ppb-L. Four replicates were performed for each of seven challenge concentrations within this range for each of the 31 compounds.

Chemometric analyses of sensor array response patterns were performed using Monte Carlo simulations in conjunction with extended disjoint principal components regression (EDPCR) to estimate expected recognition rates for the components of co-eluting mixtures.[41,42] Monte Carlo simulations superimpose random error on calibrated sensor-array response patterns, which are then classified by EDPCR to determine if the co-eluting components giving rise to the composite response pattern can be recognized and discriminated with low error.[42] Noise levels of 0.0017, 0.0024, 0.015, 0.0082 V, and sensitivity errors of 1%, 2%, 8%, 8% for C8, OPH, HME, and CCN, respectively, were used in the model. Iterative analysis (n=500) over a predefined range of concentrations yields statistical estimates of discrimination.

2.3 Results and Discussion

2.3.1 Basic Operation

In the previous prototype, event sequencing and set points were controlled by an embedded microcontroller. As the chassis temperature increased, the reference voltages for the column temperatures and carrier gas inlet pressure drifted from their initial settings. As a result, retention times would increase over time from cycle to cycle. This problem was solved in the current prototype by shifting control to the laptop computer. Highly stable flow rates, column temperatures, and retention times were achieved. For

example, in one test of 36 consecutive analytical cycles (6-hr) the average outlet flow rate (1.59 mL/min), measured at eight randomly selected times, varied by < 0.030 mL/min. The temperatures of both columns were consistently within 0.5 ºC of set-point values (generally biased low) and varied by < 0.6 C during a given analytical cycle. For temperature-programmed operation actual temperatures were virtually superimposable on set-point values.

To test the sampling and desorption functions, the sensor array was replaced with an FID and replicate samples of n-octane at 32 ppb-L were analyzed at a column temperature of 90 ºC (isothermal). Peak areas were reproducible to within +/- 4% (RSD) with splitless injection and to within 6% (RSD) with a 6:1 split injection (n=6). Similar testing of the vapor generator, using n-decane as the calibrant (no test vapor), yielded peak area variations of 10% (RSD, n=10) indicating some variability in the quantity of vapor injected from the generator assembly. In all cases, retention times were reproducible to ± 1 sec even after 40 continuous analytical cycles.

The TE cooler used in the 2nd-generation instrument maintained the array temperature to within ±1 °C of set-point temperatures (typically 20-26 °C) for at least six hours of continuous operation. Accordingly, vapor sensitivities were quite stable as well. For example, over 20 continuous analytical cycles, the integrated peak areas from preconcentrated samples of toluene vapor (34.5 ppb-L) varied by only 4-7% (RSD) around their average values for an array coated with C8, OPH, DPA, and HME MPNs.

Over a period of two months, periodic calibrations revealed that sensitivity values would drift by as much as 60%, and one sensor (HME) showed a consistent gradual decline in sensitivity. With the exception of the HME-coated sensor the drift in sensitivities was cyclic and similar for all sensors. There was enough of a difference, however, to cause significant changes in relative response patterns. Such variations in MPN-coated CR sensors have been noted in the literature,[38] and appear to be related to changes in the interparticle distances within the thin films. The practical implication of this phenomenon is that re-calibration of the instrument and re-establishment of the response pattern library would be needed roughly every two weeks.

2.3.2 Column Efficiencies

The chromatographic efficiency of each column was determined independently using n-octane as the test compound and house methane to determine hold-up times. Samples were loaded onto the PCI and injected with a split ratio of 4.4:1. Isothermal column temperatures of 40 and 30 °C were used for the first and second column, respectively, with an FID detector. The k values of octane are 4.2 and 1.3 for the first and second column, respectively, and the corresponding H_{min} values are 0.027 and 0.051cm (Figure 2-2a), which were found at optimal average linear velocities of 8.6 and 9.1 cm/s, respectively. Thus, each column could produce a maximum N of 3700 and 2000 plates per meter, respectively.

Plotting the rate of plate production as a function of average velocity (Figure 2-2b) indicates that the optimum practical gas velocity (OPGV) is ~25 cm/s, which corresponds to a volumetric flow rate at the dual-column outlet of 0.8 mL/min at 30 °C. This is 2.8 times the optimal velocity and results in a ~2-fold increase in H (Figure 2-2a).

2.3.3 Extracolumn Band Broadening

Band broadening from the PCI and sensor array are potentially important factors affecting separation efficiency. Contributions to band broadening from adsorbent preconcentrators similar to that used here have been studied previously,[15,30,35] and therefore were not explored in detail here. Although rapid heating rates and high flow rates through a PCI serve to minimize broadening, analyte volatility is also an important co-factor. Contributions to band broadening from the sensor array could arise from the finite volume of the detector cell as well as the rates of sorption and desorption of eluting vapors in and out of the interface layers on the sensors. Contributions from fluidic interconnections and electronic time constants are typically small relative to these two factors, however, evidence suggests that in this prototype adsorption on unheated interconnection surfaces may be significant for less volatile analytes (*vida infra*).

Golay plots were constructed for n-nonane using data generated with the PCI (splitless) and then with a heated 0.1-mL sampling loop injector connected via a heated 6-port valve to the inlet of the first column (column = 50°C; k = 4.9; FID; valve and sample loop = 180 ºC). Values of H_{min} were 0.068 and 0.10 cm for the loop and PCI,

respectively. Accordingly, using the method described by Bemgard et al.[43] to fit the data to the Golay-Gouichon equation yielded an instrument dead time value ~40% higher when using the PCI in splitless mode.

Golay plots were also constructed for n-nonane using data generated with the sensor array installed (22.5 °C) and then with an FID in place of the array. The loop injector was used in both series of tests. Using the sensor coated with the OPH MPN, the Golay plots were nearly superimposable, yielding a value of H_{min} of 0.071 cm with the sensor compared to 0.068 cm with the FID. Consistent with this, the average ratio of $W_{1/2}$ values (i.e., OPH:FID) was 1.1.

Subsequent tests with C_{10}-C_{12} n-alkanes gave OPH:FID $W_{1/2}$ ratios of 1.1 1.4, and 2.4, respectively (splitless PCI injection; temperature programmed separations). Thus, the peaks widths for compounds less volatile than n-decane become significantly broader with the sensor(s). Among the different sensors in the array, $W_{1/2}$ values for these n-alkanes were generally in a ratio of 1:1:1.1:1.2 for sensors coated with C8, OPH, HME, and CCN MPNs, respectively. The DPA-coated sensor, in separate tests, gave peaks widths about 1.2 times those coated with OPH and C8. The slight increase in peak width observed for the MPNs with polar tail groups may be due to longer diffusion times or possibly to longer film relaxation times arising from the stronger inter-ligand interactions extant in films of these MPNs.

2.3.4 Flow Rate Effect on Sensor Response

Among the distinguishing features of the MPN-coated CR array as a GC detector is that the sensor responses depend on the vapor concentration and not on the vapor mass. This allows for miniaturization without loss of sensitivity because the response depends on partitioning of vapors into the interface layer.[38] However, since peaks emanating from the column have a finite residence time in the detector cell, kinetic factors must be considered. Figure 2-3 shows the effect of flow rate on the peak width, height, and area for n-octane and n-nonane from the OPH-coated sensor and from an FID placed immediately downstream from the CR array. The 0.1-mL heated sample loop was used and the amount injected was 156 ng (i.e., 50 and 70 ppb-L for n-octane and n-nonane, respectively).

Values of $W_{1/2}$ decrease non-linearly with increasing flow rate and to a similar extent for both vapors with both detectors. The retention time, t_R, decreases similarly and, in fact, $W_{1/2}$ is directly proportional to t_R (Figure 2-3a). The peak height passes through a maximum for both vapors with the sensor but steadily increases for both vapors with the FID. The peak area decreases in a manner similar to that of $W_{1/2}$ but less sharply at the lower flow rates for both vapors with the sensor and is nearly invariant for both vapors with the FID. All sensors behaved similarly.

To interpret these results it is important to recognize that the responses of the sensors and the FID are also affected by the changes in the injection bandwidth and time on the column accompanying changes in flow rate through the system, and that some of the observed behavior can be ascribed to these factors. For example, over the range of flow rates examined the retention time of n-octane and n-nonane decreased by about 19-fold. In general, the less time a compound spends on the column the less band dispersion that occurs and the narrower its peak. Another factor is the dilution of the vapor concentration accompanying the higher flow rate during desorption. These two factors affect the peak parameters simultaneously but to different extents over the range of flow rates considered. The peak width is expected to decrease due to both of these factors. The shapes of the $W_{1/2}$ curves suggest the superposition of two factors. In fact, it appears that the decrease in $W_{1/2}$ can be attributed almost entirely to these factors, since similar behavior is seen for both types of detectors and both vapors.

The flow rate dependence of the peak height for the sensors is consistent with this interpretation (Figure 2-3b). At low flow rates there is a roughly linear increase in peak height, consistent with peak sharpening as the retention time decreases. At about 0.35 mL/min for both vapors, however, a plateau is reached and at higher flow rates (> 0.9 mL/min for n-octane and >0.5 mL/min for n-nonane) the trend reverses and the peak heights gradually decline due to the dilution effect becoming dominant. Note that the overall change in peak height is not very large: the ratio of maximum-to-minimum peak height is only ~2 and the RSD around the average peak height is only 17% and 24% for n-octane and n-nonane, respectively.

For the FID, the peak height also increases linearly up to about 0.6 mL/min for both vapors and then continues to increase but at a steadily declining rate for both vapors.

That is, the peaks continue to become sharper over the entire flow rate range as reflected by the increase in mass/time measured by the FID, but at a decreasing rate over the range in which the sensor(s) exhibit a decreasing height due to a decrease in mass/volume. This indicates that the peaks get sharper at a rate exceeding that at which they are being diluted, such that the mass/time continues to increase despite the mass/volume decreasing. The relative magnitude of the effect on the FID peak height is similar for both vapors. The difference in behavior between the concentration-dependent sensor and the mass-sensitive FID is quite dramatic.

The changes in peak area are, of course, a function of the combined changes in peak width and peak height. For the sensor, the peak area decreases at a high rate at first and then more gradually at the higher flow rates (Figure 2-3c). This behavior tracks that of the peak width, consistent with the relatively small change observed in peak height for the sensors. However, dilution must be occurring over the entire range of flow rates or else the peak area would show some sort of discontinuity at ~0.6 mL/min. The roughly constant peak area from the FID reflects the countervailing influences of the (decrease in) $W_{1/2}$ and (increase in) peak height.

Figure 2-3d shows the relative response pattern for n-octane at three flow rates: the lowest, highest, and mid-range values. Some variations are observed, but they are not significant and can be attributed to normal variations in sensor responses. The responses for the polar CCN-coated sensor to this alkane vapor were quite low and quite variable due to the effects of baseline noise, so they were omitted from the patterns in Figure 2-3d. These results confirm that the flow rate effects are similar for all of the sensors.

A possible alternative explanation for these trends in peak width and peak height is that the sorption/desorption kinetics of the vapors in the MPN films become slow relative to the residence time of the vapor in the detector cell as the flow rate increases, or that film relaxation following exposure is slow. If this were the case, one might see a decrease in peak width and peak height, and therefore in peak area, because the vapor would pass through the detector cell before sorption equilibrium could be achieved. If the residence time of the vapor in the detector cell is large relative to the time it takes the vapors to reach the sensor surface and diffuse into and out of the film, then such effects should not be important.

The vapor residence times within the 3 µL detector cell range from 1.1 sec to 0.055 sec for flow rates of 0.16 to 3.3 mL/min, respectively. The diffusion coefficients of n-octane and n-nonane in air at 26 ºC are both ~0.06 cm^2 s^{-1}.[44] Assuming diffusive transport, it would require only 1.4 ms for the vapors to traverse the height of detector cell (125 µm). The diffusion coefficients of vapors in the MPN films are not know but are likely to be similarly to, perhaps a bit larger than, those of vapors in rubbery amorphous polymers. Using a value of $D_{film} = 10^{-8}$ cm^2 s^{-1} from literature reports on the diffusion coefficient determined for toluene in different polymer and carbon-loaded polymer films[45-47] and assuming one dimensional diffusion, it would require 18 ms to traverse a 200 nm film. Thus about 20 ms is required for vapor diffusion, which is much smaller than the residence time even at the highest flow rate tested. Thus, it is not likely that these kinetic factors are influencing the peak parameters and behaviors depicted in Figure 2-3.

The practical implications of the results are significant. At low flow rates the peak area is extremely sensitive to flow rate, such that a change of 0.1 mL/min can lead to a change in peak area of 20% for the example shown in Figure 2-3 at flow rates in the range of 0.1-0.3 mL/min. This demands tight control on flow rate in this regime. At higher flow rates the dependence is greatly reduced, but so is the sensor response (i.e., sensitivity). Most subsequent experiments in this study were performed at a flow rate of 0.8-1.0 mL/min, which represents a compromise between these two factors. The relatively weak dependence of peak height on flow rate is useful in establishing LODs, since LODs are determined by peak-height sensitivities.

2.3.5 Split-Flow Injection

As discussed above, injection bands generated by the PCI are larger than those from heated-loop injector. Although less-volatile compounds can be focused at the head of the separation column if it is initially at low temperature, such focusing is not possible with compounds having vapor pressures above a few torr without actively cooling the column.[32] Therefore, reducing desorption/injection bandwidths is generally desirable because it enhances chromatographic efficiency and resolution. At 150 °C/s, the heating rate of the PCI is quite high and could not be increased further, leaving only the carrier gas flow rate through the PCI as a variable to explore. Split-flow injection has been

shown to improve resolution in portable and micro-scale GCs,[15,35] but at the expense of sensitivity. In fact, the loss of sensitivity is generally larger than the gain in peak resolution. However, the latter is often the more important factor in complex mixture analysis.

Mixtures of C_7-C_{12} n-alkanes (22 to 37 ppb-L; 150-160 ng injected) were tested at five discrete column outlet flow rates from 0.42 to 2.1 mL/min under split and splitless operation (column temp. = 90°C; FID). The pressure restriction of the split-control valve allowed a maximum split ratio of only 7.3:1, which decreased over the range of column flow rates examined. For brevity, only those results obtained at a column outlet flow rate of 0.7 mL/min, which is close to the OPGV, and at a split ratio of 6.6:1 are discussed in detail.

Results are summarized in Table 2-1 and Figure 2-4. As expected, split-flow injection leads to reductions in $W_{1/2}$ and, consequently, to increases in column efficiency, N, and peak resolution, R. Under the conditions of analysis (column = 90°C, isothermal), little or no on-column focusing is expected, so the changes in $W_{1/2}$ can be attributed to the higher flow rate through the PCI alone. Reductions in $W_{1/2}$ increase from 1.8-fold for n-heptane to 3.1-fold for n-dodecane, reflecting the greater influence of the desorption flow rate on less-volatile vapors. Although the resolution generally increases down the homologous series from C_7 to C_{12} (Table 2-1), as shown in Figure 2-4 the retention time decreases significantly for C_{11} and C_{12}, and since R is proportional to $t_R/W_{1/2}$ the improvement in resolution for these compounds is less than what would be expected on the basis of $W_{1/2}$ alone. Accordingly, the value of N calculated on the basis of C_{12} is also lower than expected on the basis of $W_{1/2}$ alone, because N is proportional to $(t_R/W_{1/2})^2$. For the lower alkanes in the series there is no change in t_R and the reductions in $W_{1/2}$ afforded by the split injection lead to commensurate increases in R and N.

Of course, a portion of the improvement in R is due merely to the reduced injection mass, which is nominally 13% of the splitless injection mass. By approximating the peaks as triangles and comparing calculated $W_{1/2}$ values to those observed experimentally, it appears that for C_7-C_{10} the decrease of $W_{1/2}$ is due almost entirely to the decrease in injection mass, while for C_{11} and C_{12} the decrease of $W_{1/2}$

exceeds that attributable to the decrease in injection mass alone by 12% and 22%, respectively.

Peak areas for the C_7-C_{10} alkanes with split-flow injection are only 12% of those under splitless conditions, consistent with the split ratio. For C_{11} and C_{12}, the peak area ratios are 0.14 and 0.17, respectively. Although these higher values might be due to integration errors associated with the broadness of the peaks, the desorption efficiency (recovery) of these relatively low-volatility vapors is higher with split-flow injection (higher total flow rate through PCI) than with splitless injection. Assuming 100% desorption efficiency with the split injection, the corresponding desorption efficiencies for splitless injection of C_{11} and C_{12} are approximately 85% and 72%, respectively [note: desorption efficiency = peak area ratio/(1+ split ratio)]. Experimental tests confirm that residual quantities of these compounds consistent with (somewhat lower, in general) these estimates of desorption efficiency are detected if the PCI is actuated a second time without any additional sampling.

These results confirm earlier reports showing that the gain in resolution is less than the loss in sensitivity when using split-flow injection.[15] In this study, 2-3-fold increases in resolution are accompanied by 6-8-fold reductions in sensitivity. Furthermore, for the lower alkanes, the increase in resolution can be ascribed almost completely to the reduced mass of the split injection. In addition, these results show that for compounds more volatile than n-undecane the injection bandwidth from a PCI is limited by the heating rate of the PCI, whereas for less volatile vapors the bandwidth is also affected by the flow rate through the PCI.

2.3.6 Temperature Effect on Sensor Array Response

As shown above, although $W_{1/2}$ values from the FID and the CR sensors in the array are comparable for the more volatile compounds, those from the sensors are much broader for the less volatile vapors than those from the FID under the same separation conditions. Factors that would contribute to peak broadening in the sensor array for these vapors include smaller diffusion coefficients, lower evaporation rates, and adsorption on surfaces in the flow path. Since diffusion coefficients do not differ greatly across this range of compounds (at 22.8 ºC, D of n-alkane C_9, C_{10}, C_{11}, and C_{12} is 0.055, 0.052, 0.050, 0.048 $cm^2\ s^{-1}$, respectively),[44] diffusion rates alone cannot account for the degree

of peak broadening observed for the less volatile compounds in this series, and it is likely that other factors are affecting the mass transport process. Regardless, by increasing the temperature of the sensor array, the rates of all relevant processes should increase which, in turn, should decrease $W_{1/2}$. However, since the vapor-film partition coefficient, K, will also decrease, there will be a tradeoff between resolution and sensitivity.

The temperature dependence of K for low vapor concentrations over a finite temperature range can be described by the Arrhenius-type relationship:[48]

$$K = K_0 e^{-\Delta H_s / RT} = K_0 e^{(\Delta H_v - \Delta H_m)/RT} \qquad (1)$$

where K_0 is the pre-exponential term, R is the gas constant, ΔH_s is the molar heat of sorption, ΔH_v is the molar heat of vaporization, and ΔH_m is the partial molar heat of mixing, which is zero in the ideal case. Assuming sorption approaches steady-state, the sensor response (peak area) is proportional to K,[38] and the relationship between the peak area and temperature can be expressed as follows:

$$ln \frac{A_{T_1}}{A_{T_2}} = \frac{\Delta H_v}{R}\left(\frac{1}{T_1} - \frac{1}{T_2}\right) \qquad (2)$$

where A_T is the peak area at a given temperature and T_2 for this study is 296 K (i.e., 22.8 ºC). A plot of $\ln(A_{T1}/A_{T2})$ versus $1/T_1$-$1/T_2$ should yield a line with a slope equal to $\Delta H_v/R$.

To examine the effect of the sensor temperature on resolution and sensitivity, a mixture of C_9-C_{12} n-alkanes was analyzed at each of five sensor temperatures from 23-43 ºC. Due to the fact that the other three sensors were too noisy when this experiment was performed, only results from the OPH-coated sensor are reported. Injections (62-144 ng; 17-28 ppb-L; splitless) were made with the PCI and the columns were temperature programmed to accelerate the separations.

Results are summarized in Table 2-2 and reveal the expected trends. Values of $W_{1/2}$ decrease by 1.1-2.4 fold over the temperature range, with the effect be larger for the less volatile compounds, and the peak areas decrease by 2.3-5 fold, again with the effect

being more prominent for the less volatile compounds. Since N varies with the inverse square of $W_{1/2}$, increases in N range from 1.2 to 4.8-fold. Peak height and peak area track each other quite closely. The resolution of neighboring peaks increases by 1.1-1.6 fold. Overall, as with the split flow experiments, the gain in resolution is about half the loss in sensitivity.

Plots of $\ln(A_{T1}/A_{T2})$ versus the difference in inverse temperature were approximately linear for all vapors ($r^2 > 0.98$) permitting estimates of ΔH_v for each compound. Results, shown in Table 2-3 indicate that while the estimates are close enough to literature values to conclude that sorption thermodynamics govern sensor responses, the amount of error in several of the estimates suggests that there are other factors contributing to the apparent ΔH_v values. The large negative error (-23%) for nonane is hard to explain. For decane, the error is very small, -4%, which is negligible. For low-volatile undecane and dodecane, the 26% and 28% errors was possibly due to the wall-adsorption (cold spot effect of the array). At low temperature (22.8 ºC) the peak areas were smaller than they should be, so the relative ($A_T/A_{22.8ºC}$) was higher, resulted in positive errors.

As with the split-flow experiments the decreases in $W_{1/2}$ can be attributed the decreased mass uptake by the MPN films at higher temperatures, or due to both of the decreased mass uptake at higher temperature and temperature effect. Assuming a peak is a triangle, if the peak area and height are known, theoretical $W_{1/2}$ can be calculated from peak area and height. For all the vapor-temperature combination, measured values are all > the calculated values. For C_9, the measured $W_{1/2}$ to calculated $W_{1/2}$ ratio is 1.7 to 1.6 with the temperature being increased from 22.8 to 42.7 ºC, indicating that an extra 5% ((5% = (1.7-1.6)/1.7)) reduction in $W_{1/2}$ is due to the ~2-fold increase in sensor temperature alone (beside the $W_{1/2}$ reduction due to the reduced mass uptake). Similarly, an extra 15%, 39%, and 37% reduction in $W_{1/2}$ is due to increase temperature effect alone for n-alkane C_{10} to C_{12}, respectively.

2.3.7 Analysis of Complex Mixture with Tunable Separation and Pattern Recognition

One of the primary advantages of sensor array detection is the use of response patterns to identify, or recognize, compounds eluting from the separation module. In many cases it is possible to use this capability identify the components of partially resolved or unresolved (i.e., co-eluting) mixtures from their composite response pattern.[30,41,42] This feature eases the burden on the separation module, since baseline resolution of all components in a mixture is not always necessary, and by the same token can permit acceleration of the analysis. However, in cases where the number of co-eluting compounds exceeds three or where the co-eluting compounds have similar response patterns, errors in recognition can occur. By use of the pressure tuning and temperature programming features of the separation module, best advantage can be taken of the capabilities of the array detector. This 'functional integration' of the separation and detection components of this system is an essential feature of the instrument.

To illustrate this functional integration, a mixture of 31 VOCs and SVOCs, comprising common indoor and outdoor contaminants from several functional-group classes,[51] which span a 1700-fold range of vapor pressure, was analyzed. The compounds have been assigned numbers and are listed in Table 2-4. A CR array freshly coated with the following MPN films was installed: C8, OPH, HME, and CCN. Using splitless PCI injection and an outlet flow rate of 0.9 mL/min, an initial separation was attempted using the same temperature program for both columns. The representative chromatogram from the C8 sensor presented in Figure 2-5a shows that there are five binary co-elutions (i.e., compounds 5/6, 14/15, 24/25, 27/28, and 29/30) and one ternary co-elution (i.e., compounds 20/21/22). By maintaining the same temperature program for the first column, but changing that for the second column the resolution improves such that there are only three binary co-elutions and one ternary co-elution (i.e., 13/14, 21/22, 27/28, 23/24/25, respectively, Figure 2-5b). This illustrates the value of independent temperature programming of the columns.

The relative response patterns for the nine compounds that co-elute with at least one other compound are presented in Figure 2-6. Visual inspection shows that while the patterns of the first six compounds are quite similar, there are subtle differences that

might permit their discrimination. The differences in the patterns for the compounds involved in the ternary co-elution are more apparent. Analysis by Monte Carlo simulation coupled with EDPCR classification models constructed for the nine individual compounds and their binary and ternary mixtures was performed over a concentration range of 1-5xLOD for each compound. The resulting estimates of the recognition rates were 96, 96, and 97% for the binary mixtures of 13/14, 21/22, and 27/28, respectively. That is, the statistical estimate of the ability to differentiate the mixture from its two components ranges from 96-97% for these mixtures. Using 95% recognition as a minimum threshold rate for satisfactory performance, these results indicate it would not be necessary to separate the binary mixtures because they could be resolved by use of pattern recognition. For the ternary mixture, on the other hand, the estimated recognition rate is only 87%, despite the apparent differences in patterns among the components. Therefore, the ternary mixture would require further separation to avoid confusing the mixture for one of the three possible binary component mixtures or one of the individual components.

As it turns out, compound 23 could be separated from compounds 24 and 25 by junction-point pressure modulation because these compounds are resolved on the first column. By opening the pressure-tuning valve for 3 s just after compound 23 has passed the column junction point (i.e., at t = 242 sec), sufficient distance is created to achieve complete resolution of compound 23 from the binary mixture of 24/25 at the outlet of the second column. EDPCR-Monte Carlo analysis yielded a recognition rate of 98% for the binary mixture of 24/25, so the problem was solved. An additional pressure modulation (for 3 sec at t = 252 sec) was required, however, to avoid the co-elution of compound 23 with the compounds 21/22. As shown in the final trace of Figure 2-5c, in a net separation time of seven minutes, 23 of the compounds are completely resolved and the remaining binary co-elutions can by differentiated/identified by use of pattern recognition. The traces from all four CR sensors under these conditions are presented in Figure 2-7, and the response patterns for all 31 compounds are provided Appendix 4 accompanying the dissertation.

The chromatograms from the CR array sensors shown in Figure 2-7 represent the best separation achievable in the minimum amount of time. For compounds 1-20, most

values of $W_{1/2}$ are < 3.0 sec for the C8 and OPH sensors, and fractionally broader for the HME and CCN sensors. For the later-eluting compounds, peak widths become significantly larger. Similar trends have been observed in our previous study of MPN-coated CR arrays as GC detectors and for polymer-coated SAW sensors arrays used as GC detectors in the first-generation instrument. As in those previous studies, the $W_{1/2}$ values observed with the sensor and an FID are similar for early eluting compounds (data not shown), but are much broader from the sensors for the later-eluting compounds. Furthermore, if the FID is used downstream from the sensor array significantly broader peaks are observed than with the FID installed in place of the array. The available evidence suggests that wall adsorption in the array detector cell and (unheated) interconnecting capillaries contributes significantly to the problem. Since diffusion coefficients do not decrease significantly for these compounds relative to the early eluting compounds, rates of diffusion within the MPN films are not likely to be important factors. It is possible, however, that evaporation rates may be significantly slower for the later eluters and that this also contributes to the broadening of the peaks.

Values of t_R for the 31 vapors were reproducible to within 1.0% (RSD, n = 28, four replicates at seven concentrations). The integrated peaks areas were typically reproducible to within 5-10% (RSD, n = 4), although larger variations were also found at very low concentrations for a few of the less volatile compounds on the HME and CCN (RSD > 20%).

The instrument was calibrated with the 31 vapors under the separation conditions just established. For this, the set of compounds was divided into three subsets for which there were no co-elutions and calibration curves were generated over a 100-fold concentration range in each component by use of a series of Tedlar bags and different injection volumes (see Experimental Section). The vapor concentration range differed for each vapor, depending on the sensitivity of the sensors to that compound, with lower concentrations (~0.1-10 ppb-L) being used for the later-eluting compounds whose responses were generally larger than those of the earlier-eluting (i.e., more volatile) compounds (3-300 ppb-L).

Plots of peak area (or peak height) versus vapor concentration (in ppb-L) were linear through the highest concentration tested for 80% of all the sensor-vapor

combinations (124 combination in total, forced-zero regression $r^2 > 0.95$ as the criterion, most of the r^2 were > 0.99). Calibration curves for the five compounds with the lowest vapor pressures, i.e. n-undecane, acetophenone, n-dodecane, naphthalene, and n-tridecane (compounds 27-31 in Table 2-3) were nonlinear, owing to a combination of factors, including, wall adsorption on interconnecting components in the system and low desorption efficiency from the PCI. For these compounds calibration data, i.e. sensitivity and LOD, were obtained by a single-point calibration.

The LODs generally decrease (sensitivities increase) with decreasing vapor pressure of the analyte as expected for sorption-dependent sensors (Table 2-3).[34,38] This trend is consistent across most of the vapors for all four CR sensors, though some exceptions are observed in this trend, which can generally be attributed to the mitigating influence of vapor-MPN interactions. Note that the sensitivities of α-pinene, naphthalene, and n-tridecane are much lower than expected. For α-pinene, this was, at least partly due to partial decomposition during thermal desorption, as evidenced by small additional peaks generated when analyzing this compound alone in separate tests. For naphthalene and tridecane wall adsorption and low desorption efficiencies were contributory.

Naphthalene and n-tridecane notwithstanding, calculated LODs range from 3.9 ppt for n-dodecane (C8 sensor) to 20 ppb for methyl cyclohexane (CCN sensor), assuming a 1 L sample volume. Note that the LOD values do not necessarily correlate with the sensitivity values because of differences in the baseline noise for each sensor. In general, the OPH sensor gave the highest sensitivity for most compounds, followed closely by the C8 sensor. However, the noise level fo the C8 sensor was lower, leading to lower LODs for the C8 sensor. The more polar coatings, HME and CCN, generally showed lower sensitivity toward most vapors and higher noise levels. That higher sensitivities were not observed for some of the polar analytes with these sensors challenges the noton that the thiolate tail group dictates affinity (partition coefficieints) in the MPN films. Yet, the data collected in this study appears to show that this is indeed the case and the HME has the highest LODs for all the vapors.

Compared to the earlier prototype, which employed an array of polymer-coated surface acoustic wave (SAW) sensors as the detector,[30] this instrument provides LODs

that are from 3-55 times lower for the 17 compounds tested on both instruments. This can be ascribed to a combination of factors, including the higher inherent sensitivity of the CR sensors,[34,38] more precise control of the temperature ramps in each separation column, which yields sharper peaks, and better thermostatting of the CR array.

2.4 Conclusion

This study has characterized the performance of a novel, second-generation, portable GC prototype and illustrated the tradeoffs associated with several key operating variables. Enhancements in design have led to significant improvements in overall performance relative to the previous prototype.[30] Of particular note are the improved control and stability of fluidic and thermal functions of the system, and the reduction in detection limits.

Although the on-board PCI permits the collection of large-volume air samples, injection bandwidths remain relatively broad and represent a limiting factor in achieving high chromatographic efficiencies, particularly for less volatile compounds (i.e., those with vapor pressures < 1 torr). As shown here, in addition to on-column focusing, the option of using split-flow injection can improve resolution for these less-volatile compounds. While the loss of sensitivity is generally larger than the gain in resolution, detection limits in the parts-per-trillion concentration range are relatively easy to achieve for such compounds, making the tradeoff of sensitivity less important. Notably, for compounds higher volatile than undecane the increase in resolution (decrease in peak width) associated with split-flow injection appears to be due almost entirely to the reduced injection mass. It should be kept in mind, however, that the split ratio employed here was quite low, and that higher split ratios may permit greater resolution.

The influence of flow rate on responses from the CR sensor array is significant and noteworthy. While low flow rates lead to higher sensitivity, the sharp dependence of the peak area on the flow rate below a rate of 0.5 mL/min (measured at the outlet of the columns) favors operating at higher flow rates where the dependence is much lower. Unfortunately, the loss of sensitivity at higher flow rates is substantial. The behavior observed for the sensors is quite different from that for the FID used as a reference detector, owing to the different response mechanisms of these detectors (i.e.,

concentration sensitivity vs. mass-flow sensitivity). Curiously, the peak heights of the sensors show much less sensitivity to flow rate than does the peak area, and since LODs are calculated on the basis of peak height, they will be less subject to variations from flow rate changes. To our knowledge, this is the first investigation of flow rate effects on microsensor arrays used as GC detectors.

The study of temperature effects on sensor responses revealed results that were more or less expected. Reductions in the partition coefficient at elevated temperature lead to reductions in sensitivity. For more volatile compounds, the loss in sensitivity is not accompanied by commensurate improvements in resolution, however, for less volatile compounds, resolution improves by virtue of a narrowing of peaks. Since such compounds give rise to unusually broad peaks at lower temperatures, and sensitivities are inherently high because of their large partition coefficients, it is worth considering operating an array at elevated temperature when targeting less volatile compounds in an analysis. With small arrays it might be feasible to increase the array temperature on-the-fly during an analysis after the more volatile vapors have passed through the detector. The primary contributor to peak broadening appears to be non-specific wall adsorption on unheated surfaces in the flow path beyond the column. Redoubling efforts to deactivate such surfaces is warranted as well as minimizing the lengths of connections between the column and the detector cell housing the array.

As shown in the analysis of the complex mixture, the combination of temperature- and pressure-tuned separations with detection by an MPN-coated CR sensor array is very powerful. Full advantage was taken of using response patterns from the array to ease the column separation burden and reduce total analysis time; the 31-component mixture was adequately separated in just seven minutes. At the current sampling pump flow rate, a complete analysis could be completed in about 16 minutes. LODs were generally in the sub-ppb range for a 1-L air sample, which are sufficiently low to detect VOCs and SVOCs in applications such as indoor air quality monitoring, ambient air monitoring, homeland security, and trace breath analysis (see Chapter 4).

The capabilities of this prototype greatly exceed those of the first-generation prototype and rival those of portable GC-MS instruments. Compared with the first-generation prototype, the new design enhancements incorporated into the second-

generation prototype have improved the reliability, sensitivity, resolution, flexibility, and convenience. However, there are still some shortcomings to address. One of the primary remaining issues relates to the analysis of low-vapor-pressure compounds. Desoprtion efficiencies tend to be low for these compounds and the calibration curves are invariably non-linear due, apparently, to wall adsorption on unheated surfaces in the flow path. Although cold spots in this instrument have been minimized, there are two locations where they remain: between the PCI and the first column and between the end of the second column and detector cell. Although the inlet could be heated, the presence of the (stainless steel) tee fitting makes it difficult to heat and cool rapidly at low power. The capillary between end of the column and the sensor array cannot be heated too much because it would result in a reduction in sensitivity in the concentration-dependent sensors in the array.

Another unresolved problem with the instrument relates to the MPN coatings used as interface materials on the CR array. The mechanism of the sensor response has not been fully understood and the long-term stability of responses from the sensors is low, demanding re-calibration on the order of every two weeks. The baseline resistance of the sensors also drifts over time, which requires frequent adjustment of the feedback resistance in the circuitry used for sensor response transduction.

Table 2-1. Result comparison between split- and split-flow injection operation.

Compound	Ratio of parameter value (split:splitless)[a]						
	t_R[b]	peak area	peak height	LOD[c]	$W_{1/2}$[d]	N[e]	R[f]
n-heptane	1.0	0.12	0.21	4.8	0.54	3.5	
n-octane	1.0	0.12	0.23	4.3	0.50	4.2	2.0
n-nonane	1.0	0.12	0.28	3.6	0.45	5.3	2.2
n-decane	1.0	0.12	0.34	2.9	0.35	8.5	2.7
n-undecane	1.0	0.14	0.40	2.5	0.32	8.9	2.7
n-dodecane	0.8	0.17	0.40	2.5	0.33	6.0	2.1

[a] Column outlet flow rate is 0.7 mL/min for both split and split-flow injection, split ratio is 6.6:1 for split-flow injection
[b] t_R: retention time.
[c] LOD: limit of detection.
[d] $W_{1/2}$: full peak width at half peak height.
[e] N: column efficiency parameter plate number, $N = 5.45 * (t_R/W_{1/2})^2$
[f] R: resolution between alkanes C_n and C_{n-1},

$$R = 2 * \frac{t_{R(2)} - t_{R(1)}}{W_{b(1)} + W_{b(2)}} = 1.18 * \frac{t_{R(2)} - t_{R(1)}}{W_{1/2(1)} + W_{1/2(2)}}$$

Table 2-2. Temperature effect on peak parameters from OPH sensor.

sensor temp. (ºC)	n-nonane (C_9)	n-decane (C_{10})	n-undecane (C_{11})	n-dodecane (C_{12})
		$W_{1/2}$(T) : $W_{1/2}$ (22.8 ºC)[a]		
25.6	1.00	0.97	0.87	0.85
30.5	0.94	0.84	0.70	0.63
37.9		0.80	0.65	0.48
42.7	0.88	0.79	0.59	0.46
		N(T) : N(22.8 ºC)[b]		
25.6	1.01	1.06	1.32	1.38
30.5	1.14	1.42	2.06	2.52
37.9	--[c]	1.54	2.35	4.43
42.7	1.29	1.59	2.91	4.76
		peak area (T) : peak area (22.8 ºC)		
25.6	0.90	0.84	0.89	0.96
30.5	0.66	0.57	0.59	0.62
37.9		0.46	0.38	0.34
42.7	0.43	0.32	0.22	0.20
		peak height (T) : height (22.8 ºC)		
25.6	0.77	0.86	0.91	0.98
30.5	0.67	0.62	0.60	0.72
37.9	--	0.51	0.38	0.47
42.7	0.47	0.35	0.23	0.27
	R (T) : R (22.8 ºC)[d]			
	C_9-C_{10}	C_{10}-C_{11}	C_{11}-C_{12}	
25.6	1.00	1.08	1.12	
30.5	1.09	1.21	1.31	
37.9	--	1.30	1.52	
42.7	1.15	1.33	1.62	

[a] $W_{1/2}$: full peak width at half peak height.

[b] N: column efficiency parameter plate number, $N = 5.45 * (t_R/W_{1/2})^2$

[c] Data missed due to large noise of the sensor.

[c] R: resolution between alkanes C_n and C_{n+1},

$$R = 2 * \frac{t_{R(2)} - t_{R(1)}}{W_{b(1)} + W_{b(2)}} = 1.18 * \frac{t_{R(2)} - t_{R(1)}}{W_{1/2(1)} + W_{1/2(2)}}$$

Table 2-3. Experimental and reference values of ΔH_v.

		ΔHv (KJ/mol)		
compound	r^{2} [a]	ref.[b]	cal.[c]	error (%)[d]
n-nonane	0.985	43.8	33.3	-24
n-decane	0.988	45.7	44.1	-3
n-undecane	0.994	48.0	61.3	28
n-dodecane	0.983	52.7	65.8	25

[a] R-squared values of Arrhenius plots.
[b] Reference data from ref. 50.
[c] Calculated values from the Arrhenius slope.
[d] Error (%) = (calculated value – reference value) x 100/reference value.

Table 2-4. Calibration data summary for the 31 vapors.

#	vapor	Pv (torr)[a]	RT/s	LOD (ppb)[b] C8	OPH	HME	CCN
1	ethyl acetate	93.7	53	0.61	0.72	5.6	2.5
2	benzene	95.2	62	0.51	0.58	6.3	2.7
3	trichloroethylene	69	76	0.47	0.55	5.0	2.6
4	methyl cyclohexane	46	90	0.85	1.1	20	10
5	methyl isobutyl ketone	19.9	100	0.22	0.26	2.6	1.0
6	toluene	28.4	112	0.22	0.24	2.7	1.2
7	2-hexanone	11.6	127	0.20	0.21	2.0	0.88
8	tetrachloroethene	18.6	141	0.27	0.31	3.8	1.9
9	n-butyl acetate	11.5	147	0.18	0.21	1.8	0.90
10	chlorobenzene	12	164	0.11	0.11	1.4	0.61
11	ethylbenzene	9.6	178	0.11	0.11	1.5	0.65
12	m-xylene	8.29	185	0.12	0.13	1.6	0.69
13	3-heptanone	2.6	199	0.12	0.12	1.4	0.59
14	o-xylene	6.61	201	0.083	0.10	1.2	0.47
15	n-nonane	4.45	217	0.067	0.082	1.5	0.77
16	isopropylbenzene	4.5	225	0.065	0.070	1.0	0.40
17	a-pinene	4.75	237	0.24	0.29	6.1	2.3
18	n-propylbenzene	3.42	246	0.049	0.050	0.92	0.40
19	4-ethyl toluene	3	253	0.051	0.049	1.1	0.32
20	2-ethyl toluene	2.61	265	0.031	0.032	0.61	0.21
21	1,2,4-trimethylbenzene	2.1	276	0.032	0.037	0.61	0.21
22	3-octanone	2	276	0.053	0.050	0.75	0.32
23	1,4-dichlorobenzene	1	286	0.035	0.036	0.69	0.17
24	sec-butylbenzene	1.75	288	0.027	0.028	0.58	0.20
25	n-decane	1.43	290	0.027	0.041	0.78	0.29
26	d-limonene	1.98	303	0.036	0.041	0.88	0.34
27	n-undecane	0.412	329	0.0049	0.0055	0.14	0.04
28	acetophenone	0.397	342	0.023	0.024	0.22	0.051
29	n-dodecane	0.136	357	0.0039	0.0040	0.15	0.039
30	naphthalene	0.085	374	0.11	0.089	2.1	0.41
31	tridecane	0.0558	397	1.03	1.0	26	8.5

[a] Vapor pressure at 25 ºC from Ref. 52;

[b] LOD calculated as 3σ/sensitivity, where σ is the RMS baseline noise (smoothed via binomial 40 point running average with the Grams software; σ = 1.7, 2.4, 15, and 8.2 mV for C8, OPH, HME and CCN, respectively) and the sensitivity is determined on the basis of peak height (rather than peak area). For those vapors with non-linear calibration curves, LODs were estimated by extrapolation of the (linear) low-concentration range.

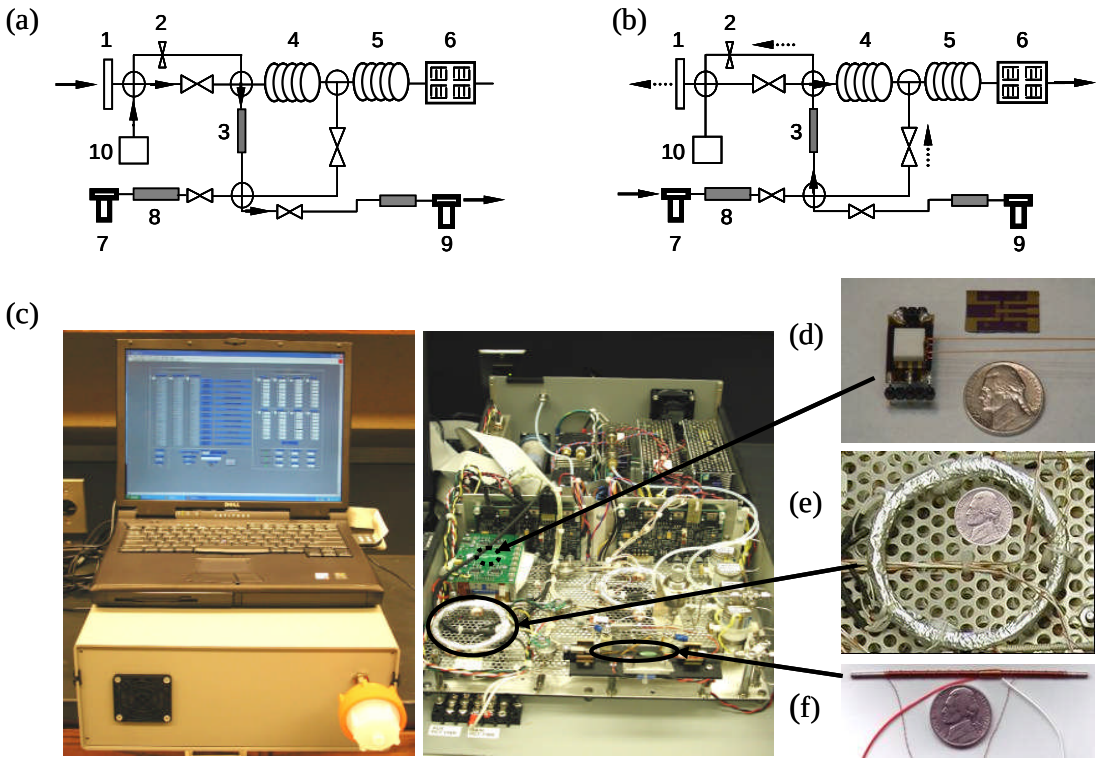

Figure 2-1. Block diagram and photos of the analytical sub-system: (a) flow direction during sampling; (b) flow direction during dry-purge (optional); (c) photos instrument underneath a laptop PC (left) and inside view (right); (d) 4-sensor substrate with intergidital electrodes (right), Macor lid (white square structure), and assembled 4-chemiresistor array with inlet/outlet capillary tubing and header pins for electric connection (underneath the PCB in the photo); (e) column wrapped with heater wire and thermocouples; (f) assembled PCF with heater and k-type thermocouple. Components in the block diagram: 1. inlet filter, 2. split control valve, 3. PCI, 4. 1st column, 5. 2nd column, 6. sensor array, 7. analysis pump, 8. scrubber, 9. sample pump.

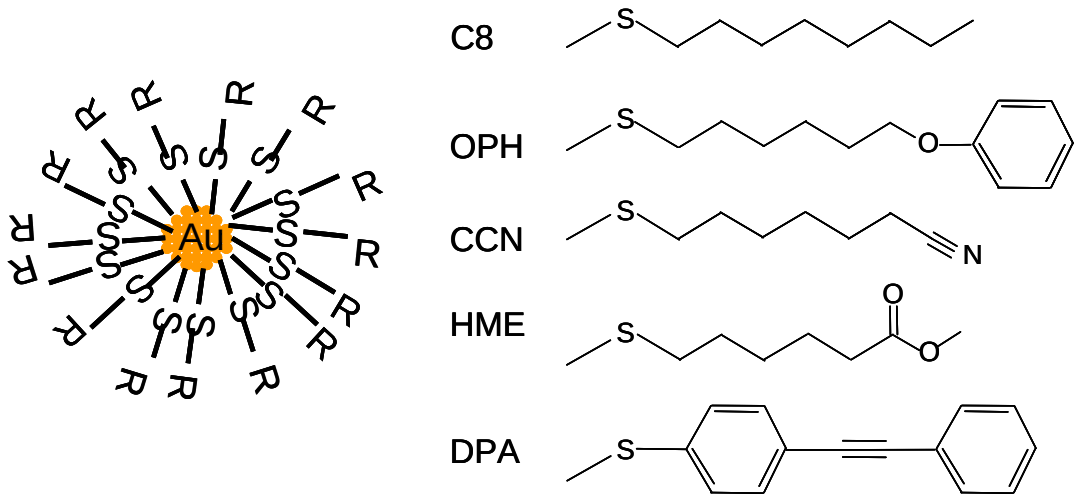

Figure 2-2. Cartoon of nanoparticle (left) and structures of the ligands of the MPNs used in this study. MPNs: n-octanethiolate (C8), 1-mercapto-6-phenoxyhexane (OPH), 7-mercaptoheptanitrile (CCN), 4-mercaptodiphenylacetylene (DPA) and methyl 6-mercaptohxanoate (HME).

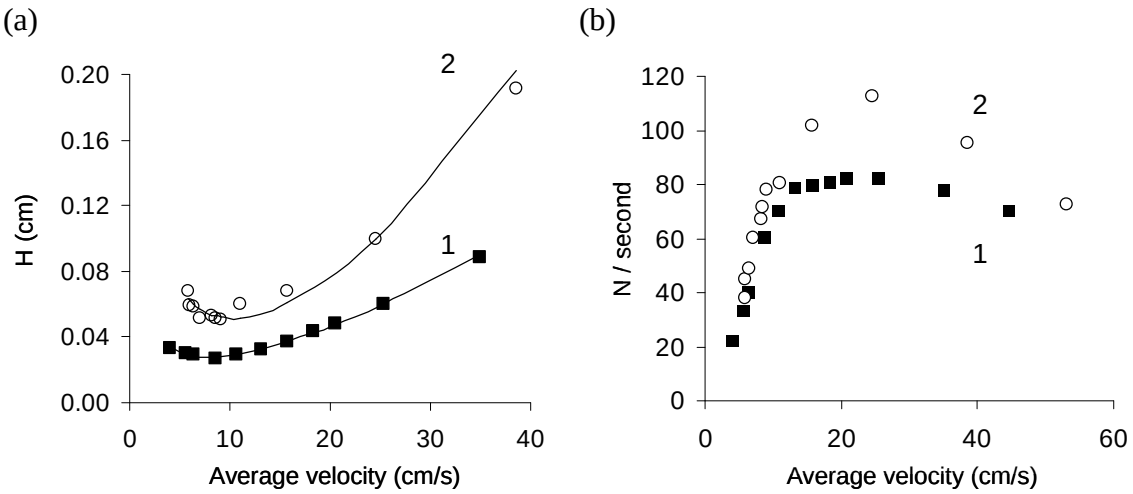

Figure 2-3. (a) Plots of height equivalent to a theoretical plate versus average carrier gas velocity with n-octane; (b) plots of plate numbers per second versus average carrier gas velocity with octane. 1) 1st column, 40 °C, k=4.2; 2), 2nd column, 30 °C, k=1.3.

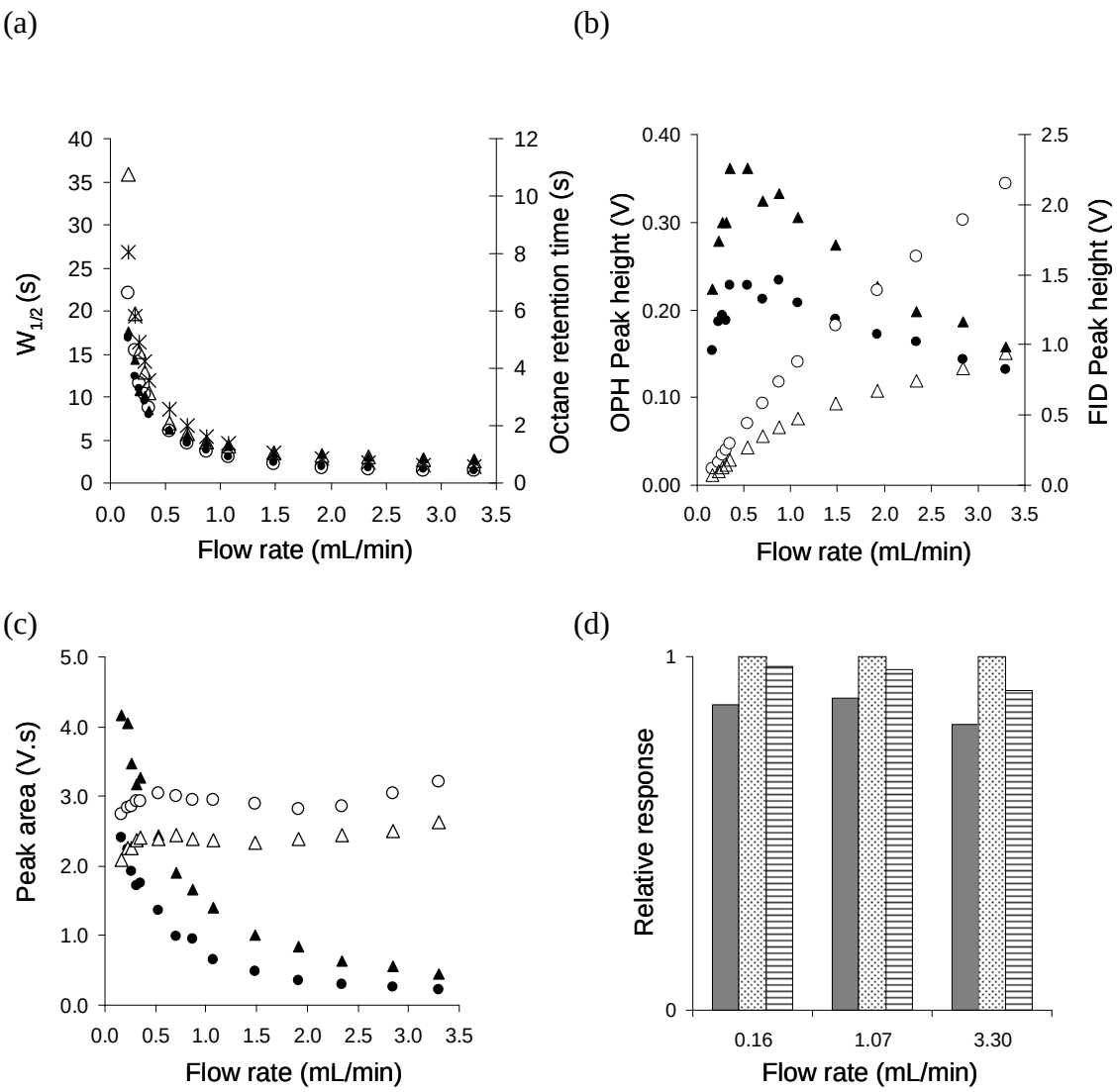

Figure 2-4. Flow rate effect on sensor response: (a) Peak width at half peak height and octane's retention time versus flow rate; (b) Peak height versus flow rate; (c) Peak area versus flow rate; (d) Response patterns of octane at different flow rates. Circle: octane from OPH; unfilled circle: octane from FID; triangle: nonane from OPH; unfilled triangle: nonane from FID; star: octane retention time; For the bar chart, fully filled column: C8; column filled with dots: OPH; column filled with lines: DPA.

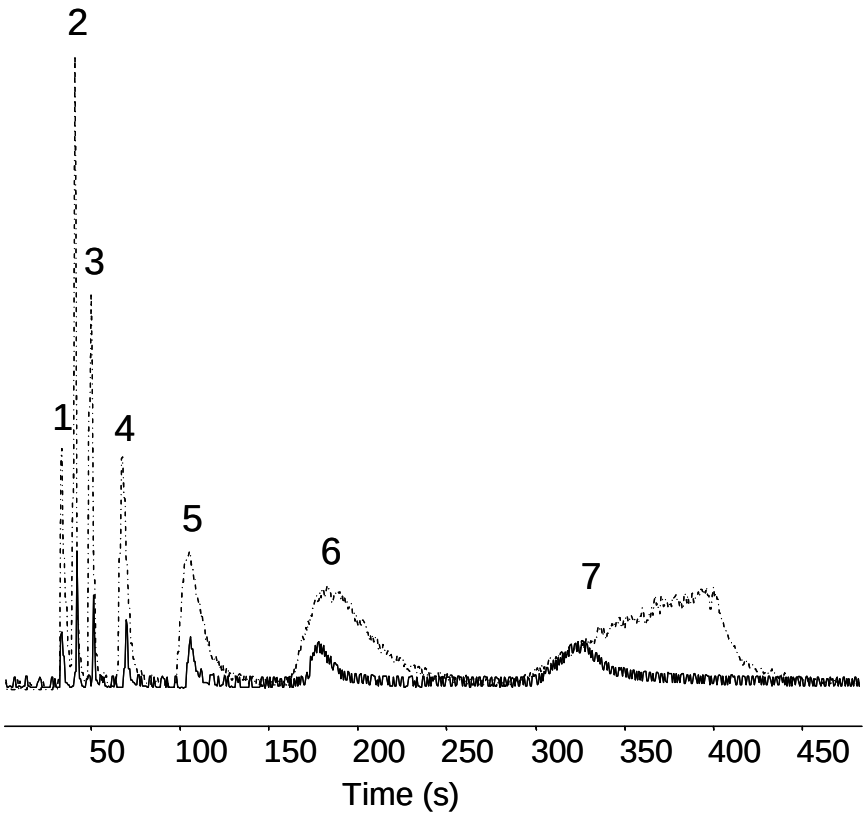

Figure 2-5. FID chromatograms under split- and splitless- flow injection operations. Solid line: split-flow; Dash line: splitless-flow. 1: methane; 2: n-heptane; 3: n-octane; 4: n-nonane; 5: n-decane; 6: n-undecane; 7: n-dodecane.

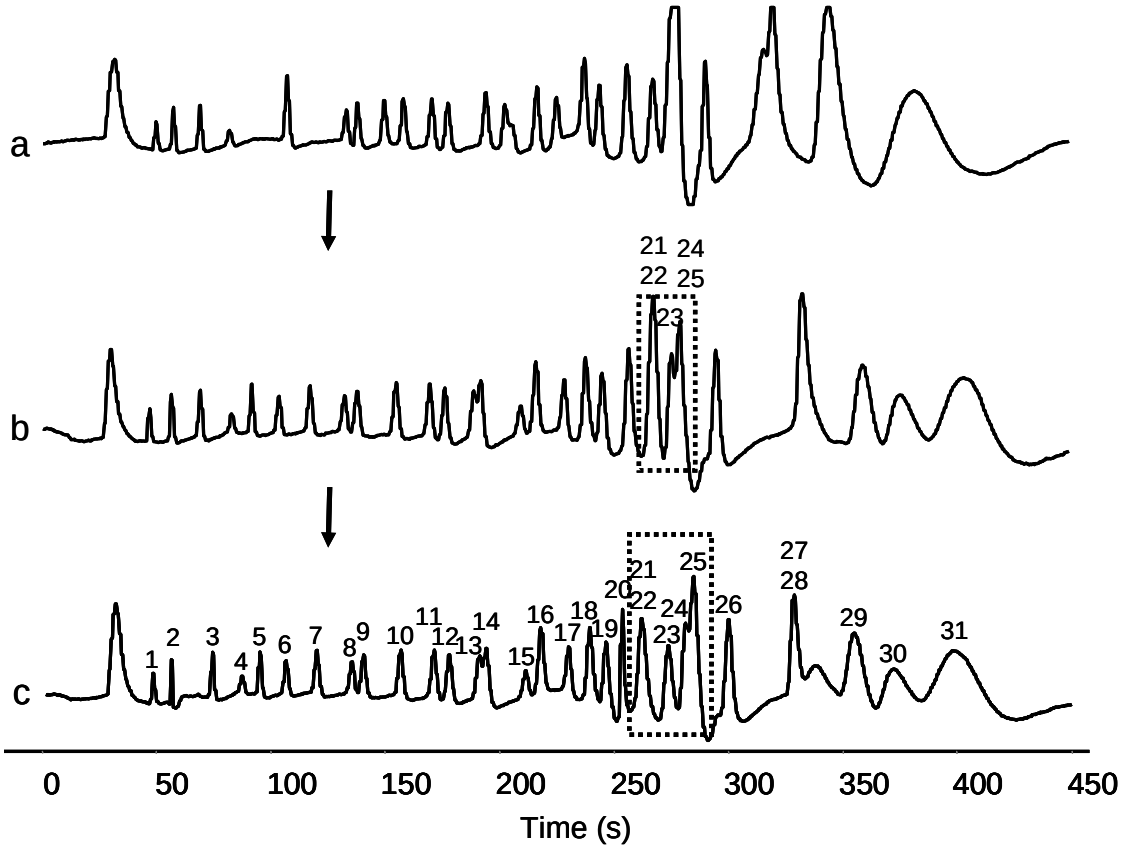

Figure 2-6. Tuned separation of 31-component mixture (for brevity, only C8 traces were shown, numbers correspond to the compounds listed in Table 2-4: (a) both columns at the same temperature programs, 30ºC for 70 s, increase to 82.5ºC at 0.25ºC /s, then increase to 150ºC at 3.38ºC /s, hold; (b) two columns at the different temperature programs. Column 1, the same as used in (1); Column 2, 50ºC for 70 s, increase to 100ºC at 1.00ºC /s, hold; (c) same temperature program as b, pressure tuning at t = 242 s for 3 s and at t = 252 s for 3 s.

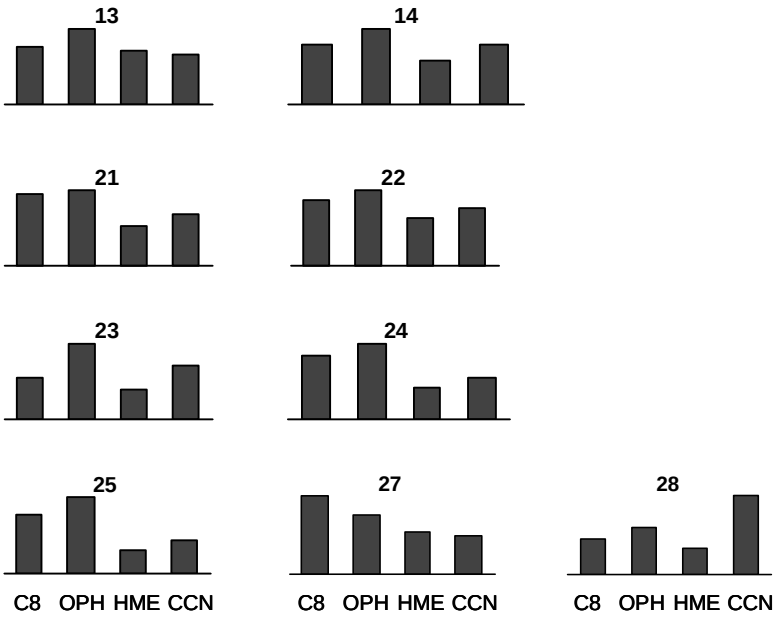

Figure 2-7. Relative response patterns of compounds that coeluted in Figure 2-6b. The identities of the compounds can be found in Table 2-4.

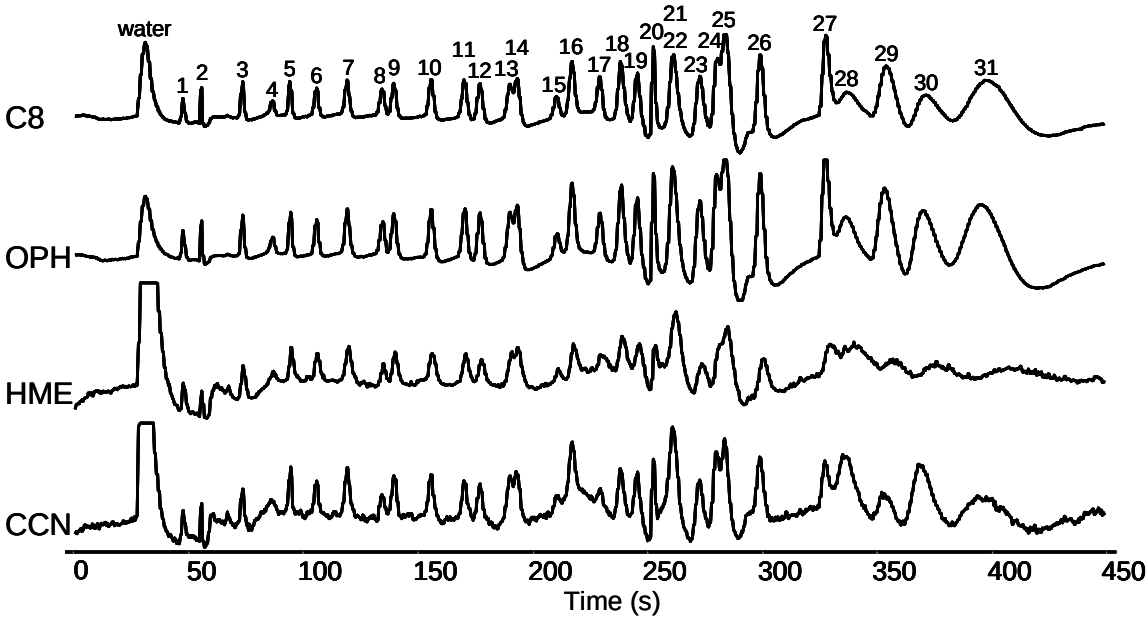

Figure 2-8. CR-array chromatogram traces of tuned separation of 31-component mixtures. Numbers correspond to the compounds listed in Table 2-4. GC conditions are the same as those in Figure 2-5(c).

2.5 Reference

1. Hering S. V. ed. *Air Sampling Instruments,* American Conference of Governmental Industrial Hygienists, Cincinnati, Ohio, 7th edn., 1989.
2. Miller, D. L.; Woods, J. S.; Grubaugh, K. W.; Jordon, L. M. *Environmental Science & Technology* **1980**, *14*(1), 97-100
3. Barker, N. J.; Leveson, R. C. *American Laboratory* **1980**, *12*(12), 76.
4. Photovac, Inc., http://www.photovac.com (accessed Feb. 2008).
5. SRI Instruments, http://www.srigc.com (accessed Feb. 2008).
6. Microsensor System Inc. http://microsensorsystems.com (accessed, March, 2008).
7. Varian, Inc., http://www.varianinc.com (accessed Feb. 2008).
8. Agilent Technologies, http://www.home.agilent.com (accessed Feb. 2008).
9. Inficon, http://www.inficon.com (accessed Feb. 2008).
10. Electronic Sensor Technology, http://www.estcal.com (accessed Feb. 2008).
11. RVM Scientific Inc., http://www.rvmscientific.com (accessed Feb. 2008).
12. Sloan K. M.; Mustacich R. V.; Eckenrode B. A.; *Field Anal. Chem. Technol.* **2001**, *5*(6), 288-301.
13. SLS Micro Technology (SLS), http://www.sls-micro-technology.de (accessed Feb. 2008).
14. Defiant Technologies, http://www.defiant-tech.com (accessed Feb. 2008).
15. Lu, C. J.; Steinecker, W. H.; Tian, W. C.; Agah, M.; Potkay, J. M.; Oborny, M. C.; Nichols, J.; Chan, H.; Driscoll, J.; Sacks, R. D.; Pang, S. W.; Wise, K. D.; Zellers, E. T. *Lab On A Chip* **2005**, *5*, 1123-1131.
16. Lewis, P. R.; Manginell, R. P.; Adkins, D. R.; Kottenstette, R. J.; Wheeler, D. R.; Sokolowski, S. S.; Trudell, D. E.; Byrnes, J. E.; Okandan, M.; Bauer, J. M.; Manley, R. G.; Frye-Mason, G. C. *IEEE Sens. J.* **2006**, *6*(3), 784-795.
17. Sanchez, J. M.; Sacks, R. D. *J. Sep. Sci.* **2007**, *30*(7), 1052-1060.
18. Liu, X.; Pawliszyn, J. *Int. J. Environ. Anal. Chem.*, **2005**, *85*(15), 1189-1200.
19. Dziuban, J. A.; Mroz, J.; Szczygielska, M.; Malachowski, M.; Gorecka-Drzazga, A.; Walczak, R.; Bula, W.; Zalewski, D.; Nieradko, L.; Lysko, J.; Koszur, J.; Kowalski, P. *Sens. Actuators, A*, **2004**, *115*, 318-330.
20. Ji, J.; Deng, C. H.; Shen, W. W.; Zhang, X. M. *Talanta* **2006**, *69*(4), 894-899.
21. Smith, P. A.; Sng, M. T.; Eckenrode, B. A.; Leow, S. Y.; Koch, D.; Erickson, R. P.; Jackson Lepage, C. R.; Hook, G. L. *J. Chromatogr. A* **2005**, *1067*, 285-294.
22. Griffin Analytical technologies, http://www.griffinanalytical.com (accessed Feb. 2008).
23. Ericson, R. P.; Tripathi, A.; Maswadeh, W M.; Snyder, A. P.; Smith, P. A. *Anal. Chim. Acta* **2006**, *556*(2), 455-461.
24. Femtoscan, http://www.femtoscan.com (accessed Feb. 2008).
25. Lambertus, G. R.; Fix, C. S.; Reidy, S. M.; Miller, R. A.; Wheeler, D.; Nazarov, E.; Sacks, R. *Anal. Chem.* **2005**, *77*(23), 7563-7571.
26. Jia, C. R.; Batterman, S.; Godwin, C. *Atmos. Environ.* **2008**, doi: 10.1016/j.atmosenv.2007.11.055.
27. Batterman, S. A.; Peng, C. Y.; Braun, J. *Atmospheric Environment* **2002**, *36*(39-40), 6015-6030.
28. Zhong, Q.; Veeneman, R. A.; Steinecker, W. H.; Jia, C.; Batterman, S. A.; Zellers, E. T. *J. Environ. Monit.* **2007**, *9*, 440-448.

29. Jia, M. Y.; Koziel, J.; Pawliszyn, J. *Field Anal. Chem. Technol.* **2000**, *4*, 73-84.
30. Lu, C. J.; Whiting, J.; Sacks, R. D.; Zellers, E. T. *Anal. Chem.* **2003**, *75*(6), 1400-1409.
31. Lu, C. J.; Zellers E.T. *Anal. Chem*. **2001**, *73*, 3449-3457.
32. Lu. C.J.; Zellers E.T. *Analyst* **2002**, *127*, 1061-1068.
33. Lu, C. J.; Jin, C.; Zellers, E. T. *J. Environ. Monit.* **2006**, *8*(2), 270-278.
34. Cai, Q. Y.; Zellers, E. T. *Anal. Chem.* **2002**, *74*, 3533-3539.
35. Whiting, J. J.; Sacks, R. D. *J. Sep. Sci.* **2006**, *29*(2), 218-227.
36. Grall, A. J.; Sacks, R. D. *Anal. Chem.* **1999**, *71*(22), 5199-5205.
37. Grall, A. J.; Zellers, E. T.; Sacks, R. D. *Environ. Sci. Technol.* **2001**, *35*, 163-169.
38. Steinecker, W. H.; Rowe, M. P.; Zellers, E. T. *Anal Chem.* **2007**, *79*, 4977-4986.
39. Rowe, M. P.; Plass, K. E.; Kim, K.; Kurdak, C.; Zellers, E. T.; Matzger, A. J. *Chem. Mater.*, **2004**, *16*, 3513–3517.
40. Wohltjen, H.; Snow, A. W. *Anal Chem.* **1998**, *70*, 2856-2859.
41. Zellers, E. T.; Batterman, S. A.; Han, M.; Patrash, S. J. *Anal. Chem*. **1995**, *67*, 1092-1106.
42. Park, J.; Groves, W. A.; Zellers, E. T. *Anal. Chem*. **1999**, *71*, 3877-3886.
43. Bemgard A. K.; Blomber L. G. *Anal. Chem.* **1989**, *61*, 2165-2171.
44. Nelson, G. O. *Gas Mixture: Preparation and Control.* Lewis Publishers: New York, 1992.
45. Kummer, A. M.; Hielemann, A.; Baltes, H. *Anal. Chem.* **2004**, *76*(9), 2470-2477.
46. Briglin, S. M.; Lewis, N. S. *J. Phys. Chem. B* **2003**, *107*, 1103-11042.
47. Feller, J. F.; Langevin, D.; Marais, S. *Synthetic Metals* **2004**, *144*(1),81-88.
48. Jennings W., Mittlefehldt E., Stremple P. *Analytical Gas Chromatography, 2nd ed.*, Academic Press, San Diego, CA, 1997, p145.
49. Littlewood, A. B. *Gas Chromatography*, Academic press: New York, 1970.
50. CRC handbook of chemistry and physics, 61st edition, editor Robert C. Weast, Melvin J. Astle, CRC press, Inc. Boca Raton, FL 33431, 1980-81, Pag3 C-482
51. Jia, C.; Batterman, S.; Chernyak, S. *J. Environ. Monit.* **2006**, *8*(2), 1029-1042.
52. Howard, P. H.; Meylan, W. M. *Handbook of Physical Properties of Organic Chemicals*, Lewis: New York, 1997.

Chapter 3

Rapid Determination of Environmental Tobacco Smoke Markers in Complex Mixture of Indoor Air Contaminants*

Abstract

The adaptation of the second-generation prototype to the determination of vapor-phase markers of environmental tobacco smoke (ETS) is described. A dual-stage adsorbent preconcentrator was used with the two series-coupled separation columns that can be independently temperature programmed, and a chemiresistor (CR) array detector. An adsorbent pre-trap was developed to remove semi-volatile organics from the sample stream. Conditions were established to quantitatively capture two ETS markers, 2,5-dimethylfuran (2,5-DMF) and 4-ethenylpyridine (4-EP, as a surrogate for 3-EP), and to separate them from the 34 most prominent co-contaminants present in ETS using ambient air as the carrier gas. Response pattern of 4-EP was unique, and the separation time was reduced by 16% by taking advantage of the capability of the CR array to discriminate between the components of simple coelutions. Projected detection limits are 0.58 and 0.08 ppb for 2,5-DMF and 4-EP, respectively, assuming a 1-L sample volume, which are sufficiently low to determine these markers in typical smoking-permitted environments. A complete analysis can be performed every 15 minutes.

---

* This chapter has been published, with minor modifications, in *J. Environ. Monit.* **2007**, 9, 440-448.

3.1 Introduction

Environmental tobacco smoke (ETS) is a complex mixture of compounds collectively classified by the International Agency for Research on Cancer as a carcinogenic substance.[1] The complexity of ETS and the presence of confounding sources of some ETS constituents in many environments have impeded accurate exposure assessments and have led to efforts to find surrogate measures of ETS.[2] Vapor-phase nicotine (VPN) is the most widely used marker of ETS, but it is not ideal because of its low volatility and unpredictable decay rate.[3] A pyrolysis product of nicotine, 3-ethenylpyridine (3-EP), has been reported as an alternative ETS marker.[3,4] Concentrations of 3-EP correlate better with ETS particle concentrations and other gas-phase ETS components than do those of VPN, it is found exclusively in the vapor phase, and its decay follows first-order kinetic models. Average concentrations of 3-EP measured in indoor environments where smoking is permitted typically range from 0.8-6.3 $\mu g/m^3$ (0.18-1.5 ppb), with average personal exposure levels generally somewhat lower (0.4-0.7 ppb). Exposures rarely exceed 4.5 ppb.[5-9]

Appendix 3 provides a detailed review of reported determinations of 3-EP and VPN from smoking and non-smoking environments.

Another compound, 2,5-dimethylfuran (2,5-DMF), has also been identified as a vapor-phase marker of ETS.[10,11] In tests designed to simulate ETS levels in an office environment, 2,5-DMF concentrations were found to range from 2.4–30 $\mu g/m^3$ (0.6-7.5 ppb).[10,11] Concentrations of 2,5-DMF in the breath of passively exposed non-smokers averaged 6.8 ppb, while those in the breath of smokers averaged 94 ppb immediately after smoking.[11]

The most widely reported methods for determination of 3-EP in indoor air entail sorbent-tube sampling followed by gas-chromatograph-mass-spectrometry (GC-MS) or GC-nitrogen-phosphours detector (GC-NPD) analysis.[6,8,9,12] Similarly, samples of 2,5-DMF vapor can be captured by canister or on Tenax-TA adsorbents and analyzed by GC-MS.[10,11] Although such methods are undoubtedly reliable, the availability of portable instrumentation capable of monitoring ETS markers *in situ* would facilitate exposure assessments and interventions by allowing a greater number of measurements to be collected at lower cost and much higher temporal resolution, as well as providing

immediate feedback to affected populations. Unfortunately, relatively few portable instruments are available with the capability for analyzing the components of complex vapor mixtures,[13-19] and the cost, complexity, and/or size of those with such capabilities preclude their use for extended or routine monitoring campaigns. Although Gordon et al. have described a fieldable breath analyzer,[11] there are no published reports on the determination of ambient concentrations of vapor-phase ETS markers with portable direct-reading instrumentation.

This chapter describes the adaptation of the second-generation prototype instrument to the determination of ETS markers in synthetic air samples also containing the major co-contaminants encountered in environments where smoking is permitted. In this study, air samples were collected from a local bowling alley where smoking is allowed and analyzed by conventional methods to identify and quantify the two ETS markers 2,5-DMF and 3-EP and the major co-contaminants. Mixtures of these were then generated in the laboratory and conditions were established for the determination of the markers using a combination of retention times and the response patterns obtained from the CR-array detector. Since at the outset of the study 3-EP was not commercially available, its isomer, 4-EP, was used as a surrogate.[12] A pre-trap was developed for removing semi-volatile organic compounds (SVOCs) from the sample. Preconcentration factors and desorption efficiencies for the ETS markers were verified and chromatographic conditions were established to separate the markers from other contaminants in the shortest possible time. Using Monte Carlo simulations coupled with pattern recognition analysis of sensor-array responses, it was possible to determine the degree of discrimination achievable between the markers and possible co-eluting interferences and to use this information to accelerate the analysis.

3.2 Experimental

3.2.1 Instrument Features and Operating Modes

Figure 3-1 shows the layout of the analytical sub-system. Except the incorporation of a pre-trap, and the use of a two-stage preconcentrator/injector (PCI) in this system, the other features were the same as those in Figure 2-1 of Chapter 2. A detailed description

of the instrument components and the rationale for the design are provided in experimental section of Chapter 2.

The instrument has four operating modes: Sampling, Dry-purge, Analysis, and Post-analysis-purge Modes. In Sampling Mode, air is drawn through the pre-trap and the PCI at 0.13 L/min by the sampling pump. Vapors not removed by the pre-trap (see below) are captured on one of the two PCI adsorbents contained in an insulated Inconel 600® tube (1.35 mm i.d., 5-cm long). The PCI tube was packed, in order, with 3 mg each of 40/60-mesh Carbopack X and Carbopack B (separated by glass woo1), which have specific surface areas of 250 m^2/g and 100 m^2/g, respectively (Supelco, Bellefonte, PA).[23] After sampling a pre-determined air volume, typically 1 L for this study, the sampling pump is turned off and isolated from the system by an upstream valve (Figure 3-1a). An optional Dry-purge Mode can be included during which the analysis pump draws ambient air in through a second inlet port and passes it through a scrubber cartridge packed with molecular sieves and charcoal to remove water vapor and VOCs. The purified air passes through the PCI (at room temperature) to strip a portion of the water vapor from the adsorbents and to backflush it, along with any residual contaminants in the fore line, out through the sample inlet port. In Analysis Mode, the PCI is heated (via an insulated copper-wire coil) to 300 °C in < 2 sec and maintained at this temperature for 90 sec. Ambient air drawn into the system by the analysis pump is scrubbed, as in Purge Mode, and then directed through the PCI, the two separation columns, and the detector cell containing the sensor array prior to exiting the instrument. Desorbed vapors are thereby injected onto the first of the two separation columns, with the option of splitting off a portion of the desorbed flow stream (by opening the split-flow control valve) stream for the purposes of sharpening the injection band. In Post-analysis-purge Mode, the inlet valve is open, scrubbed air is driven by the analysis pump, at the same flow direction as that in the Dry-purge Mode, the PCI and the pre-trap are re-conditioned by heating to 300 ºC with back flushing for 150 sec at 0.28 L/min after the analysis.

Each CR sensors in the 4-sensor array is coated with a different gold-thiolate monolayer protected nanoparticle (MPN).[26,27] MPNs derived from the following thiols were used in this study: n-octanethiol (C8), 1-mercapto-6-phenoxyhexane (OPH), 7-mercaptoheptanitrile (CCN), methyl 6-mercaptohexanoate (HME), and 4-

mercaptodiphenylacetylene (DPA).[28] The structures of the thiolates are presented in Figure 2-2 of Chapter 2. Software written in Labview® 7.1 (National Instruments, Austin, TX) is run from a laptop computer and used to control the instrument and process the sensor output signals through separate 12 bit and 16 bit D/A data acquisition cards. Sensor output data are imported to Grams 32 (Thermogalactics, Salem, NH) for peak integration.

3.2.2 Field Samples

Air samples from a local bowling alley were collected and analyzed on two different occasions using EPA Method TO-17.[30] The GC-MS (Model 6890-5973, MS in Scan Mode, Agilent, Palo Alto, CA) was calibrated with 96 VOCs selected on the basis of their adverse health effects and prevalence as contaminants in indoor air.[31] Neither 3-EP nor VPN were included in this initial calibration library. They were added prior to analyzing samples from the second set of samples collected from the bowling alley.

3.2.3 Test Atmosphere Generation

Chemicals were obtained from Aldrich (Milwaulkee, WI), Acros/Fisher (Pittsburgh, PA), or Lancaster (Windham, NH) at ≥ 98% purity. Since 3-EP could not obtained commercially, its isomer 4-ethenylpyridine (4-EP) was used. These isomers are reported to have the same GC retention time (and similar MS fragmentation patterns),[12] consistent with their similar vapor pressures, reported to be 1.70 torr for 4-EP[32] and estimated to be 1.65 torr for 3-EP on the basis of its boiling point.[33,34] Test atmospheres of the vapors were generated in clean, dry air from a compressed-air cylinder over a range of concentrations in a series of Tedlar® bags (25 ±2 ºC) and concentrations were compared to those determined using CS_2 solutions of the analytes by GC-FID (Model 6890, Agilent).

3.2.4 Adsorbent-Bed Capacities and Desorption Efficiencies

A series of experiments was performed to identify the types and quantities of adsorbents for use in the pre-trap and PCI. The 10% breakthrough volume, V_{b10}, was determined by drawing a vapor sample through the adsorbent bed at 0.1 L/min, periodically collecting aliquots downstream in a 0.25 mL sample loop, and injecting via a

6-port valve into an HP GC.[35] In this GC, a nitrogen-phosphorous detector (NPD) was employed for experiments involving low concentrations of 4-EP and VPN, and an flame ionization detector (FID) was used for all other experiments. Desorption efficiencies were determined by injecting a known concentration of analyte(s) in air into a clean air stream being drawn through the adsorbent bed, reversing the flow and heating the adsorbent to 300 ºC to inject the captured analytes into the GC-FID or NPD. Responses were compared to those for an equivalent mass injected directly to the GC-FID or NPD. Instrument responses to relevant vapors were then compared with and without the pre-trap installed. The sample inlet was connected to one port of a 6-port valve and a miniature diaphragm pump (KNF Neuberger, Trenton, NJ) was used to draw samples at 0.13 L/min from a test atmosphere through a sample loop on a background of scrubbed air. The PCI was then heated and the desorbed vapors injected into the separation module. The PCI and pre-trap were re-conditioned after each analysis by sequentially heating them to 300 °C while backflushing with clean air.

3.2.5 Instrument Calibration

The most prominent co-contaminants found to bracket 2,5-DMF and 3-EP in chromatograms obtained from field samples were divided into three subsets for calibration. Conditions required to separate the markers in a minimum amount of time were established. Sample loops with volumes ranging from 0.010-1 mL were used to cover the desired range of injected masses. Effective (mass-equivalent) vapor concentrations were calculated according to the ratio of injection and sample volumes. For example, an aliquot of 1 mL from a sample loop containing 100 ppm of vapors is equivalent to 100 ppb in a sample volume of 1 L. Mass-equivalent calibration concentrations ranged from 0.15 - 150 ppb-L. Five replicates were performed for each challenge concentration.

3.2.6 Chemometrics

Chemometric analyses of sensor array response patterns were performed using extended disjoint principal components regression (EDPCR).[36,37] Expected recognition rates for the components of co-eluting mixtures were estimated by combining Monte Carlo simulations with EDPCR. The Monte Carlo simulations superimpose random error

on calibrated sensor-array response patterns, which are then analyzed by EDPCR to determine if the components giving rise to the composite response pattern can be determined with low error.[37] Iterative analysis (n=500) over a range of concentrations yields statistical estimates of discrimination.

3.3 Results and Discussion

3.3.1 Contaminant Profiles from Field Samples

GC/MS analysis of the first set of field samples collected from the bowling alley yielded more than 100 detectable peaks, 35 of which could be identified as among those in the initial spectral library used for identification (Table 3-1). These target compounds accounted for 44% of the collected mass (using toluene-equivalent mass for the unidentified fraction). Concentrations ranged from 0.06 ppb (sec-butylbenzene) to 50 ppb (toluene). The concentration of 2,5-DMF was 0.56 ppb. Since 3-EP was not included in the calibration library for this analysis, its presence and concentration could not be verified.

Subsequently, GC conditions were adjusted, the spectral library augmented, and a second set of field samples was collected, in this case from an area within the bowling alley with a greater number of active smokers. Appendix 4-2 presents the chromatogram from the 1-L sample with the major peaks identified by reference to Table 3-1. A total of 40 compounds (60% of VOC mass) were identified at concentrations of 0.061 ppb (n-butylbenzene) to 29 ppb (d-limonene). Table 3-1 presents the average concentrations (RSD < 20% for most vapors). The concentrations of 2,5-DMF and 3-EP were 1.2 and 2.0 ppb, respectively. VPN was also found in these samples; however, it could not be accurately quantified because of variable desorption efficiencies observed in experiments with VPN-spiked adsorbent tubes. As shown in Table 3-1, the VOC profiles are quite consistent between the two sampling campaigns.

3.3.2 Pre-Trap

An adsorbent pre-trap was developed in order to minimize accumulation of SVOCs within the instrument. VPN (p_v = 0.038 torr) was the most-volatile and most polar of the SVOCs detected during field sampling, and was therefore chosen as the

sentinel 'cutoff' vapor for assessing pre-trap capacity. A 2-mg bed of the lower-surface-area graphitized carbon, Carbotrap C (10 m^2/g, 20/40 mesh, Supelco) challenged (0.1 L/min) in individual tests with ~450 ppb of VPN or 4-EP gave V_{b10} values of 1 L and 0.020 L, respectively. This V_{b10} value for VPN matches the desired benchmark sample volume. Furthermore, the 4-EP reached saturation within just 0.3 L, indicating a minimal amount of retention. Breakthrough of 2,5-DMF (60 ppb) was immediate and saturation was reached within 0.1 L indicating that this vapor is unretained. The VPN V_{b10} value remained within 15% of the initial value after 18 breakthrough-reconditioning cycles indicating good medium-term stability of the pre-trap.

The pre-trap was then challenged with a mixture of VPN (350 ppb) and 18 other compounds (p_v range = 0.00143 to 28.4 torr). Concentrations were 450 ppb for 4-EP, 50 ppb for 2,5-DMF, and from 10-15 ppb for the remaining 16 compounds (#8, 10, 13, 15, 17, 22, 25, 26, 31, 33, 34, 36, 38, and 40-42 in Table 3-1). Results for 4-EP and 2,5-DMF were unaffected but the VPN V_{b10} value decreased to 0.66 L. For a sample volume of 1 L the VPN breakthrough fraction, however, was only 42% indicating that the majority of the VPN was being trapped. Given the expectation for higher capacity at lower (i.e., more realistic) VPN concentrations, this level of performance was considered acceptable.

Subsequent tests were performed with and without this pre-trap installed in the instrument. A test atmosphere containing the two ETS markers and nine other vapors (p_v range = 0.14 to 95 torr, #3, 6, 8, 13, 17, 22, 25, 34, and 36 in Table 3-1) was generated and aliquots injected by sample loop and flushed with 1-L of clean air. Mass-equivalent concentrations ranged from 0.9 to 200 ppb-L. In all cases there was <5% reduction in detected concentrations when the pre-trap was installed compared to when it was not. An additional test series with the four SVOCs VPN, n-tridecane, n-tetradecane, and n-pentadecane added to the mixture indicated that the trapping efficiency of tridecane was 60% and those for the remaining vapors were ≥ 85%.

The PCI and the pre-trap were re-conditioned by heating to 300ºC with backflushing for 150 sec at 0.28 L/min after each of the previous samples. After 48 complete analytical cycles there was no apparent reduction in the performance of the PCI

or pre-trap, and the reproducibility of peak areas for the 11-vapor mixture was better than 8% (RSD) for all vapors (based on the C8-coated CR).

3.3.3 PCI

A 3-mg bed of Carbopack B challenged with 700 ppb of 4-EP in air at 0.1 L/min gave a V_{b10} of 3.5 L. In the presence of 18 additional vapors (#8, 10, 13, 15, 17, 22, 25, 26, 31, 33, 34, 36, 38, and 40-42 in Table 3-1), each at 10-25 ppb, the 4-EP V_{b10} decreased by only 0.7 L. The 4-EP desorption efficiency averaged 37 ±2% for challenge concentrations of 1.4-18 ppb (6-72 ng), increasing to 52 ± 4% at concentrations ranging from 42-85 ppb (170-340 ng). Since no additional peaks were observed by GC-FID, we speculate that 4-EP is partially polymerizing at high temperature in the air medium within the PCI.

The 2,5-DMF, which was not retained strongly on Carbopack B (V_{b10} = 0.034 L), gave a V_{b10} of 6.2 L with a 3-mg bed of Carbopack X (100 ppb). No change in capacity was observed in the presence of benzene and trichloroethylene, which are the only other vapors in the 18-vapor mixture expected to pass through the Carbopack B and be trapped on Carbopack X along with 2,5-DMF.[20] A desorption efficiency of 90 ± 2% (n=3) was obtained, which was independent of mass loading from 0.78 - 13.1 ppb-L (3-42 ng).

Estimates of preconcentration factors can be derived under the assumption that vapors were captured from a 1-L sample volume and that the entire desorbed mass is contained in the volume of the eluting peaks. The latter is estimated by multiplying the peak width (baseline) by the desorption flow rate. Since peak widths are measured after elution, the preconcentration factor is reduced by any peak dispersion incurred during transport through the system and thus is a conservative, but practical, estimate. Using this approach, effective preconcentration factors for 2,5-DMF and 4-EP averaged ~4,800 and ~1,800 at a desorption flow rate of 1.7 mL/min. Some dependence on concentration is observed, hence the approximate values.

3.3.4 Calibration with ETS Markers and Interfering Compounds

A set of GC conditions was established under which 2,5-DMF and 4-EP were separated from the 14 most prominent interfering compounds eluting within the same broad retention-time window as these two markers. This was more difficult than

anticipated and required, ultimately, a rather unusual temperature program that held the second column at a relatively low temperature in order to separate the 4-EP from adjacent compound peaks. The 4-EP peak exhibited a long right tail, not only with the prototype instrument but also with the bench-scale GCs used in the testing described above. Pressure (stop-flow) tuning was not useful in this analysis because the 4-EP and its closest eluting co-contaminants, n-undecane and n-dodecane, were not fully separated on the first column.

The chromatograms from the CR array sensors shown in Figure 3-2 represent the best separation achievable in the minimum amount of time. Peak FWHH values are < 1.5 sec for the first eight compounds (#1-8 in Table 3-2) and then get progressively broader for the later eluting compounds due, in part, to the low temperature used for the second column. Peak widths of the early eluting compounds were similar for the sensors and for an FID used in place of the sensors for analyses performed under similar conditions (see Figure 3-3). For the later-eluting compounds sensor peaks are broader than the corresponding FID peaks, indicating that sorption kinetics in the MPN coatings on the sensors are contributory. Regardless, using the independent column temperature programming, the 2,5-DMF and 4-EP peaks are fully separated from the other 14 compounds in < 240 sec (280 sec is required for complete elution of n-dodecane). Ambient water vapor, which permeates into the Tedlar® bag containing the test atmosphere, was also detected as the earliest eluting peak (RT = 25 sec) from three of the sensors in the array, with the highest responses from the sensors coated with HME and CCN MPNs which contain polar functional groups. The unusual peak shapes from these latter two sensors indicate that the responses have exceeded the dynamic range of the sensor readout circuit.

RT values for the 16 vapors were reproducible to within 0.4% (RSD, n = 30, five replicates at six concentrations). Responses from all four CR sensors were generally reproducible (RSD < 10% for five replicates). The one notable exception was n-dodecane on the C8- and OPH-coated sensors at the lower concentrations (RSD > 20%) due to the small S/N ratios.

For benzene, TCE, and 2,5-DMF, calibration concentrations up to 150 ppb were tested. For the less volatile vapors, this range was reduced to 50 ppb due to the higher

sensitivities exhibited toward these vapors. For the first 12 vapors listed in Table 3-2, plots of peak area versus vapor concentration were linear from the sensors coated with OPH, HME, and CCN MPNs, with most linear-regression r^2 values of >0.95 (forced zero). For the C8 sensor, the first eight of these vapors also gave linear calibration curves ($r^2 > 0.95$), but n-decane, 4-ethyltoluene, and d-limonene became non-linear above 25 ppb. For the four least volatile vapors, responses from all four sensors became non-linear at higher concentrations. Since FID responses were linear for these vapors, we believe the non-linearity arises from the slow sorption-desorption kinetics in the sensor films, which results in incomplete mass transport of the vapors into the sensor coatings as the peak passes through the detector. Peak broadening also contributes to a loss of sensitivity in the tails of the peaks and a consequent negative integration bias. The linear response range for 2,5-DMF extends to at least 150 ppb while that for 4-EP extends to 10 ppb. Appendix 4 presents calibration curves of the 16 compounds.

As expected for sorption-dependent sensors, sensitivity generally increases as the vapor pressure of the analyte decreases.[26,29] This is reflected in the within-sensor sensitivity values (normalized to benzene) in Table 3-2. This trend is consistent across all vapors for the non-polar C8-coated sensor; as shown, the sensitivity for the least-volatile n-dodecane is 760 times that for the most-volatile benzene. For the other three sensors, functional-group interactions cause some deviations from this general trend. For example, the sensitivities of the HME- and CCN-coated sensors for 4-EP are 2.4 and 3 times higher than those for n-dodecane, respectively, in spite of the lower vapor pressure for the alkane.

Calculated limits of detection (LODs) range from 7.2 ppt for n-dodecane (C8-coated sensor) to 14 ppb for 2,5-DMF (CCN-coated sensor) (Table 3-2). Note that the LODs do not necessarily correlate with the sensitivity values because of differences in the baseline noise for each sensor; the CCN-coated sensor had a particularly high baseline noise level while the C8-coated sensor had very low noise. For 14 of the 16 compounds, the C8-coated CR gives the lowest LOD and the highest sensitivity. Interestingly, for 4-EP the lowest LOD is achieved with the C8-coated sensor even though it had the lowest sensitivity for this vapor among the four sensors. The calculated LODs for 2,5-DMF and 4-EP are 0.58 and 0.08 ppb, respectively.

These LODs are considered minimum values because they are based on a single sensor. If responses are needed from the entire array for vapor recognition, then the LODs increase to 14 and 0.34 ppb for 2,5-DMF and 4-EP, respectively. Compared to the earlier prototype, which employed an array of polymer-coated surface acoustic wave (SAW) sensors as the detector,[20] this instrument provides LODs that are from 20-80 times lower for the 10 compounds tested on both instruments. This can be ascribed to a combination of factors, including the higher inherent sensitivity of the CR sensors,[26,29] better thermostatting of the array, and more precise control of the temperature ramps in each separation column, which yields sharper peaks.

3.3.5 Sensor Array Pattern Recognition

In combination with the retention time, CR-array response patterns provide the means to recognize eluting vapors by reference to a library of calibrated patterns. The normalized response pattern for each vapor is shown in Figure 3-2 (also see Table 3-2). By visual inspection it is apparent that vapors from the same chemical class have patterns that are, in general, more similar than those for vapors from different classes.[26,27,38] Fortunately, chromatographic separation of homologues is relatively easy.

The 4-EP (Figure 3-2, cmpd 15) response pattern is unique among the 16 prominent ETS contaminants, while the 2,5-DMF (cmpd 3) pattern resembles those of the other aromatic vapors toluene and styrene (cmpds 4 and 8) as well as that of TCE (cmpd 2). From the tabulation of relative response ratios in Table 3-2, the largest range of responses for any vapor is about 15-fold (i.e., n-decane with HME- and C8-coated sensors), with typical ranges being 1.5- to 2.5-fold.

Since it is often possible to determine the contributions of the components of simple mixtures to the composite response pattern they produce, certain co-elutions can be tolerated without losing the ability to recognize the vapors.[20,39] The extent to which this is possible can be tested using Monte Carlo simulations coupled with EDPCR. From calibration, we established a library of relative response patterns to which synthetic patterns, generated by superimposing a typical amount of error on each response pattern, could be compared. Under the assumption of response additivity, composite response patterns for mixtures were created by summing the responses to the individual vapors. Iteratively generating and assigning an identity to each component of such synthetic

mixture samples over a range of concentrations from 1-5×LOD for each vapor yielded statistical estimates of recognition rates for the components of co-eluting mixtures. As an example, this type of analysis was performed with each of the following three pairs of vapors, which are seen to completely co-elute in Figure 3-2: toluene + methyl isobutyl ketone (cmpds 4 and 5); n-decane + 4-ethyltoluene (cmpds 9 and 10); d-limonene + 1,2,4-trimethylbenzene (cmpds 11 and 12). Results (n=500 per mixture) indicate that toluene and methyl isobutyl ketone can be recognized as components of a binary mixture at a rate of only 86%, while the components of the other two co-eluting mixture pairs can be recognized at rates of 95% and 96%, respectively. We typically apply a minimum threshold of 95% recognition to consider the determination satisfactory.[37,39] Thus, toluene and methyl isobutyl ketone would need to be chromatographically resolved for quantitative analysis, while the other pairs would not.

Focusing on the marker compounds, it turns out that there was some difficulty in separating 2,5-DMF from TCE. Monte Carlo/EDPCR analysis indicates that if these were allowed to co-elute their recognition rate would be only 46%, highlighting the need for such separation. If the temperature program of the second column is adjusted 4-EP can be made to co-elute with 1,4-dichlorobenzene and n-undecane. However, the recognition rate for this ternary mixture is only 72%. On the other hand, 4-EP could be allowed to co-elute with n-dodecane, since they can be recognized in the binary mixture at a very high rate of 97 %. (Note: although the presence of the ETS marker could still be confirmed in many of the cases where mixture recognition was found to be low, errors in quantification are invariably incurred that lead to overestimation of the ETS marker concentration).

It is also possible to use this approach to determine if all the sensors in the array are needed for a given discrimination.[37] For the 4-EP/dodecane discrimination additional simulations were run with various subsets of the four sensors in the array and it was found that only two sensors were required: 2-sensor arrays of C8+CCN, C8+HME, and OPH+CCN performed similarly, with recognition rates of >95%. Since the LOD is affected by this, one might choose the array providing the lowest LODs, which was C8+HME for the 4-EP/dodecane case. In fact this array provided low calculated LODs

for both 4-EP (0.085 and 0.18 ppb, respectively) and 2,5-DMF (0.58 ppb and 4.1 ppb, respectively).

3.3.6 Analysis of Markers in a 36-Component Mixture

The remaining 20 vapors with $p_v > 0.1$ torr found in the field samples (Table 3-1) were then added to the test mixture and analyzed by the prototype instrument (less volatile vapors would be captured by the pre-trap). The temperature program employed was the same as that used to separate the previous subset of compounds. The chromatogram traces from the C8-coated sensor and the FID (Figure 3-3), traces from other sensors omitted for brevity) show that 2,5-DMF and 4-EP are well separated from the 34 interfering compounds and that the total elution time remains at 280 sec. Assuming a 1-L sample volume, an entire analysis, which includes sampling, separation, detection, and post-sample purging and cooling of the PCI and pre-trap, can be completed within 16 minutes.

Since it was shown above that 4-EP could be recognized in the presence of n-dodecane, the 36-component mixture was analyzed again with a sharp increase in the temperature of the second column toward the end of the elution, i.e., from 58 to 150 °C over 9 sec starting at t = 203 sec. This reduced the retention time of n-dodecane by ~40 sec and resulted in co-elution of the 4-EP and n-dodecane. The peaks were also sharpened leading to a slight reduction of both LODs. The resulting C8 chromatogram is presented as the lower trace in Figure 3-3. Thus, the separation time could be reduced by 16 % (total analysis time ~ 15 minutes) by taking advantage of the capability of the sensor array to discriminate between the components of simple mixtures.

3.4 Conclusions

The determination of two vapor-phase markers of ETS, 2,5-DMF and 4-EP (as a surrogate for 3-EP), at trace levels in complex VOC backgrounds using a uniquely-equipped portable GC prototype has been demonstrated through a series of laboratory experiments. Calculated LODs and dynamic ranges for 2,5-DMF and 4-EP, assuming a 1-L sample volume, are sufficient to determine these markers in typical environmental samples.[3-10] To our knowledge this is the first reported use of a portable direct-reading instrument for this application.

Several issues related to the adaptation of this instrument to ETS-marker determinations were addressed and successfully resolved: an adsorbent pre-trap was developed to preclude SVOCs from entering the instrument and accumulating on inlet surfaces, while permitting the more volatile compounds, including the ETS markers, to pass through and be captured by the on-board preconcentrator; a two-stage preconcentrator/injector was developed that provides quantitative trapping, high preconcentration factors, and reproducible thermal injection of markers into the separation module; independent temperature programming of the dual-column separation module was used to separate the markers from 34 interfering compounds in an elution time of < 5 min; and an integrated chemiresistor array employing functionalized gold nanoparticles interface layers was used to assist in analyte recognition and to reduce the separation time. Sensor responses and GC retention times are highly reproducible and a complete sampling and analysis cycle can be completed every 15 minutes.

Results obtained here using the surrogate marker 4-EP are expected to be representative of those for the actual marker 3-EP. From the similarity of the GC retention times and vapor pressures reported in the literature (*vida supra*), we can infer similar capture efficiencies on the carbon adsorbents used in the PCI. It is also likely that 3-EP will exhibit relatively low recoveries upon thermal desorption in air as observed for 4-EP, due to the inherent reactivity of the vinyl groups in both of these compounds. By analogy with the nearly identical response patterns reported for the dimethylpyridine isomers 2,3- and 2,4-lutidine using a polymer-coated SAW sensor array,[40] we expect response patterns for 3-EP and 4-EP to be very similar as well. Finally, since partitioning into the sensor interface layers of the CR array is governed largely by vapor pressures, the LODs for these compounds should also be similar.

Table 3-1. Average concentrations (ppb) of ETS markers and co-contaminants found in a local bowling alley using EPA TO-17.[a]

No.	Compound	p_v (torr)	Field Set 1(ppb)	Field Set 2 (ppb)
1	chloroform	197	nd	0.24
2	1,1,1-trichloroethane	124	1.1	2.1
3	benzene	95.2	2.1	4.0
4	ethyl acetate	93.7	nd	16
5	carbon tetrachloride	91	0.085	0.1
6	trichloroethylene	69	1.5	1.7
7	methylcyclohexane	46	1.2	0.75
8	toluene	28.4	50	13
9	2,5-dimethylfuran	25.9	0.56	1.2
10	methyl isobutyl ketone	19.9	2.6	1.1
11	tetrachloroethylene	13	0.78	1.2
12	n-octane	10.9	nd	1.1
13	ethylbenzene	9.6	1.2	1.5
14	p-xylene	8.8	3.7	4.2
15	m-xylene	8.3		
16	o-xylene	6.6	1.1	1.2
17	styrene	6.4	4.0	4.1
18	α-pinene	4.8	0.61	0.83
19	n-nonane	4.45	0.94	1.2
20	isopropylbenzene	3.5	0.16	0.12
21	n-propylbenzene	3.4	0.78	nd
22	4-ethyltoluene	3	4.0	1.1
23	2-ethyltoluene	2.6	1.0	0.47
24	1,3,5-trimethylbenzene	2.5	1.1	0.42
25	1,2,4-trimethylbenzene	2.1	3.8	1.3
26	d-limonene	1.98	29	29
27	sec-butylbenzene	1.75	0.060	nd
28	1,2,3-trimethylbenzene	1.7	0.73	0.67
29	3-ethenylpyridine	1.65[b]	nd	2.0
30	p-isopropyltoluene	1.46	0.19	0.52
31	n-decane	1.4	3.3	1.6
32	n-butylbenzene	1.06	nd	0.061
33	1,4-dichlorobenzene	1.0	7.5	6.9
34	n-undecane	0.41	6.6	1.3
35	phenol	0.35	nd	1.5
36	n-dodecane	0.14	4.3	1.1
37	naphthalene	0.085	0.14	2.1
38	n-tridecane	0.0558	0.98	0.47
39	nicotine	0.038	nd	nq
40	n-tetradecane	0.0116	0.73	0.62
41	n-pentadecane	0.00343	0.72	0.76
42	n-hexadecane	0.00143	0.56	0.61

[a] Vapor pressure at 25 ºC from Ref. 32; [b]See text; nd = not detected; nq = detected but not quantified.

Table 3-2. Calibration data summary for the 16 vapors shown in Figure 3-2.

#	chemical	RT/ (sec)	Within-sensor relative sensitivity[a]				LOD (ppb)[b]				Normalized response pattern[c]			
			C8	OPH	HME	CCN	C8	OPH	HME	CCN	C8	OPH	HME	CCN
1	benzene	55	1.0	1.0	1.0	1.0	0.56	1.6	3.8	12	1.0	0.96	0.89	0.70
2	tri-chloroethylene	68	1.2	1.3	1.3	1.2	0.59	1.8	3.7	9.8	1.0	0.88	0.95	0.67
3	2,5-dimethylfuran	73	1.1	0.89	1.1	1.0	0.58	1.9	4.1	14	1.0	0.74	0.83	0.61
4	toluene	95	3.8	3.2	3.3	3.2	0.12	0.43	0.94	3.2	1.0	0.80	0.77	0.59
5	methyl isobutyl ketone	95	2.1	3.2	2.4	3.4	0.38	0.55	1.7	4.0	0.69	1.0	0.68	0.78
6	ethylbenzene	120	9.6	7.3	5.3	6.3	0.060	0.24	0.73	1.9	1.0	0.73	0.49	0.46
7	m-xylene	123	12	8.2	8.6	7.9	0.053	0.21	0.47	1.6	1.0	0.65	0.63	0.46
8	styrene	132	14	13	16	13	0.052	0.16	0.33	1.1	1.0	0.84	0.97	0.64
9	n-decane	147	65	9.7	4.9	8.2	0.019	0.34	1.8	3.0	1.0	0.14	0.067	0.089
10	4-ethyltoluene	149	55	19	21	18	0.020	0.16	0.37	1.2	1.0	0.33	0.34	0.23
11	d-limonene	162	104	22	23	18	0.015	0.18	0.49	1.6	1.0	0.20	0.19	0.12
12	1,2,4-trimethylbenzene	165	40	27	21	23	0.039	0.13	0.50	1.3	1.0	0.65	0.47	0.40
13	1,4-dichlorobenzene	178	41	43	36	40	0.044	0.098	0.33	0.79	1.0	1.0	0.77	0.68
14	n-undecane	187	252	49	22	37	0.011	0.070	0.17	1.4	1.0	0.19	0.077	0.10
15	4-EP	210	61	115	163	296	0.085	0.11	0.18	0.34	0.29	0.53	0.70	1.0
16	n-dodecane	254	759	149	67	100	0.0072	0.060	0.47	0.64	1.0	0.19	0.078	0.093

[a] Values of sensitivity for all vapors from each sensor have been divided by the sensitivity value for benzene. Looking column-wise shows the range of sensitivities for each sensor among the 16 test vapors;

[b] LOD calculated as 3σ/sensitivity, where σ is the RMS baseline noise (smoothed via binomial 40 point running average with the Grams software; σ = 2.7, 6.4, 15, and 36 mV for C8, OPH, HME and CCN, respectively) and the sensitivity is determined on the basis of peak height (rather than peak area). For those vapors with non-linear calibration curves, LODs were estimated by extrapolation of the (linear) low-concentration range;

[c] Normalized response ratios, used to derive the relative response patterns in Figure 3-2, were determined by dividing the peak-area sensitivity of each sensor by the largest sensitivity value among the sensors in the array for each vapor.

(a)

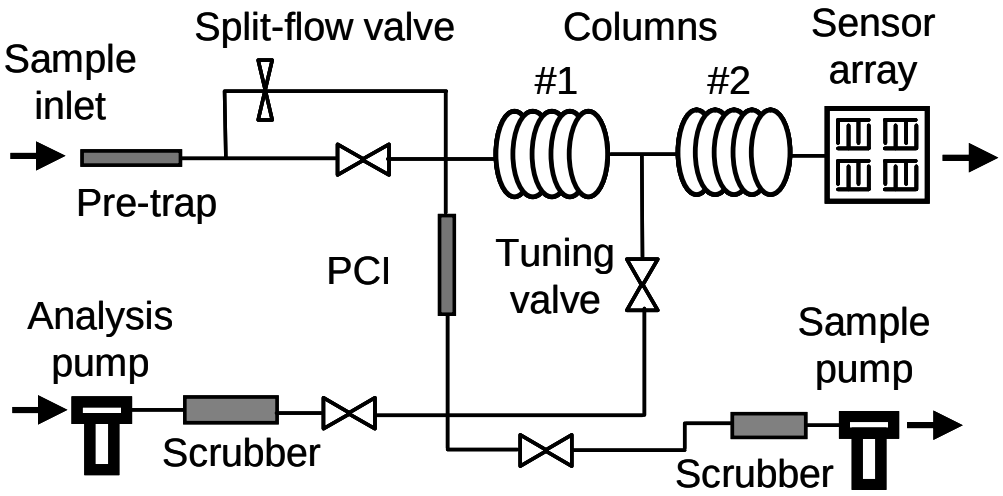

(b)

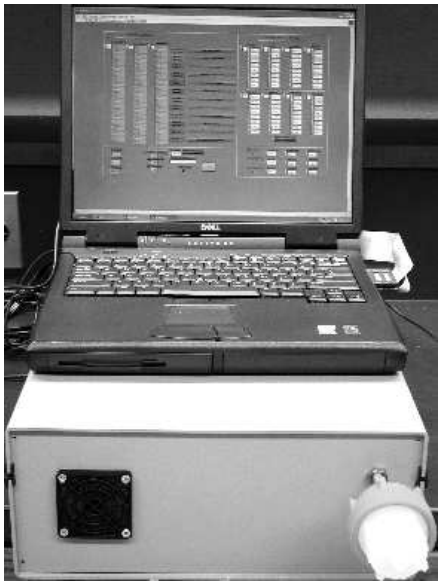

Figure 3-1. (a) Schematic of fluidic sub-system and (b) photograph of the prototype instrument beneath a laptop computer (PCI = preconcentrator/injector).

(a)

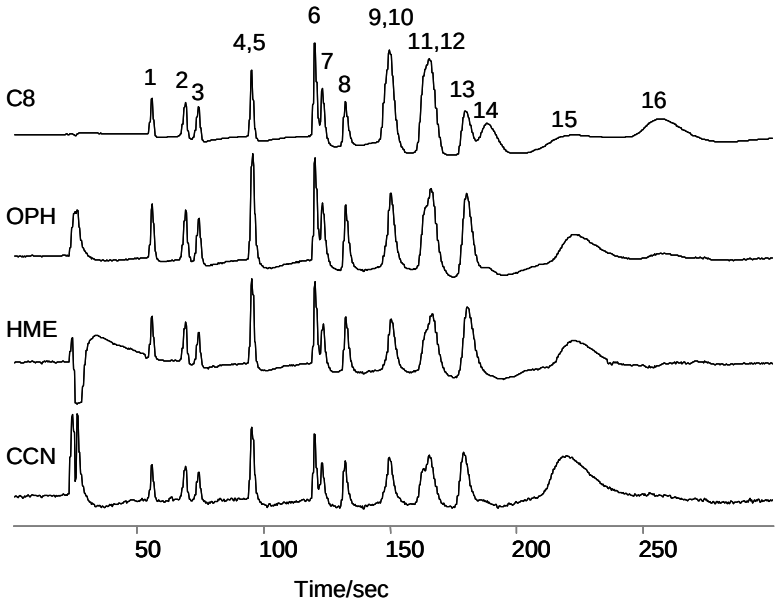

(b)

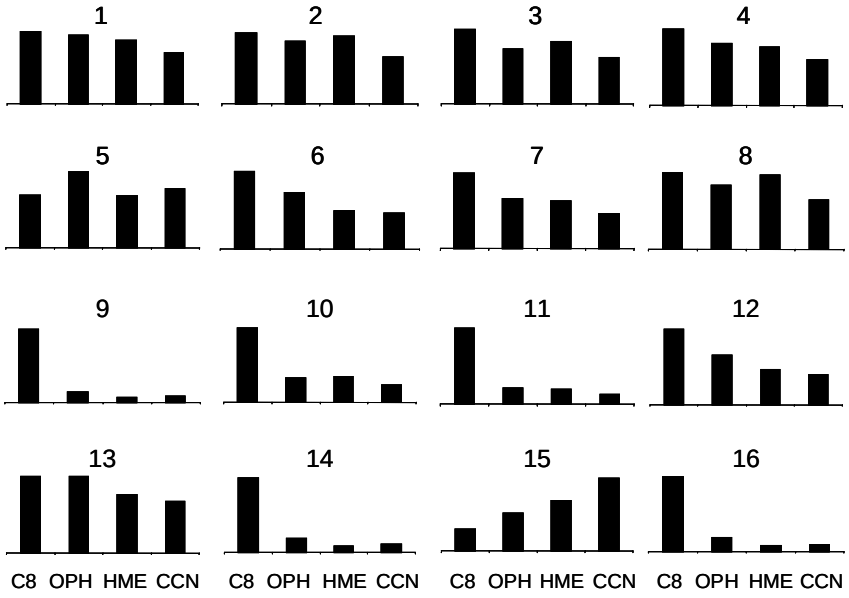

Figure 3-2. (a) CR-array chromatogram traces and (b) associated response patterns of a mixture of two ETS marker compounds and 14 co-contaminants. Numbers correspond to the compounds listed in Table 3-2. The following temperature programs were used: Column 1, 28ºC for 60s, increase to 160ºC at 2.5ºC /s, hold; Column 2, 55ºC, increase to 60ºC at 0.02ºC /s, hold. The flow rate was 1.0 mL/min and the sensor array was maintained at 21.8ºC.

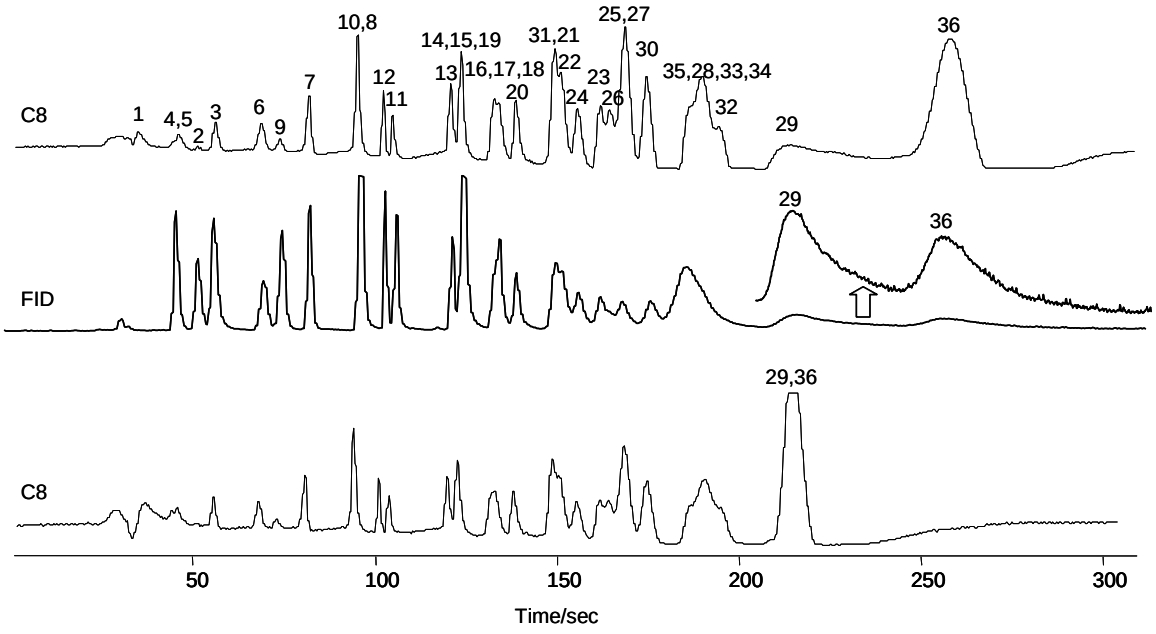

Figure 3-3. Upper trace from the C8-coated sensor shows separation of 4-EP (#29) and 2,5-DMF (#9) from 34 potential interferences in <5 minutes. Numbers correspond to the compounds listed in Table 3-1. Middle trace is from an FID used in place of the CR array for analysis of a mixture of the same compounds, excluding chloroform (inset provides enlarged view of the broad peaks for 4-EP and n-dodecane). Lower trace from the C8-coated sensor was obtained under conditions that accelerated the analysis; the contributions of 4-EP and n-dodecane to the last peak can be resolved via pattern recognition of the composite responses from the sensors in the array (see text).

3.5 References

1. International Agency for Research on Cancer, *IARC Monographs on the Evaluation of Carcinogenic Risks to Humanss*, WHO Press, Geneva, Switzerland, 2002, vol. 83.
2. Jenkins, R. A.; Guerin, M. R.; Tomkins, B. A. *The Chemistry of Environmental Tobacco Smoke: Composition and Measurement*, Lewis Publishers, Boca Raton, FL, 2nd edn., 2000, ch. 3, pp. 49.
3. Nelson, P. R.; Heavner, D. L.; Collie, B. B.; Maiolo K. C.; Ogden, M. W. *Environ. Sci. Technol*. **1992**, *26*(10), 1909-1915.
4. Hodgson, A. T.; Daisey, J. M.; Mahanama, K. R. R.; Brinke, J. Ten; Alevantis, L. E. *Environ. Int*., **1996**, *22*(3), 295–307.
5. Bohanon, H. R.; Piade, J. J.; Schorp, M. K.; Saint-Jalm, Y. *J. Exposure. Anal. Environ. Epidemiol.* **2003**, *13*(5), 378-392.
6. Hyvarinen, M. J.; Rothberg, M.; Kahkonen, E.; Mielo, T.; Reijula, L. *Indoor Air* **2000**, *10*(2), 121-125.
7. Baek S. O.; Jenkins, R. A. *Indoor and Built. Environ.* **2001**, *10*(3-4*)*, 200-208.
8. Maskarinec, M. P.; Jenkins, R. A.; Counts, R. W.; Dindal, A. B. *J. Exposure. Anal. Environ. Epidemiol.* **2000**, *10*(1), 36-49.
9. Singer, B. C.; Hodgson, A. T.; Guevarra, K. S.; Hawley, E. L.; Nazaroff, W. W. *Environ. Sci. Technol.* **2002**, *36*(5), 846-853.
10. Xie, J. X.; Wang, X. M.; Sheng, G. Y.; Bi, X. H.; Fu, J. M. *Atmos. Environ.* **2003**, *37*, 3365-3374.
11. S. M. Gordon, L.A. Wallace, M. C. Brinkman, P. J. Callahan and D. V. Kenny, *Environ. Health Perspect*., 2002, **110**(7), 689-698.
12. ASTM International. ASTM D5075-01: Standard Test Method for Nicotine & 3-Ethenylpyridine in Indoor Air; West Conshohocken, PA, 2001.
13. Harris, C. M. *Anal. Chem*. **2002**, *74*(21), 585A-589A.
14. Eiceman, G. A.; Gardea-Torresdey, J.; Dorman, F.; Overton, E.; Bhushan, A.; Dharmasena, H. P. *Anal. Chem.* **2006**, *78*(12), 3985-3996.
15. Smith, P. A.; Sng, M. T.; Eckenrode, B. A.; Leow, S. Y.; Koch, D.; Erickson, R. P.; Lepage, C. R. J.; Hook, G. L. *J. Chromatogr. A* **2005**, *1067*, 285-294.
16. Inficon Corporate, http://www.inficon.com (accessed June 2006).
17. Liu, X.; Pawliszyn, J. *Int. J. Environ. Anal. Chem.* **2005**, *85*(15), 1189-1200.
18. Dziuban, J. A.; Mroz, J.; Szczygielska, M.; Malachowski, M.; Gorecka-Drzazga, A.; Walczak, R.; Bula, W.; Zalewski, D.; Nieradko, L.; Lysko, J.; Koszur, J.; Kowalski, P. *Sens. Actuators, A* **2004**, *115*, 318-330.
19. Gao, L.; Song, Q.; Patterson, G. E.; Cooks, R. G.; Zheng, O. *Anal. Chem.* **2006**, *78*, 5994-6002.
20. Lu, C. J.; Whiting, J.; Sacks, R. D.; Zellers, E. T. *Anal. Chem.* **2003**, *75*(6), 1400-1409.
21. Lu, C. J.; Jin, C.; Zellers, E. T. *J. Environ. Monit.* **2006**, *8*(2), 270-278.
22. Zhong, Q.; Steinecker, W. H.; Zellers, E. T. manuscript in preparation.
23. Lu, C. J.; Zellers, E.T. *Analyst* **2002**, *127*, 1061-1068.
24. RVM Scientific Inc., http://www.rvmscientific.com (accessed June 2006).
25. Veriotti, T.; Sacks, R. D. *Anal. Chem.* **2001**, *73*, 814-819.
26. Cai, Q. Y.; Zellers, E. T. *Anal. Chem*. **2002**, *74*, 3533-3539.

27. Lu, C. J.; Steinecker, W. H.; Tian, W. C.; Agah, M.; Potkay, J. M.; Oborny, M. C.; Nichols, J.; Chan, H.; Driscoll, J.; Sacks, R. D.; Pang, S. W.; Wise, K. D.; Zellers, E. T. *Lab On A Chip* **2005**, *5*, 1123-1131.
28. Rowe, M. P.; Plass, K. E.; Kim, K.; Kurdak, C.; Zellers, E. T.; Matzger, A. J. *Chem. Mater.* **2004**, *16*, 3513–3517.
29. Steinecker, W. H.; Rowe, M. P.; Zellers, E. T. *J Anal. Chem*., under review.
30. U.S. Environmental Protection Agency. *TO-17, Compendium of Methods for the Determination of Toxic Organic Compounds in Ambient Air*, Report No. EPA/625/R-96/010b, 2nd edn; Washington, DC, 1997.
31. Jia, C.; Batterman, S.; Chernyak, S. *J. Environ. Monit.*, **2006**, *8*(2), 1029-1042.
32. Howard, P. H.; Meylan, W. M., Eds. *Handbook of Physical Properties of Organic Chemicals*; Lewis: Boca Raton, FL, 1997.
33. Lide, D. R. ed. *CRC Handbook of Chemistry and Physics, Internet Version 2005,* http://www.hbcpnetbase.com, CRC Press, Boca Raton, FL, 2005, sec. 3, pp 3-568.
34. Davies, C. N. *Ann. Occup. Hyg.* **1985**, *29*, 13-25.
35. Lu, C. J.; Zellers, E. T. *Anal. Chem*. **2001**, *73*, 3449-3457.
36. Zellers, E. T.; Batterman, S. A.; Han, M.; Patrash, S. J. *Anal. Chem*. **1995**, *67*, 1092-1106.
37. Park, J.; Groves, W. A.; Zellers, E. T. *Anal. Chem*. **1999**, *71*, 3877-3886.
38. Yang, C. -Y.; Li, C. -L.; Lu, C. -J. *Anal. Chimi. Acta* **2006**, *565*, 17-26.
39. Hsieh, M. D.; Zellers, E. T. *Anal. Chem*. **2004**, *76*, 1885-1895.
40. Patrash, S. J.; Zellers, E. T. *Anal. Chem*. **1993**, *65*, 2055-2066.

Chapter 4

Determination of Breath Biomarkers of Lung Cancer

Abstract

Adaptation of the second-generation portable gas chromatograph (GC) prototype instrument to determination of breath biomarkers of lung cancer is described. Seven compounds were selected as breath biomarkers based on an extensive literature review. Conditions were established to separate biomarkers from 30 interferences present in breath within 200 s. Removal of adsorbed water vapor from prconcentrator/injector (PCI) was also investigated. Purging with 500 mL dry air was found to effectively remove most of the water trapped in the PCI, with minimum loss of the marker compounds. Selected biomarkers were calibrated with the instrument. Projected detection limits ranged from 0.4 ppb (ethylbenzene-C8 sensor) to 0.2 ppm (2-methylpentane-CCN sensor), assuming a 1-L sample volume. Spiked breath samples from healthy human subjects were analyzed. Retention time and sensor response patters were used for peak identification. A fidelity test found that the marker compounds could be recognized with 95% confidence with the response patterns from only C8 and OPH sensors in the array. Measured concentrations were found to be in the same order of magnitude of the spiked values.

4.1 Introduction

Worldwide, lung cancer is the most prevalent occupational cancer. Occupational exposure to a variety of agents (e.g., asbestos, As, Be, Cd, Ni, silica, and diesel exhaust) occurs across numerous sectors and accounts for an estimated 10% of all lung cancers.[1] Detection and surgical treatment at an early stage can dramatically increase the 5-year survival rate.[2] Breath biomarker analysis has recently been cited as a promising lung cancer screening method.[3]

The use of breath as a diagnostic tool has received renewed interest in recent years as the field of metabolomics gains momentum.[4-6] With advances in instrumentation, it appears feasible to explore with greater accuracy than ever before, the correlation between clinical or pre-clinical disease states and changes in the levels of multiple breath constituents.[4,5,7] Given the rising costs of health care for an aging population, there is an increasing motivation for portable, turn-key analytical systems suitable for conducting rapid screening-level diagnostics in a hospital, clinic, or home.

The analytical challenges to using breath biomarkers as a cancer screening method are not insignificant. Although a chromatogram from the breath of an individual can contain > 150 VOCs at concentrations in the part-per-trillion range,[8,9] typically the breath in healthy individuals contain fewer than 40 VOCs at detectable levels. The study of breath VOCs as an indicator of lung cancer can be traced back to the mid-1980s.[10] Several breath VOCs have been identified as potential biomarkers of lung cancer in a number of independent studies. These include aliphatic and aromatic hydrocarbons, esters, and aldehydes,[5,11-14] which are products of lipid peroxidation of the polyunsaturated fatty acids found in cell membranes.[15] It is now generally acknowledged that no single VOC can serve as a unique biomarker, and current approaches to establishing correlations of breath biomarkers with lung cancer rely on multivariate statistical models involving groups of VOCs. As a result, sophisticated instrumentation is needed. Considered the ‘gold standard’ for multi-component analyses of volatile (or volatilizable) analytes, GC with mass spectrometer detector (GC-MS) has been the most used for investigating breath biomarkers of lung cancer.[5,11-13]

However, the GC-MS is complex, expensive, and requires a highly trained technician to operate and to interpret collected data.[6] Attempts to use electronic nose

technologies comprising standalone sensor arrays to differentiate lung cancer patients from healthy controls have been partially successful,[16-18] but have been criticized for their low sensitivity and inability to identify specific VOCs.[19] Sensors should be operated in parallel with other analytical methods if a deeper understanding is required. Micro-spectrometers are amenable to clinical breath biomarker monitoring. Unfortunately, even though progress continues toward the development of these devices based on ion-mobility,[20,21] infrared absorbance,[22,23] and mass analysis,[24,25] it is doubtful that the size, cost, and/or complexity could be reduced sufficiently to permit widespread use by the general population in the near future.

Another challenge in breath analysis is the high concentration of water vapor in breath samples. This problem includes the competition between biomarkers and water vapor for sites on the preconcentrator adsorbent, possible changes in VOC retention time on the GC column, and interference with sensor-array responses to early-eluting VOCs due to co-elution with the water peak. Different approaches have been taken to reduce the uptake of water in analytical systems. One simple option is to place a water trap, which contained hygroscopic crystals of calcium sulfate impregnated with a color indicator of water content (Dry-Rite®), in series with an adsorbent tube,[26] but some of the polar compounds can be lost also. Another simple method is to slightly heat the adsorbent trap to avoid water condensation during sampling.[8] However, the heating decreases the adsorption capacity of VOCs. To avoid the use of carbon molecular sieves which have high affinity for water vapor in the adsorbent trap is another option.[27,28] Unfortunately, carbon molecular sieves must be used when very high volatile compounds are sampled. Other adsorbent materials, like Carbotrap X which are graphitized carbons, do not have enough capacity for vapors more volatile than benzene.[29] Purging of the adsorbent with dry air prior to thermal desorption can remove most of the water from adsorbents such as XUS565[30] and Carboxen 1000,[31] and is a widely used method.

This chapter describes the adaptation of the second-generation prototype instrument to the determination of breath markers of lung cancer among a fairly complex set of interferences in synthetic and spiked breath samples. There are three major focuses. The first focus entails a critical review of literature on VOCs used as lung cancer biomarkers, and the required detection limits. Commonly encountered background

(potentially interfering) VOCs were identified on the basis of literature reports and by collecting breath samples from healthy subjects and analyzing them with a GC-MS method. The second focus involves the adjustments to the hardware, software, and operating conditions of the instrument. Efforts were made to reject as much water vapor as possible from the preconcentrated sample prior to injection into the separation stage of the instrument. Separation conditions were established to resolve biomarkers from water vapor and potential interfering VOCs. The instrument was calibrated with the biomarkers to determine sensitivities and limits of detection (LODs). Finally, the third investigation was to use the instrument to analyze breath samples spiked with biomarkers.

4.2 Experimental

4.2.1 Instrument Features and Operating Modes

Figure 2-1 shows the layout of the analytical sub-system. A detailed description of the instrument components and instrument operation was described in the experimental section of Chapter 2. Briefly the instrument has three major operating modes: Sampling, Dry-purge, Analysis. In Sampling Mode, air is drawn to the proconcentrator/injector (PCI) at a rate of 83 mL/min by the sampling pump. The PCI tube was packed, in order, with 8 mg of 40/60-mesh Carbopack B, 2.5 mg of 40/60-mesh Carbopack X, and 1.8 mg of 45/60-mesh Carboxen 1000 (separated by glass woo1), which have specific surface areas of 100, 250, and 1200 m^2/g, respectively (Supelco, Bellefonte, PA).[29] After sampling a pre-determined air volume, the sampling pump is turned off and isolated from the system by an upstream valve. A Dry-purge Mode is included during which the analysis pump draws ambient air in through a second inlet port passing it through a scrubber cartridge packed with molecular sieves and charcoal to remove water vapor and VOCs. The purified air passes through the PCI (at room temperature) to strip a portion of the water vapor from the adsorbents and to backflush it, along with any residual contaminants in the fore line, out through the sample inlet port. In Analysis Mode, the PCI is heated (via an insulated copper-wire coil) to 300 °C in < 2 sec and maintained at this temperature for 90 sec. Ambient air drawn into the system by the analysis pump is scrubbed, as in Purge Mode, and then directed through the PCI, the two separation columns, and the detector cell containing the sensor array prior to exiting the

instrument. Desorbed vapors are thereby injected onto the first of two separation columns, with the option of splitting off a portion of the desorbed flow stream (by opening the split-flow control valve) stream for the purposes of sharpening the injection band.

Each of the CR sensors in the 4-sensor array is coated with a different gold-thiolate monolayer protected nanoparticle (MPN).[32,33] MPNs derived from the following thiols were used in this study: n-octanethiol (C8), 1-mercapto-6-phenoxyhexane (OPH), 7-mercaptoheptanitrile (CCN), methyl 6-mercaptohexanoate (HME).[34] The structures of the thiolates are presented in Figure 2-2 of Chapter 2. Software written in Labview® 7.1 (National Instruments, Austin, TX) is run from a laptop computer and used to control the instrument and process the sensor output signals through separate 12 bit and 16 bit D/A data acquisition cards. Sensor output data are imported to Grams 32 (Thermogalactics, Salem, NH) for peak integration.

4.2.2 Breath Samples for the Determination of Interferences

Breath samples from five healthy subjects were collected and analyzed on two different occasions. On one occasion, two breath samples were collected from two healthy subjects. The subjects fasted at least two hours before the sample collection. Each sample was obtained following a deep breath, being held for 5 to 10 s and then exhaling slowly for 5 s to exclude the anatomical deadspace air which was ~150 mL[35] before filling a pre-cleaned 12-L Tedlar bag (SKC, Inc., Eighty Four, PA). Two duplicates of 4-L samples were collected to TO-17 adsorbent tubes from the Tedlar bag.[36] VOCs present in ambient air influence the composition and concentration of the exhaled breath.[9] Therefore it is necessary to monitor the VOCs in the environment where breath samples are taken. Indoor air samples were collected by the adsorbent tubes simultaneously when the breath samples were taken. GC-MS (Model 6890-5973, MS in Scan Mode, Agilent, Palo Alto, CA) was used to analyze the samples, and the analysis was performed by Prof. Batterman's group. The method and performance of the GC-MS system can be found in Ref 37.

4.2.3 Sample Stability in Tedlar Bags

Test atmospheres were prepared by injecting liquid samples of the seven biomarkers into a 12-L Tedlar bag prefilled with 10 L of clean dry air. The marker compounds were obtained from Aldrich (Milwaukee, WI) at ≥ 98% purity. Since these compounds were relatively volatile, their concentrations, ranging from 99 to 291 ppm, were calculated by assuming complete evaporation. At intervals of 1, 2, 2 and 3 hours samples of 0.25 mL sample were introduced to the instrument by a flow of clean air via an extra six-port valve, preconcentrated by the PCI, thermally desorbed to the columns for separation, and detected with an flame ionization detector (FID) which was installed in place of the sensor array. Three replicates were performed for each interval. Since this investigation involved only short-term storage of samples in a Tedlar bag, the samples were held for no more than eight hours.

4.2.4 Water Vapor Removal with Dry-Air Purge

Since some of the biomarkers are very volatile, Carboxen 1000 was necessary for sample preconcentration. Carboxen 1000 has a high affinity for water vapor.[27] High content of water vapor trapped in the PCI and desorbed to the columns was expected to cause several problems: 1) decrease in capacity of Carboxen 1000 for target compounds; 2) possible degradation of columns, especially the polar one; and 3) difficulty in determining early eluting peaks due to interference from the large water peak from sensors. Water vapor in the breath samples trapped by Carboxen 1000 in the PCI can be partially removed by dry-air purge prior to thermal desorption.[31] To test the efficiency of this method, a 500-mL water-saturated air sample was drawn to the PCI in the system followed by dry-air purge. The remaining water in the PCI was then thermally desorbed/injected into the columns, and detected by the CR sensor array, which was sensitive to water vapor. Water-saturated air was generated by flowing clean air from a cylinder through a fritted bubbler which contained distilled water into a Tedlar bag. After the optimal volume of air for dry-purge was determined, a 5-L water-saturated air sample containing the biomarkers of low concentrations were tested with and without dry-purge. A sample volume of 5 L was the anticipated value for actual breath samples based on the

LODs of the sensors. By comparing the peak area from the CR sensors of the biomarkers obtained from tests with and with without dry-purge the sample loss was evaluated.

4.2.5 Instrument Calibration

Test atmospheres containing biomarkers were generated in Tedlar bags with concentrations ranged from 69 to 1180 ppm, depending on the vapor pressures. Conditions were established for separating the marker compounds in a minimum analysis time. These biomarkers were divided into two non-coeluting subsets for calibration. The sample inlet of the instrument was connected to an external auto-sampler, which was designed specifically to aid in laboratory testing of the instrument. This auto-sampler employed a low-dead-volume 6-port valve (Model EH4C6WE, Valco Instruments Co. Inc., Houston, TX) and a KNF mini-diaphragm pump. This auto-sampler was controlled by Labview. During sample collection, the 6-port valve was set at the injection position, and 1 L of scrubbed air was drawn at 83 mL/min. The air was passed through the sample loop pre-loaded with vapors, and through the PCI where the vapors were trapped on the adsorbents. The sample loop volume ranged from 10 μL to 2 mL. Effective (mass-equivalent) vapor concentrations were calculated according to the ratio of injection and sample volumes. For example, an aliquot of 1 mL from a sample loop containing 100 ppm of vapors is equivalent to 100 ppb in a sample volume of 1 L. The calibrated equivalent concentrations ranged from 0.7 – 2360 ppb for 1-L sample. There were four replicates for each challenge concentration.

4.2.6 Analysis of Spiked Breath Samples

Using the procedure described in Section 5.2.2, breath samples from healthy subjects were collected in 12-L Tedlar bags. Mixtures of seven biomarkers alone, or seven biomarkers plus 30 interferences of ppm concentration level were prepared in a separate 12-L Tedlar bag, using the procedure described in the Section 5.2.5. Fifty mL of this high concentration vapor was spiked to another 12-L Tedlar bag prefilled with 10 L clean air for dilution. Next, 50 mL of these diluted vapors were spiked into the Tedlar bag prefilled with breath samples. Spiked breath samples of 5 L were introduced to the instrument followed a dry-purge, then were analysized.

4.3 Results and Discussion

5.3.1 Breath Biomarkers of Lung Cancer

A number of studies have been carried out in order to investigate the relationship between lung cancer and certain VOCs from breath. Conclusions from these studies are not entirely consistent, and the identity of VOCs as biomarkers of lung cancer has not been clearly established.[16] Most of the studies later than 1999[11,38,39] chose marker compounds based on the 1999 study of Phillips et al.[12] Table 4-1 lists the VOCs which were found to be associated with lung cancer in a few representative studies. From this table, the inconsistency in selecting biomarkers is obvious, and no single VOC can serve as the breath biomarker of lung cancer. Instead, a set of VOCs must be used to developed statistical models for screening purposes.

A recent paper by Poli et. al.[11] selected compounds mostly based on the Phillips's study (1999).[12] This paper not only identified, but also quantified the selected VOCs. This has been the most persuasive study on this subject by far. Therefore our study focuses on biomarkers of lung cancer based on the finding of the Poli paper. By assigning scores to the compounds based on their concentration difference between non-small cell lung cancer (NSCLC) patient group and the other three groups, i.e. chronic obstructive pulmonary disease (COPD) group, smoker group, and control group, compounds were selected based on the total scores. Scoring rule was: score = 1 when the concentration found from the NSCLC patient group was significantly different than that found from one other group; score = 0 when the concentration difference was insignificant. Using this rule, four compounds are selected: 2-methylpentane, and ethylbenzene, toluene, and benzene. Considering other studies, four additional endogenous compounds often cited as biomarker of lung cancer were also included in the investigation. These included isoprene,[12-13] pentane,[5,11] and ethylpropionate.[13] Although several studies have shown that isoprene, which always exists in breath, was not significantly associated with lung cancer,[11] increased level of this compound can serve as an indicator of some health effects.[40] Therefore, isoprene was also selected in our target list.

In summary, four endogenous compounds: isoprene, pentane, 2-methylpentane, heptane, ethylpropionate, and three smoking-related compounds: benzene, toluene, ethylbenzene were selected as the breath biomarkers of lung cancer.

4.3.2 VOC Profiles from Breath Samples of Healthy Subject

The GC-MS analysis found 63 compounds at least once from the eight breath samples collected from five healthy subjects, with sample volumes ranging from 2.5 to 5.0 L. Note that the compound identification was based on both of calibration and ion library search. Among these, 19 compounds were detected at ≥ 50% frequency, only d-limonene was detected from all the samples. Thirty-five compounds had concentration ≤ 1.0 $\mu g/m^3$, with highest being 80.6 $\mu g/m^3$ (33.9 ppb) for acetone. From the six indoor air samples collected simultaneously with the breath samples, with sample volumes ranging from 2.0 to 4.0 L, 48 compounds were detected at least once. Among these, 28 compounds were detected at ≥ 50% frequency, 12 compounds were detected from all the samples. The highest concentration was 42.0 $\mu g/m^3$ (14.2 ppb) for butanone.

Comparing the breath and indoor air VOCs, it was found that the former was significantly influenced by the latter. Therefore, the indoor air VOCs should be considered. These critera were set to determine the interferences: 1) detected at ≥ 50% frequency in all eight breath samples; 2) detected at ≥ 50% frequency in all six lab air samples; 3) detected at least once from the breath with retention times within those of 1) and 2). Based on these criteria, 30 compounds were selected as the interferences in this project. These compounds are listed in Table 4-2, along with the marker compounds. In total there are 37 compounds with 6500-fold range in vapor pressures. Six of these 37 compounds were detected once. It should be noted that four of the biomarkers (isoprene, benzene, toluene, and ethylbenzene) also matched these critera. Concentration ranges found from the breath and lab air samples are given in this table. Concentrations of the biomarkers found in breath samples from Ref. 11 are also listed. The concentrations found in the literature investigation are higher than those found from our samples.

4.3.3 Sample Stability in Tedlar Bags

Tedlar bags are made of polyvinyl fluoride (PVF), and water vapor can permeate through the PVF film when there is a concentration gradient between the air inside the

bag and ambient air.[41] Studies by Groves et. al. showed that Tedlar bags are suitable for collecting breath samples due to its water removal capability through permeation and minimum sample loss.[42]

Since sample loss due to storage in the Tedlar bag depends on the types of vapors, it was necessary to investigate the possible sample loss of the biomarkers. As shown in Figure 4-1, within eight hours of storage in a Tedlar bag, the peak area (from FID) was relatively stable. The exception was ethylpropionate, whose peak area increased by 23%, peak area changes of all the others ranged from 4% to 15%. No appearant trend of sample loss with increasing storage time was found. These results matched the literature that the storage in Tedlar bags resulted in only small, if any, sample loss for non-polar compounds.[43]

4.3.4 Water Vapor Removal by Dry-Air Purge

As shown in Figure 4-2, without dry-air purge the water peaks from a water-saturated air sample of 0.5 L from all the four sensors were extremely large, especially from the HME sensor, which was out of the detection range of the circuitry. The baseline of HME did not recover until 280 s, and it took ~160 s for baselines of the other three sensors to recover. Another big problem associated with the large water peak was that early eluting biomarkers, such as isoprene, pentane, 2-methylpentane, benzene would merge or be lost in the water peak, making it difficult to analyze the peaks of these compounds.

With a purge volume of 500 mL, most of water was removed from the PCI, with a removal rate of 87% (average of C8, OPH, and CCN, standard deviation ±3.7%), and it took 42, 60, 128, and 85 s for the baseline of C8, OPH, HME, CCN, respectively, to recover. Increasing the purge volume to 1 L and 5 L did not further increase the water removal rate.

The potential loss of VOCs due to dry-purge was investigated. The seven biomarkers of high concentrations were injected to a 12-L Tedlar bag prefilled with water-saturated clean air. The final concentrations were in a range of 6-21 ppb for isoprene, pentane, 2-methylpentane, benzene, heptane, ethylpropionate, toluene, and ethylbenzene, respectively. Samples of 5 L were analyzed with and without purging with 0.5-L dry air. Chromatograms from these two analyses are shown in Figure 4-3. As seen

from the figure, without dry-purge, all the peaks of biomarkers were affected by the huge water peak with HME sensor, seven were affected with CCN sensor, six were affected with C8 and OPH sensors. It was impossible to obtain the peak information of the early eluting compounds, especially isoprene, pentane, and 2-methylpentane. Only peaks of toluene and ethylbenzene could be correctly integrated. By comparing the peak areas from these two analyses, sample loss of toluene was 17% (average of C8 and OPH, with a standard deviation of 4.2%) due to dry-purge, and the loss of ethylbenzene was 23% (average of C8 and OPH, with a standard deviation of 0.6%).

Comparing the chromatograms of a dry sample and a 5-L water-saturated sample with dry-air purge, as shown in Figure 4-4, no retention time shift was observed associated with the latter sample and dry-purge. However, band broadening of benzene was observed. According to the expected vapor distribution on this three-stage adsorbent PCI,[29] benzene is the most volatile compound captured by Carbopack X. With the presence of high content of water vapor, Carbopack X which has low water affinity can adsorb some amount of the moisture,[44] and benzene vapor might be displaced to the downstream Carboxen 1000 during sampling. During dry-purge which was at the opposite direction of sampling, part of the benzene vapor trapped on Carboxen 100 might be swept back to Carbopack X. Each of the factors, i.e. benzene being trapped on and desorbed from Carboxen 1000, and it being distributed on the two adsorbents, could cause band broadening of benzene peak. Peak shapes of later eluting compounds which were mainly captured by Carbopack B were not affected by the presence of water and dry-purge process.

4.3.5 Instrument Calibration with Biomarkers

The strategy was to separate the marker compounds from each other and from the interferences while minimizing the analysis time. With this in mind, since more than half of the interferences had lower vapor pressures than ethylbenzene which was the least volatile biomarker, it was possible to increase the column temperature after ethylbenzene eluted, and accelerate the elution for all of the interferences which elute after ethylbenzene. A set of conditions were established under which the total separation time was less than 200s for the 37-component mixture. Isoprene and pentane coeluted. With the presence of water, these coeluting peaks further coeluted with water. Compared with

the CR response to water, the responses of these two compounds were very small. Increasing the concentrations of these compounds during calibration did not have an impact on the area of the coelutiong peak. Therefore, it was concluded that the instrument in the current status of development was not able to analyze these two marker compounds. The other five biomarkers were well separated from each other and from the interferences. Figure 4-4 shows the CR chromatograms for the 37 compounds from a dry sample. Note that even with a dry sample, water peak was always present in the chromatograms due to the permeation of water from ambient air into the Tedlar bag.

In the course of this study, two different CR arrays were used, with both having the same coating, i.e. C8, OPH, HME, and CCN. The first array was broken due to an accident, and the other array was made and used in the test. With the first array, calibrations were performed with concentrations at 50- or 200-fold ranges, depending on the sensitivity of a specific compound. There were seven concentration levels, each having four replicates. For the reason mentioned above, isoprene and pentane were excluded for the construction of the calibration curves. Responses from all the CR sensors were generally reproducible (RSD < 10% for four replicates), except the lowest concentration point at which there was sensor response (RSD ranged from 20-40%). Plots of peak area versus vapor concentration were generally linear except for two combinations which were toluene-CCN, and ethylbenzene-OPH, whose R^2 of calibration curves were 0.94, and 0.97, respectively. The R^2 of calibration curves for all the other vapor-sensor combinations were >0.99.

After the accident, calibration was performed with the second sensor array. Calibration data reported below were obtained with the second sensor array. Assuming the good linearity and precision were also obtained with the second array, in order to reduce time in this study, the calibration was performed with only three concentration levels, with a 20-fold range. There were four replicates for each concentration level. As expected, responses were reproducible, with an RSD < 10% for all the concentration levels. Calibrations curves were all linear (R^2 >0.99).

The sensor response sensitivity generally increases as the vapor pressure of the analyte decreases, as expected for the sorption-based sensor responses.[32,33] The relative sensitivities of the marker compounds for the same sensor were listed on Table 4-3.

Sensitivities of ethylbenzene from C8, OPH, HME, and CCN were 51, 88, 101, and 66 times higher than those of 2-methylpentane, respectively. Also listed on Table 4-3, cross-sensor sensitivity ratios were obtained by dividing sensitivities (calibration slopes of peak area vs. concentration) for a given vapor by that for the most sensitive sensor in the array. These ratios were the relative response patterns of the compounds. Plotted as bar charts, the response patterns were given in Figure 4-5. Vapors from the same functional group classes have similar patterns, e.g. benzene, toluene, and ethylbenzene. These response patterns can be used together with retention times to identify vapors.

Limits of detection (LODs) were determined by multiplying the standard deviation of baseline for each sensor by a factor of three and then dividing by the slope of calibration curve constructed by the peak height vs. concentration. LODs of these marker compounds from this new array were somewhat higher than those from the previous array. Except for 2-methylpentane, LODs of C8, OPH, and CCN ranged from 0.32 to 5.7 ppb, assuming a 1-L sample. CCN had the highest LODs, due to its highest noise level and relatively lower response, ranging from 5.5 to 20 ppb (excluding 2-methylpentane). LODs of 2-methylpentane were very high, ranging from 10 ppb from C8 to 208 ppb from CCN. LODs for the five biomarkers are listed on Table 4-3. With these LODs, relatively large sample volumes are required. By comparing these LODs and the concentrations found by Poli et al,[11] listed on Table 4-2, if only the most sensitive sensor, i.e. C8, was used, a sample size of 3 L was necessary. If detection by all the sensors in the array is required, the sample volume must be increased to 61 L.

4.3.6 Fidelity Test of Sensor Response Patterns for Vapor

As described in Section 5.3.5, for a specific vapor, responses (sensitivities) from different sensors in the array were not the same. This was based on the differential vapor-sensor interaction. A sensor response pattern can be treated as a crude spectrum, and be used for vapor recognition. As seen in Figure 4-5, response patterns of vapors from the same chemical class are similar. Fortunately, GC separation of the homologous vapors is readily achieved. For vapors completely resolved by GC columns, response patterns add one more dimension on top of retention time to determine the analytes. Pattern recognition for a simple coeluting mixture is also possible by determining the contribution of the components in the mixture to the composite response pattern they

produce.[33] In our case, after excluding isoprene and pentane, the remaining five biomarkers were fully separated from each other, and from the 30 possible interferences. Therefore our focus is on the pattern recognition for single vapors.

When dealing with an actual field sample, to assign a peak at a certain retention time or a retention time window, in the case of coelutions, which is defined as the retention time range covering the specific coeluting peaks, is by comparing the measured response pattern to the response pattern from the calibration. Since deviation of response pattern occurs due to the fluctuation in sensor response under different environmental conditions or by the sensors themselves, one big question to ask is how much deviation can be tolerated, or how much confidence we have in this assignment. To answer this question, i.e. to reliably identify resolved peaks, it is required to place a statistical threshold on the allowable degree of deviation in response patterns, and a pattern fidelity test should be performed. Recently a multivariate statistical goodness-of-fit method was successfully applied to the test of pattern fidelity for vapor recognition with response patterns from a polymer-coated surface acoustic wave (SAW) sensor array.[45] Details of this fidelity test can be found in Ref. 45. The follow text is the brief description of this method. “Calibration data are used to define clusters in the 3-dimensional space whose boundaries are defined by the spread among replicate sensor array response vectors for a given vapor over the range of calibrated concentrations. The Mahalanobis distance is calculated and used to establish a spatial threshold (boundary) for deciding whether subsequent sample vectors fall within an acceptable distance from the cluster mean to be considered to have been generated by the vapor corresponding to that cluster. In order to establish decision rules with known error rates, the *F* statistic is used, with the degree of freedom determined by the sample size and number of sensors in the array. A confidence level of 95% was selected in all cases.”

In our study, the same fidelity test method was used. First 12 sets of calibration response patterns (relative sensitivity ratio) for each marker compound were used to determine the spatial threshold. A fidelity test was performed for each of the data set in order to examine the reliability of these thresholds. For all the 12 data sets of each compound tested, there was at most only one data set, which was obtained with the lowest or highest concentration level for the calibration, that was not within the threshold.

Therefore the threshold was regarded reliable. Then these thresholds were used for the fidelity test of measured response patterns from breath samples of healthy subjects spiked with lung cancer biomarkers, or spiked with both of biomarkers and possible interferences.

The sample volume of each analysis was 5 L, and a dry-purge using 500-mL of clean dry air was applied to each sample after the cycle. Five breath samples were spiked only with the biomarkers, and four with both biomarkers and the 30 interferences. The spiked concentrations varied from sample to sample. Listed on Table 4-4, spiked concentrations were estimated ranging from a few ppt to 100 ppb, most of which were greater than the 5-L LODs (5-L LOD equaled to LOD of 1-L sample divided by 5). The exact volumes of breath samples collected in the 12-L Tedlar bag were not know, but estimated to be between 10 to 12 L. The spiked concentrations were calculated based on a volume of 10 L, and for a 12-L volume the concentrations were decreased by 17%. The concentration ranges were reported on Table 4-4. Thirty-six chromatograms were generated from the four sensors for the nine samples. Looking at the chromatograms, no significant peaks outside of the retention time windows of spiked compounds were observed, indicating that the breath samples were very ‘clean’ or the concentrations of VOCs in the breath samples were below the 5-L LODs. Besides peaks of isoprene and pentane, peak of 2-methylpentane was also found to completely overlap with the big water peak from all sensors even with dry-purge, and was not included in the fidelity test.

Results of fidelity test for the remaining four biomarkers, benzene (BZ), ethylpropionate (EPRO), toluene (TOL), and ethylbenzene (EBZ) from the nine spiked breath samples are listed on Table 4-4. Responses from all the four sensors were used to construct the response pattern of the 4-sensor array, and if peaks were too small, and integration was not possible, peak area was assigned zero. Fidelity test found that none of the nine response patterns of benzene from the nine samples were within the 95% confidence level. Better results were obtained for ethylpropionate, ethylbenzene, and especially toluene. Seven out of nine patterns of toluene were recognized within 95% confidence level. It was obvious that water peak interfereed peaks of benzene, ethylpropionate from HME and CCN, resulting in poor results of fidelity test. The water peak effect on benzene was the most serious. The benzene peak was much broader from

samples of high relative humidity (RH), and under dry-purge process, as explained in Section 5.3.4, but the calibration was performed with dry samples. The detectability of much broader peaks from HME, and CCN which were less sensitive than C8, and OPH decreased. There were only two measurable peaks of benzene from HME for all the nine samples. CCN had no measurable peaks at all. As stated before, the response of non-detectable peak was assigned zero at the pattern. Therefore none of patterns from the 4-CR array matched the response patterns generated from calibrations at all. If only the response from C8 and OPH were used to generate response pattern, the fidelity test showed that 100% of the measured patterns were within the 95% confidence level of the threshold. Similarly, for the other three biomarkers, low responses from HME and CCN were due to low concentration and were also the cause of < 100% recognition. If only responses from C8 and OPH sensors are considered, all the measured patterns were within the 95% confidence level of the threshold. The results from the fidelity test indicated that first, detectable responses from all the sensors were required if the fidelity test was performed with the patterns from the 4-sensor array from calibrations; second, an array containing only C8 and OPH sensors were adequate for response pattern recognition for these resolved marker compounds.

4.3.7 Quantification of Biomarkers from Spiked Breath Samples

Concentrations of the biomarkers in the spiked breath samples of Section 5.36 were estimated by combining responses from all the sensors in the array with following equation:[46]

$$C_i = \frac{(M_{i1}S_{i1} + M_{i2}S_{i2} + M_{i3}S_{i3} + M_{i4}S_{i4})}{(S_{i1}^2 + S_{i2}^2 + S_{i3}^2 + S_{i4}^2)} \qquad (1)$$

where C_i is the concentration of vapor i, M_{ij} is the response of each sensor j, and S_{ij} is the sensitivity (slope of the calibration curve). If there was no peak or the peak from a specific sensor was not detectable, the M and S of this sensor was not included in the equation. This calculated concentration was then corrected by the sample loss due to dry-purge (Section 4.3.4), which was 23% and 17% for ethylbenzene and toluene, respectively. Since the sample loss for benzene and ethylpropionate was not able to obtained, an arbitrary value 17% was chosen. Quantification results were not satisfactory, with most of measure concentrations being lower than the spiked concentration, and with

most of the measurement errors being greater than 20% (Table 4-4). The negative bias in most of the measured concentrations was possibly due to the difference in procedures of calibration and analysis of spiked breath sample. First, the calibration was performed with high concentrations, i.e. ppm level and small sample injection (< 1 mL). While the analysis of spiked breath samples were performed at low concentrations, i.e. ppb levels, and large sample volumes (5 L). The adsorption efficiency of the PCI might be lower for the very diluted breath samples than the samples of high concentrations for calibration. Second, the investigation of possible sample loss due to storage in Tedlar bag was performed with dry samples of high concentrations (ppm levels), and no sample loss was found due to storage within the 8-hour period. Sample loss for the spiked breath samples at very low concentrations and high humidity condition might occur.

4.4 Conclusions

This study has explored the application of the second-generation instrument to the determinations of breath biomarkers of lung cancer. Several challenges were encountered in this project and were overcome. The first challenge was the selection of the breath biomarkers of lung cancer. Seven compounds were selective based on literature review. The second issue was associated with the high water content present in breath sample. Without any water rejection method, it was impossible to detect most of the marker compounds. The majority of water vapor adsorbed in the PCI was removed by dry-air purge, with minimum sample loss of the biomarkers. The third challenge was to separate the biomarkers from interferences in the breath samples. Good resolution was obtained for the biomarkers among possible interferences. Less than 200 seconds were required for the separation of a 37-compound mixture. Analysis of breath samples from healthy subjects spiked with biomarkers and possible interferences provided an estimation of how accurate the determinations of biomarkers with actual breath samples could be. A fidelity test showed that response patterns from only C8 and OPH in the array could be used with the retention times (windows) to identify the marker compounds successfully. Concentrations measured by the responses from the sensor array were in the same order of magnitude of the spike concentraions, although negative bias was found for most of the samples.

Two significant issues have not been resolved with this study. First, although most of the water was removed by dry-purge, the remaining water peaks from all four sensors, especially HME, were still relatively large. This directly resulted in the difficulty to determine three of the seven biomarkers, isoprene, pentane, and 2-methylpentane which coeluted with water. It is necessary to investigate another method to remove the water vapor completely from the sample before it is introduced to the system. Alternatively, avoiding MPNs with polar functionality can help to reduce the water peak problem. Secondly, although prevalent concentrations of biomarkers are unknown, it is expected that they would be low. Because of this low concentration, it is necessary to improve the LODs of this system in order to collect sample relatively small volumes. Benefits from small sample volumes include reducing the burden of water removal, and the sampling time, which reduces the total analysis time.

Table 4-1. VOCs selected as marker compounds from literature.

	Marker VOCs from breath for lung Cancer from literature				
#	O'neill et al., 1988[13]	Phillips et al., 1999[12]	Phillips et al., 2003[5]	Deng et al., 2004[38]	Poli et al., 2005[11]
1	acetone	3-methylnonane	4-methyloctane	hexanal	1,2,4-trimethylbenzene
2	methyl isobutenoate	1,2,4-trimethylbenzene	butane	heptanal	2,2,4,6,6-pentamethylheptane
3	acetophenone	1,4-dimethylbenzene	2-methylhexane		2-methylpentane
4	alkyl benzene (C9H12)	1-heptene	3-methylhexane		benzene
5	alkyl benzene (C9H12)	1-hexene	3-methyltridecane		decane
6	benzaldehyde	1-methyl-2-pentylcyclopropane	5-methyldecane		ethylbenzene
7	benzene	1-methylethenylbenzene	7-methyltridecane		heptane
8	butanone	2,2,4,6,6-pentamethylheptane	heptane		isoprene
9	dichlorobenzene	2,4-dimethylheptane	pentane		octane
10	dichloromethane	2-methylheptane			pentane
11	ethylbenzene	3-methyloctane			styrene
12	ethylpropanoate	benzene			toluene
13	hexane	cyclohexane			xylenes
14	isoprene	decane			
15	methyl naphthalene	hepatanal			
16	methylethylbenzene	hexanal			
17	methylpentane	isoprene			
18	naphthalene	methylcyclopentane			
19	nonanal	propylbenzene			
20	phenol	styrene (ethylbenzene)			
21	propenal	trichlorofuoromethane			
22	styrene	undecane			
23	tetrachloroethylene				
24	toluene				
25	trichloroethane				
26	trichlorofluomethane				
27	trimethylbenzene				
28	trimethylheptane				

Table 4-2. Breath biomarkers and interferences.

#	compound	RT/s[a]	P_v (torr)[b]	highest conc. (ppb)[c] breath[c]	indoor[d]	lit.[e]	#	compound	RT/s	P_v (torr)	highest conc. (ppb) breath	indoor
1	**isoprene**	29	551	13	nd	147	20	p-xylene,m-xylene	145	8.29	0.014	0.028
2	**pentane**	31	514	nd	nd	16	21	o-xylene	150	6.61	0.053	0.062
3	**2-methylpentane**	37	211	nd	nd	3.4	22	styrene	150	6.4	0.014	0.028
4	acetone	41	231	34	0.0084		23	3-heptanone	150	2.6	0.34	nd
5	ethylacetate	44	93.7	0.90	nd		24	n-nonane	150	4.45	0.21	0.074
6	butanone	45	95.3	0.91	14		25	a-pinene	163	4.75	0.59	0.022
7	tetrahydrofuran	47	162	0.73	11		26	n-propyl benzene	165	3.42	0.024	0.010
8	**benzene**	53	95.2	0.27	0.38	2.3	27	4-ethyl toluene	168	3	0.077	0.041
9	trichloroethylene	63	69	0.13	0.061		28	1,3,5-trimethylbenzene	170	2.48	0.016	0.014
10	n-heptane	70	46	0.54	0.12		29	2-ethyl toluene	173	2.61	0.018	0.016
11	**ethylpropanoate**	71	35.8	nd	nd		30	1,2,4-trimethylbenzene	179	2.1	0.051	0.049
12	**toluene**	91	28.4	0.31	0.50	3.9	31	n-decane	179	1.43	0.15	0.034
13	hexanal	106	11.3	0.29	0.46		32	d-limonene	180	1.98	4.8	0.108
14	1-octene	110	17.4	0.48	nd		33	p-isopropyltoluene	180	1.46	0.23	0.0018
15	tetrachloroethene	116	18.6	0.027	0.016		34	1,2,3-trimethyl benzene	183	1.69	0.018	0.016
16	n-octane	167	14.1	0.20	0.12		35	benzaldehyde	185	0.127	0.45	0.31
17	nonanal	118	0.37	0.66	0.60		36	n-dodecane	191	0.136	0.085	0.033
18	chlorobenzene	134	12	0.054	0.0087		37	naphthalene	198	0.085	0.015	0.015
19	**ethylbenzene**	142	9.6	0.046	0.064	0.6						

[a] Retention times from correspond to those from Figure 4-3; [b] vapor pressure at 25 ºC from Ref.47; [c] highest concentration from breath samples detected with GC-MS; [d] highest concentration from indoor air samples detected with GC-MS; [e] Median concentration found from patients of lung cancer from Ref. 11; nd = not detected; compounds in bold fonts are selected as biomarkers of lung cancer.

Table 4-3. Calibration data summary of five biomarkers shown in Figure 4-5.

#	RT/s	Vapor (abbreviation)	LOD (ppb)[a]				Within-sensor relative sensitivity[b]				Normalized response pattern[c]			
			C8	OPH	HME	CCN	C8	OPH	HME	CCN	C8	OPH	HME	CCN
3	25	2-methylpentane (2MPEN)	10	28	84	208	1.0	1.0	1.0	1.0	1.0	0.55	0.45	0.27
8	35	benzene (BEN)	1.6	2.3	5.7	20	6.1	10	13	13	1.0	0.90	0.96	0.57
11	47	ethyl propionate (EPRO)	1.0	1.1	2.9	10	8	17	22	20	0.81	0.94	1.0	0.55
12	60	toluene (TOL)	0.58	0.84	2.3	9.9	21	33	39	25	1.0	0.86	0.85	0.33
19	100	ethylbenzene (ETB)	0.32	0.44	1.3	5.5	51	88	101	66	1.0	0.94	0.90	0.35

[a] LOD calculated as 3σ/sensitivity, where σ is the RMS baseline noise (smoothed via binomial 40 point running average with the Grams software; σ = 2.4, 2.8, 8.4, and 14 mV for C8, OPH, HME and CCN, respectively) and the sensitivity is determined on the basis of peak height (rather than peak area).

[b] Values of sensitivity for all vapors from each sensor have been divided by the sensitivity value for 2-methylpentane. Looking column-wise shows the range of sensitivities for each sensor among the five biomarkers.

[c] Normalized response ratios, used to derive the relative response patterns in Figure 4-5, were determined by dividing the peak-area sensitivity of each sensor by the largest sensitivity value among the sensors in the array for each vapor.

Table 4-4. Response pattern recognition and concentrations of spiked breath samples.

Breath sample[a]	Spiked conc. (ppb)[b]				Measurement error (%)[c]				4-CR array Pattern kept at 95% confidence level?				2-CR array[c] Pattern kept at 95% confidence level?			
	BZ	EPRO	TOL	EBZ	BZ	EPRO	TOL	EBZ	BZ	EPRO	TOL	EBZ	BZ	EPRO	TOL	EBZ
S1	11	8.8	3.8	3.3	6.9	19	54	44	no	yes	yes	yes	yes	yes	yes	yes
S2	11	8.8	3.8	3.3	-47	-36	-47	-22	no	no	yes	yes	yes	yes	yes	yes
S3	11	8.8	3.8	3.3	-26	-13	-1.2	9.2	no	no	yes	yes	yes	yes	yes	yes
S4	11	8.8	3.8	3.3	-34	-37	3.5	-8.0	no	yes	no	yes	yes	yes	yes	yes
S5	84	83	34	4.1	-77	-73	-65	-59	no	no	yes	yes	yes	yes	yes	yes
S6	0.8	0.83	0.33	0.05	-100	6.7	322	281	no	no	no	no	yes	yes	yes	yes
S7	4.1	4.2	1.6	0.25	-78	-42	17	38	no	no	yes	no	yes	yes	yes	yes
S8	4.1	4.2	1.6	0.25	-51	-57	32	21	no	no	yes	no	yes	yes	yes	yes
S9	84	83	34	4.1	-89	-73	-63	-56	no	no	yes	no	yes	yes	yes	yes
							Count of "yes"		0	2	7	5	9	9	9	9
							Percentage for "yes"		0%	22%	78%	56%	100%	100%	100%	100%

[a] Samples S1-S5 only spiked with biomarkers; Samples S6-S9 spiked with both biomarkers and 30 interferences; Except ethylbenzene (EBZ) in samples S6-S8, spiked concentrations are > LODs (for 5-L sample) from all sensors.
[b] Approximated spiked concentrations, see Table 4-2 for compound names.
[c] Measurement error (%) = (measured conc. – spiked conc.) x 100/spiked conc.
[d] Responses from C8 and OPH sensors in the array were used for fidelity tests.

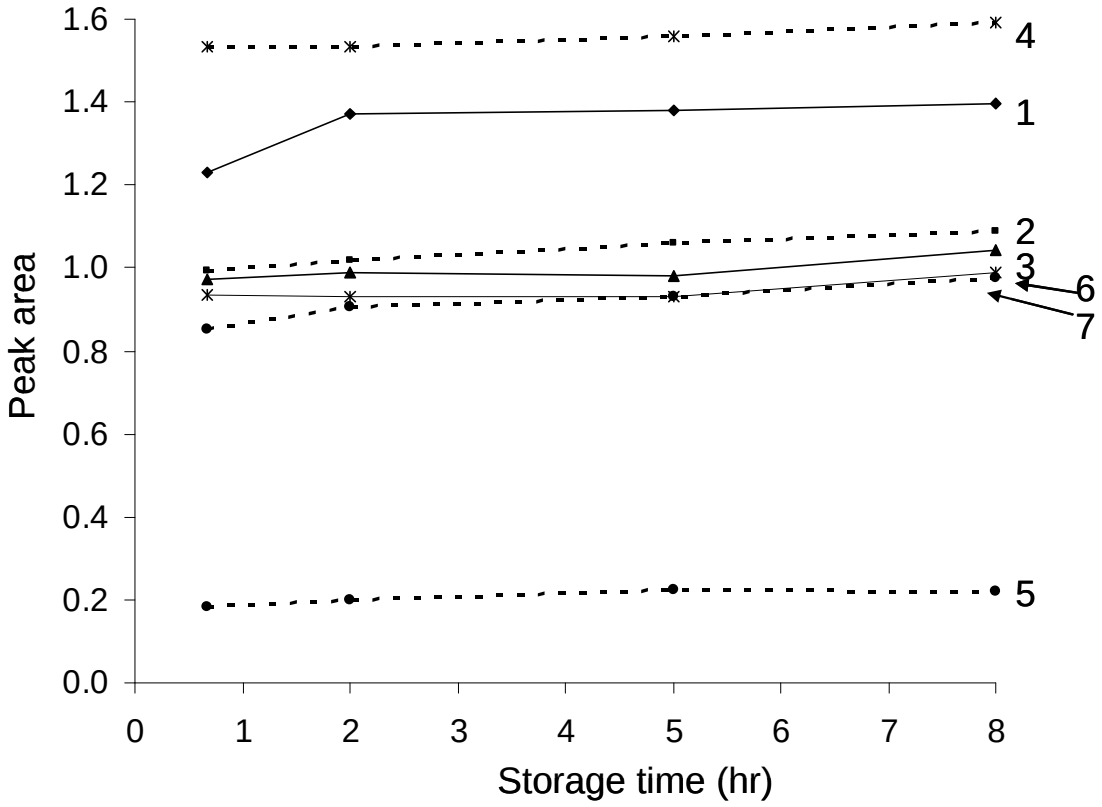

Figure 4-1. Stability of marker compounds stored in a Tedlar bag within eight hours. Samples were detected with FID which replaced the sensor array in the instrument. Compounds: 1. isoprene, 2. pentane, 3. 2-methylpentane, 4. benzene, 5. ethylpropionate, 6. toluene, 7. ethylbenzene.

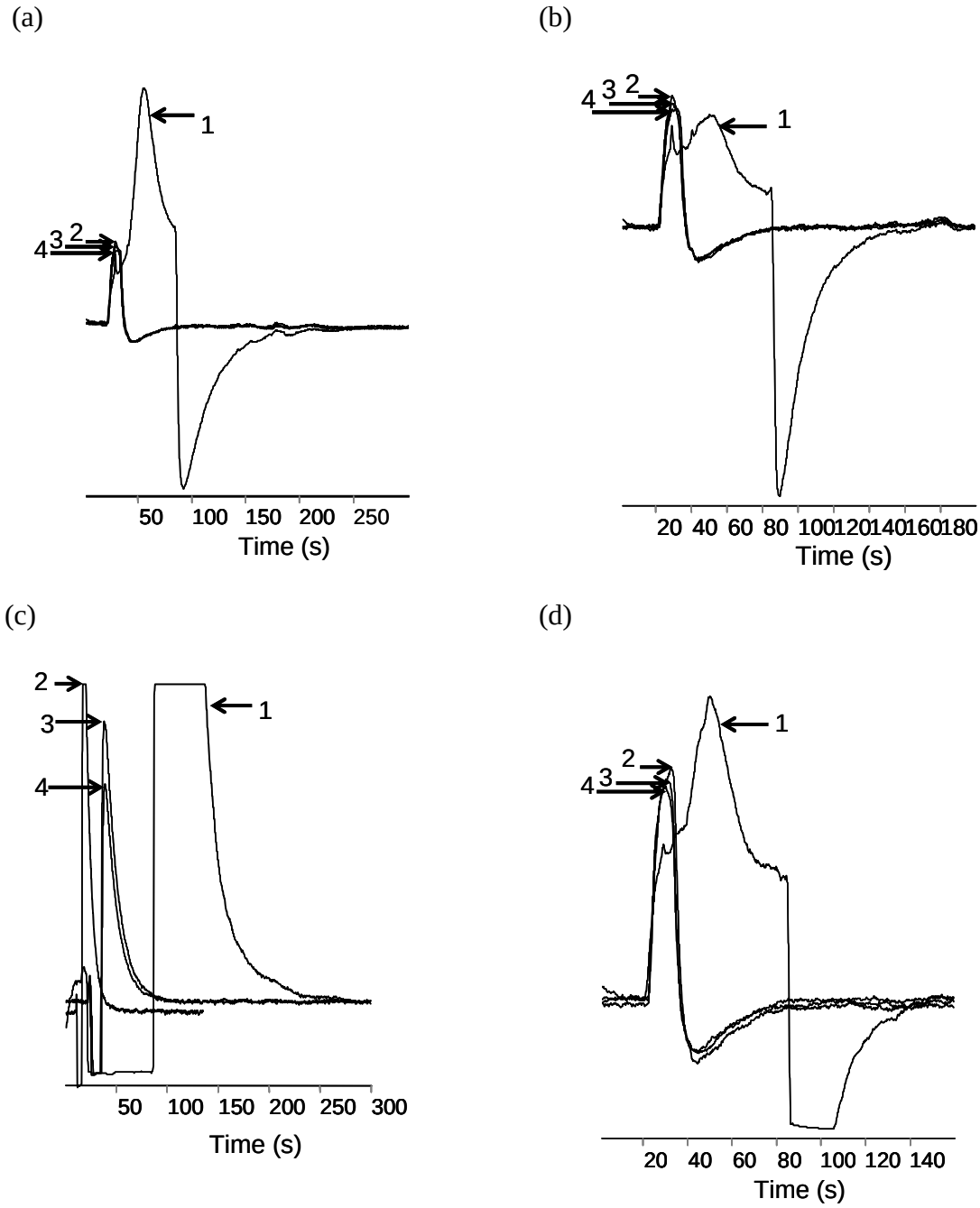

Figure 4-2. Sensor responses to water vapor after sampling 0.5 mL of water-saturated air followed by dry-air purge at different volumes, thermal desorption, and elution from the columns. Sensors: (a) C8; (b) OPH; (C) HME, (d) CCN; Dry air volume: (1) without dry purge; (2) 0.5 L; (3) 1 L; (4) 5 L.

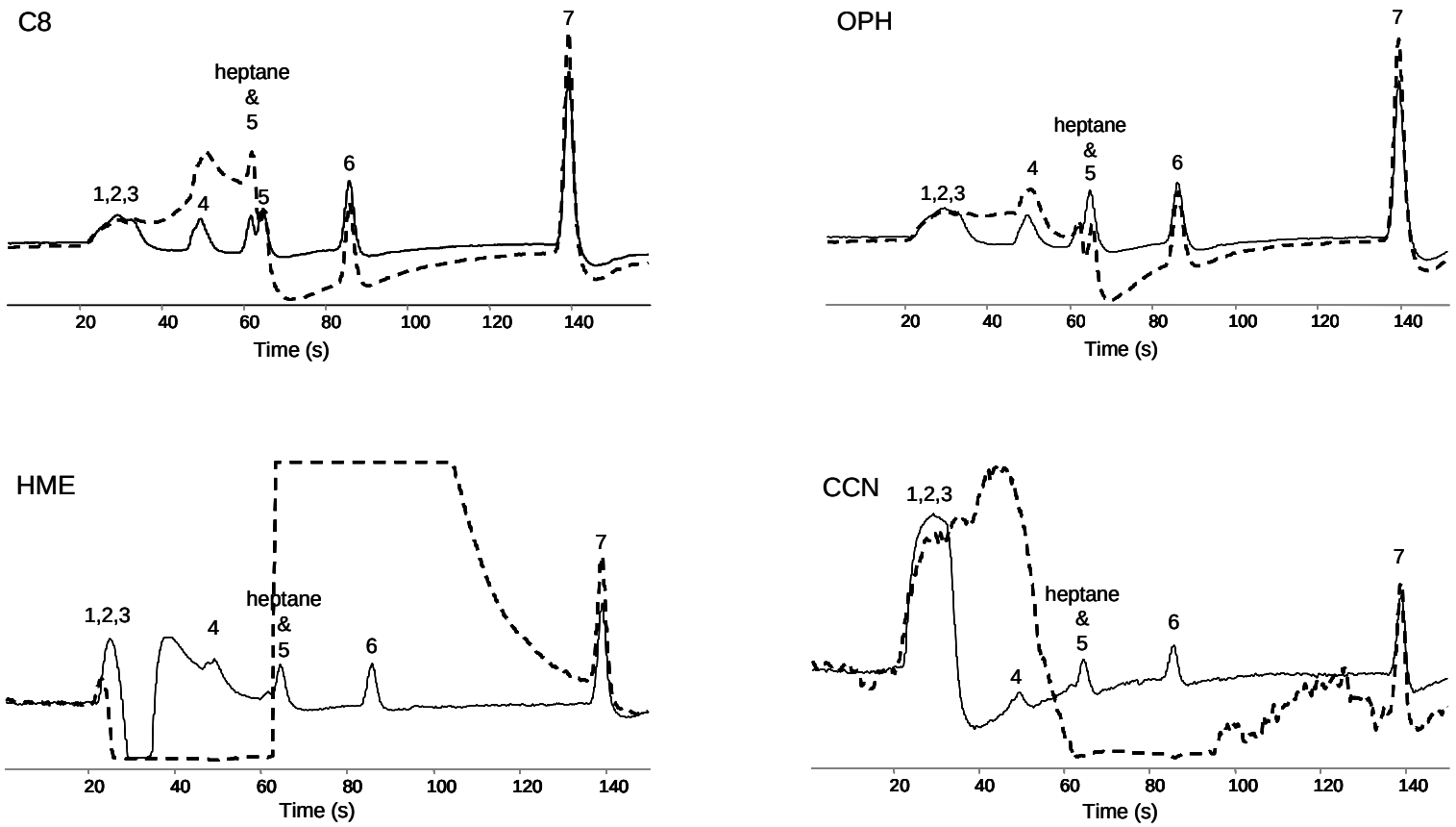

Figure 4-3. Sensor responses to 5-L samples of water-saturated air containing biomarkers with or without dry-purge. Dash lines: without dry-air purge; solid lines: with dry-air purge; compounds and concentration: 1. pentane, 16 ppb; 2. isoprene, 15 ppb; 3. 2-methylpentane, 8.3 ppb; 4. benzene, 21 ppb; 5. ethylpropionate, 16 ppb; 6. toluene, 6.9 ppb; 7. ethylbenzene, 6.0 ppb, heptane, 12 ppb.

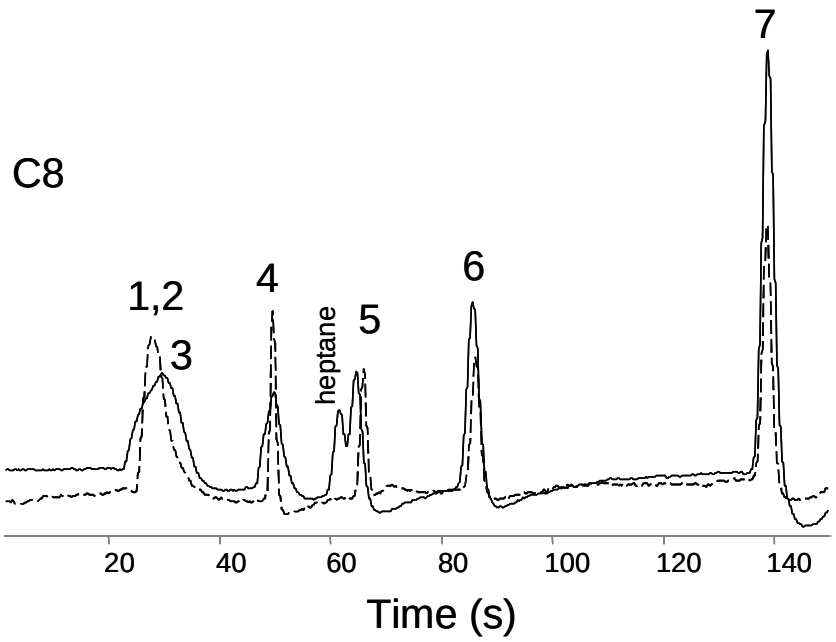

Figure 4-4. Sensor responses to dry sample (dash line) and 5-L water-saturated sample with dry-purge. Compounds: 1. isoprene, 2. pentane, 3. 2-methylpentane, 4. benzene, 5. ethylpropionate, 6. toluene, 7. ethylbenzene.

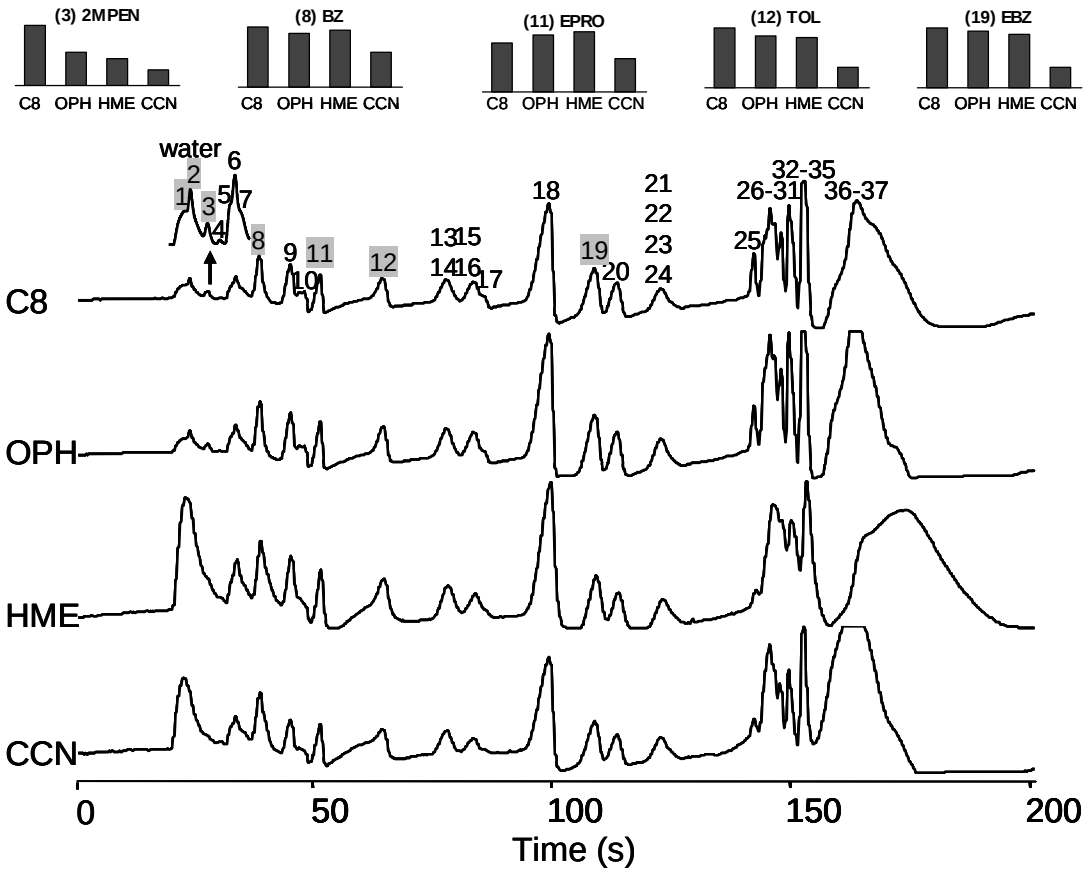

Figure 4-5. CR-array chromatographic traces and response patterns of 5 marker compounds (bar charts on top of the figure). Compound numbers on the bar charts and chromatograms correspond to those on Table 4-3.

4.5 References

1. World Health Organization, World Health Report 2002.
2. CancerCare, www.lungcancer.org.
3. Mcwilliams, A.; Lam, S. *Curr. Opin. Pulmonary Med.* **2005**, *11*, 272-77.
4. Di Francesco, F.; Fuoco, F.; Trivella, M. G.; Ceccarini, A. *Microchem. J.* **2005**, *79*, 405-410.
5. Phillips, M.; Cataneo, R. N.; Cummin, A. R. C.; Gagliardi, A. J.; Gleeson, K.; Greenberg, J.; Maxfield, R. A.; Rom, W. N. *Chest* **2003**, *123*, 2115-23.
6. Manolis, A. *Clin. Chem.* **1983**, *29*, 5-15.
7. Turner, A. P. F.; Magan, N. *Nat. Rev.* **2004**, *2*, 161-166.
8. Phillips, M. *Anal. Biochem.* **1997**, *247*, 272-78.
9. Phillips, M.; Herrera, J.; Krishnan, S.; Zain, M.; Greenberg, J.; Cataneo, R. N. *J. Chromatogr. B* **1999**, *729*, 75-88.
10. Gordon, S. M.; Szidon, J. P.; Krotoszynski, B. K.; Gibbons, R. D.; Oneill, H. J. *Clin. Chem.* **1985**, *31*, 1278-82.
11. Poli, D.; Carbognani, P.; Corradi, M.; Goldoni, M.; Acampa, O.; Balbi, B.; Bianchi, L.; Rusca, M.; Mutti, A. *Respir. Res.* **2005,** *6*.
12. Phillips, M.; Gleeson, K.; Hughes, J. M. B.; Greenberg, J.; Cataneo, R. N.; Baker, L.; Mcvay, W. P. *Lancet* **1999**, *353*, 1930-33.
13. O'neill, H. J.; Gordon, S. M.; Oneill, M. H.; Gibbons, R. D.; Szidon, J. P. *Clin. Chem.* **1988**, *34*, 1613-18.
14. Chanin, T. D.; Merrick, D. T.; Franklin, W. A.; Hirsch, F. R. *Curr. Opin. Pulmonary Med.* **2004**, *10*, 242-47.
15. Ost, D.; Shah, R. D.; Fein, D.; Fein, A. M. *Chest* **2003**, *123*, 1788-92.
16. Mazzone, P. J.; Hammel, J.; Dweik, R.; Na, J.; Czich, C.; Laskowski, D.; Mekhail, T. *Thorax* **2007**, *62*(7),565-568.
17. Di Natale, C.; Macagnano, A.; Martinelli, E.; Paolesse, R.; D'arcangelo, G.; Roscioni, C.; Finazzi-Agro, A.; D'amico, A. *Biosens. Bioelectron.* **2003**, *18*, 1209-18.
18. Machado, R. F.; Laskowski, D.; Deffenderfer, O.; Burch, T.; Zheng, S.; Mazzone, P. J.; Mekhail, T.; Jennings, C.; Stoller, J. K.; Pyle, J.; Duncan, J.; Dweik, R. A.; Erzurum, S. C. *Am. J. Respir. Crit. Care Med.* **2005**, *171*, 1286-91.
19. Phillips, M. *Am. J. Respir. Crit. Care Med.* **2005**, *172*, 1060.
20. Xu, J.; Whitten, W. B.; Ramsey, J. M. *Anal. Chem*. **2003**, *75*, 4206.
21. Miller, R. A.; Nazarov, E. G.; Eiceman, G. A.; King, A. T. *Sens. Actuators A* **2001**, *91*, 301.
22. Charlton, C.; De Melas, F.; nberg, A.; Croitoru, N.; Mizaikoff, B. *IEE Proceedings-Optoelectronics* **2003**, *150*, 306.
23. Hocker, G. B.; Youngner, D.; Deutsch, E.; Volpicelli, A.; Senturia, S.; Butler, M.; Sinclair, M.; Plowman, T.; Ricco, A. J. *Technical Digest Solid-State Sensor and Actuator Workshop*, Hilton Head SC, June, 2000, pp. 89-91.
24. Siebert, P.; Petzold, G.; Hellenbart, A.; Muller, J. *Appl. Phys. A.* **1998**, *67*, 155.
25. Moxom, J.; Reilly, P. T. A.; Whitten, W. B.; Ramsey, J. M. *Anal. Chem*. **2003**, *75*, 3739.
26. Phillips, M.; Greenberg, J. *J. Chromatogr. Biomed. Appl.* **1991**, *564*, 242-49.
27. Helming, D.; Vieling, L. *Anal. Chem.* **1995**, *67*, 4380.

28. Gawloski, J.; Gierczak, T.; Jezo, A.; Niedzielski, J. *Analyst* **1999**, *124*, 1553
29. Lu, C.J.; Zellers, E. T. *Analyst* **2002**, *127*, 1061-1068.
30. Groves, W. A.; Zellers, E. T.; Frye, G. C. *Anal. Chim. Acta* **1998**, *371*, 131-43.
31. Lu, C. J. *Dissertation*, University of Michigan, Ann Arbor, Michigan, 2002.
32. Cai, Q. Y.; Zellers, E. T. *Anal. Chem.* **2002**, *74*, 3533-3539.
33. Lu, C. J.; Steinecker, W. H; Tian, W. C.; Agah, M.; Potkay, J. M.; Oborny, M. C.; Nichols, J.; Chan, H.; Driscoll, J.; Sacks, R. D.; Pang, S. W.; Wise, K. D.; Zellers, E. T. *Lab On A Chip* **2005**, *5*, 1123-1131.
34. Rowe, M. P.; Plass, K. E.; Kim, K.; Kurdak, C.; Zellers, E. T.; Matzger, A. J. *Chem. Mater.*, **2004**, *16*, 3513–3517.
35. Vander, A. J.; Sherman, J. H.; Luciano, D. S. *Human Physiolog*. 3rd Edt., New York: McGraw-Hill, 1980.
36. US EPA, TO-17, *Compendium of Methods for the Determination of Toxic Organic Compounds in Ambient Air*, Report No. EPA/625/R-96/010b, US Environmental Protection Agency, Washington, DC, 2nd edn, 1997.
37. Jia, C.; Batterman, S.; Chernyak, S. *J. Environ. Monit.* **2006**, *8*(2), 1029-1042.
38. Deng, C. H.; Zhang, X. M.; Li, N. *J. Chromatogr. B-Anal. Technol. Biomed. Life Sci.* **2004**, *808*, 269-77.
39. Giardina, M.; Olesik, S. V. *Anal. Chem.* **2003**, *75*, 1604-14.
40. Karl, T.; Prazeller, P.; Mayr, D.; Jordan, A.; Rieder, J.; Fall, R.; Lindinger, W. *J. Appl. Physiol* **2001**, *91*, 762-770.
41. Cariou, S.; Guillot, J. M. *Anal. Bioanal. Chem* **2005**, *384*, 468.
42. Groves, W. A.; Zellers, E. T. *Am. Ind. Hyg. Assoc. J.* **1996**, *57*, 257-63.
43. Lipari, F. *J. Chromatogr.* **1990**, *503*, 51.
44. Fastyn, P.; Kornacki, W.; Gierczak, T.; Gawlowski, J.; Niedzielski, J. *J. Chromatogr. A* **2005**, *1078*(1-2), 7-12.
45. Lu, C. J.; Jin, C.; Zellers, E. T. *J. Environ. Monit.* **2006**, *8*(2), 270-278.
46. Sharaf, M. A.; Illman, D. L.; Kowaski, B. R. in *Chemometrics*, John Wiely and Sons Inc., New York, 1986
47. Howard, P. H.; Meylan, W. M *Handbook of Physical Properties of Organic Chemicals*, Lewis, New York, 1997.

Chapter 5

Conclusions

An improved portable gas chromatograph (GC) with several novel design features has been developed and characterized. The work described in this dissertation builds upon previous work by students in the Zellers Group without which the advances incorporated into the current prototype would not have been possible. The key analytical components of this portable GC are a mini multi-adsorbent preconcentrator/injector (PCI), two series-coupled 4.5-m low-thermal-mass separation columns capable of independent temperature programming and junction-point pressure tuning, and a detector consisting of an integrated array of four chemiresistor (CR) sensors coated with Au-thiolate monolayer-protected nanoparticles (MPN). Scrubbed ambient air is used as the carrier gas. The CR array replaced an array of polymer-coated SAW sensors used in the first-generation prototype and has afforded much lower detection limits. Other important modifications made to the instrument and explored in this research are an inlet particle filter, (optional) adsorbent pre-trap for removing gas-phase compounds with very low vapor pressures, carrier gas, split-flow injection, active sensor temperature control by a thermoelectric cooler, an on-board calibration-vapor generator, a LabVIEW program for instrument control and operation, and a wireless communication module for remote operation of the instrument.

For all the applications of interest, limits of detection (LODs) in the low- or sub-parts-per-billion are needed. The on-board PCI is capable of quantitatively capturing and concentrating volatile and semi-volatile organic compounds (VOCs and SVOCs) from large-volume air samples and desorbing them into a smaller injection volume, making it possible to achieve the low LODs required. Use of multiple adsorbents with different specific surface areas permits the efficient capture and desorption of (S)VOCs spanning a wide range of volatility and functionality. The small size of the PCI coupled with the

option to increase the desorption flow rate via a split-flow injection option, minimizes band broadening of the injection plug which, in turn enhances chromatographic efficiency. The tradeoff of enhanced chromatographic resolution versus loss of sensitivity was characterized and it was found that for most VOCs the increase in resolution could be attributed entirely to the reduction in the size of chromatographic peaks due to the reduced injection mass, whereas for SVOCs there was a fractional improvement attributable to peak sharpening from the split-flow injection.

The use of columns with different stationary phases permits separation of compounds that are both polar and non-polar, which would not be separated as well on a column of similar length having only a single polarity. Stop-flow "tuning" of retention via control of the pressure at the midpoint between the two columns was used to advantage for the separation of pairs of compounds that would otherwise co-elute. Independent temperature programming of each column was also used to enhance and accelerate separations. Generally speaking, the independent and fast column temperature programming feature is much more powerful than the pressure tuning feature of the separation module. However, both features are important for separating complex (S)VOC mixtures and making best use of the capability of the CR-array detector to discriminate among certain compounds via pattern recognition of array response patterns, as shown in Chapters 2, 3, and 4.

The use of a microfabricated CR array as the detector in a field portable instrument has many advantages: simple design and support circuitry, no need for support gases, small size and weight, low power consumption, and the generation of response patterns that can be used for vapor recognition. In both the first- and second-generation prototypes, the MPN-coated CR sensors exhibited higher sensitivity and lower LODs than the polymer-coated SAW sensors used originally in the first-generation prototype. For the majority of the (S)VOCs analyzed, LODs in the parts-per-trillion concentration could be achieved with modest sample volumes of one liter or less. Response patterns from the CR array can be used together with retention times for identifying eluting compounds. Indeed, the combination of array response patterns and retention time is extremely useful for multi-vapor analysis. For fully resolved peaks, response patterns add one more dimension on top of retention times for vapor identifications. Response

pattern recognition allows for certain co-elutions because the components giving rise to the composite response pattern can be determined by the pattern recognition algorithms.

Band broadening, particularly for less volatile compounds, occurs with the sensor array because of adsorption on the walls of the unheated detector cell and interconnecting capillary between the detector and the column outlet. This shortcoming can be addressed by operating the sensor array at elevated temperature, though at a cost of decreased sensitivity. Sensor sensitivity is also influenced by the flow rate through the detector cell. The investigation of flow rate effects on sensor response in a GC system performed here provides a detailed assessment of this important operating variable. A combination of effects was identified and the implications on the performance of the instrument were characterized.

There are some disadvantages of using this new type of MPN-coated CR sensor array as the detector. Of greatest concern is the instability of sensor responses and shifts in baseline resistance values that occur over the course a one or two weeks. This demands re-calibration to re-establish the pattern recognition library and also changes in the reference resistors that are used in the signal processing circuitry. Further exploration of the causes of these changes in sensor performance is warranted in order to improve the longer term stability.

The advantages of using ambient air as the carrier gas are the increased portability and reduced maintenance scheduling compared to systems that use onboard carrier gas tanks. Drawbacks associating with using air as the carrier gas include the passing of residual water vapor through the system, the need to limit the operating temperature of the columns to < 180 ºC, and lower optimal flow rates (compared to, say, He or H_2 carrier gases).

The user-defined and user-friendly LabVIEW program for instrument control and operation developed in this research runs on a laptop computer and has many advantages over the built-in microprocontroller used in the first-generation prototype. There is more flexibility in setting the operation commends with individual components and greater stability of fluidic and thermal conditions. In fact, the most significant problem with the first-generation prototype was the retention time shift associated with the on-board

microcontroller whose reference voltages, used for carrier pressure and column controls, decreased when the chassis temperature increased.

The capabilities of this prototype greatly exceed those of the first-generation prototype and rival those of portable GC-MS instruments. Compared with the first-generation prototype, the new design enhancements incorporated into the second-generation prototype have improved the reliability, sensitivity, resolution, flexibility, and convenience. However, there are still some shortcomings to address. One of the primary remaining issues relates to the analysis of low-vapor-pressure compounds. Desoprtion efficiencies tend to be low for these compounds and the calibration curves are invariably non-linear due, apparently, to wall adsorption on unheated surfaces in the flow path. Although cold spots in this instrument have been minimized, there are two locations where they remain: between the PCI and the first column and between the end of the second column and detector cell. Although the inlet could be heated, the presence of the (stainless steel) tee fitting makes it difficult to heat and cool rapidly at low power. The capillary between end of the column and the sensor array cannot be heated too much because it would result in a reduction in sensitivity in the concentration-dependent sensors in the array.

Despite these shortcomings, the capability of the second generation prototype to address several practical monitoring problems has been demonstrated. First, it was adapted to determine two airborne markers of environmental tobacco smoke (ETS) among complex interferences (Chapter 3). As part of this effort, an adsorbent pre-trap was successfully installed to remove unwanted SVOCs from the sample stream. The two ETS markers were successfully separated from the 34 most prominent co-contaminants present in ETS and the calculated LODs are sufficiently low to determine these markers in typical smoking-permitted environments.

In a second project exploring potential applications of the prototype, it was adapted to determine seven breath biomarkers of lung cancer (Chapter 4). A key challenge in this application is removing water vapor from the sample stream. Although most of the water can removed by dry-air purge, the responses to water vapor from all four sensors, but especially the sensors with the more polar interface layers, are still relatively large. This impedes the determinations of early-eluting target compounds. It is

necessary to investigate a more effective method to remove the water vapor from the sample or to use MPNS with nonpolar functionality. Secondly, further reductions in LODs for the more volatile compounds are needed. Collecting an air sample of larger volume is possible, but, in addition to requiring longer sampling time, larger air sample volume results in a more serious water problem as mentioned above. In spite of these issues, instrument operating conditions were established to separate the seven biomarkers from each other and from 30 common endogenous and exogenous (S)VOC interferences in under three minutes. Breath samples spiked with the biomarkers and interferences were successfully analyzed.

To our knowledge this is the first reported application of a portable GC to these types of investigations. With additional work aimed at solving some of the remaining challenges, instruments employing the technologies and approaches embodied in this prototype GC should find wide application in many areas of environmental health science, and should have significant positive impacts on assessing exposures to harmful (S)VOCs in occupational, residential, and outdoor environments, as well as in monitoring the health status of workers and the general population.

Appendices

Appendix 1. Calibration Data with the 1st-Generation Instrument (Chapter 1)

Calibration curves (CR sensors: square = C8, circle = OPH, triangle = CCN)

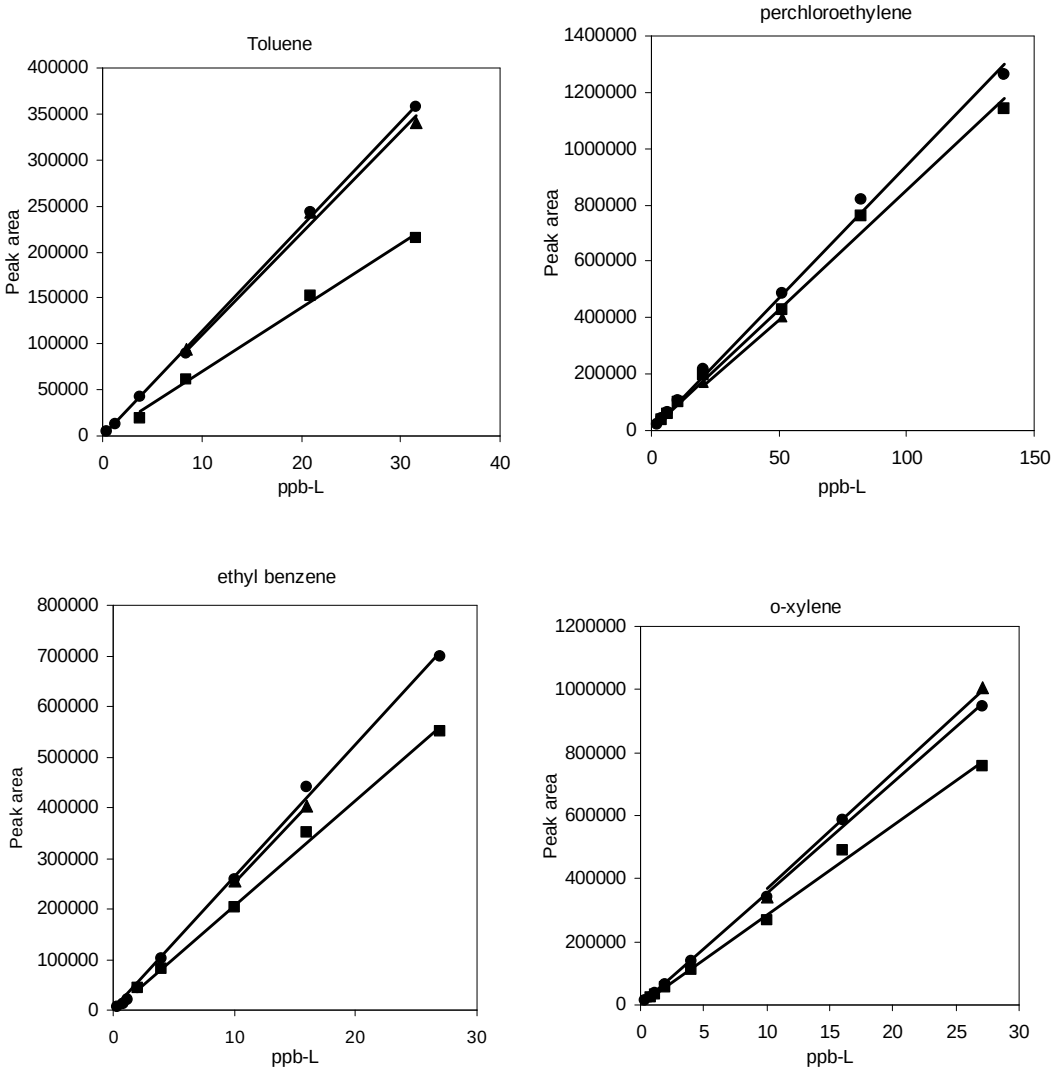

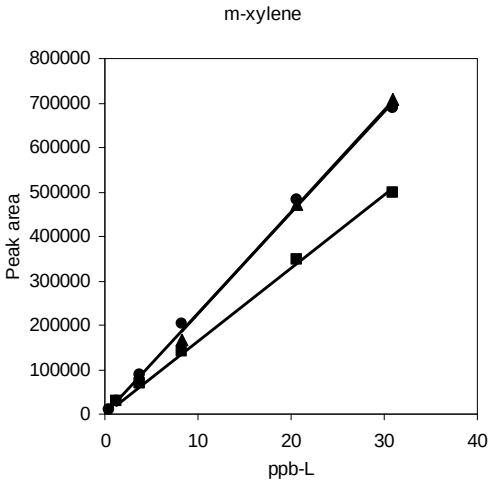
m-xylene
Peak area
ppb-L
800000
700000
600000
500000
400000
300000
200000
100000
0
0
10
20
30
40

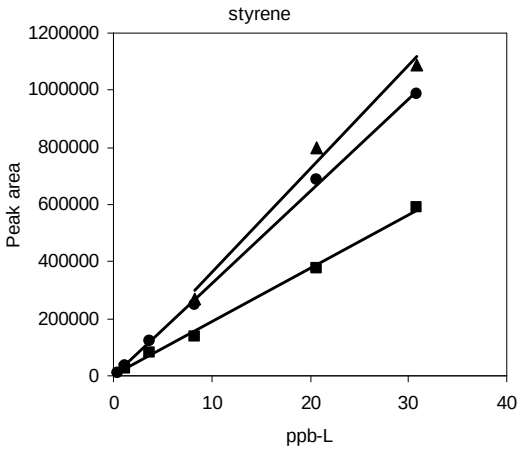
styrene
Peak area
ppb-L
1200000
1000000
800000
600000
400000
200000
0
0
10
20
30
40

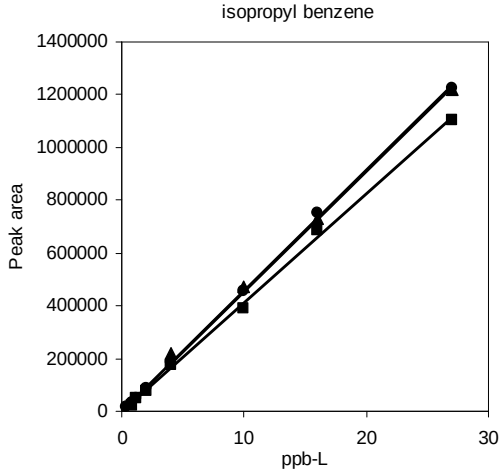
isopropyl benzene
Peak area
ppb-L
1400000
1200000
1000000
800000
600000
400000
200000
0
0
10
20
30

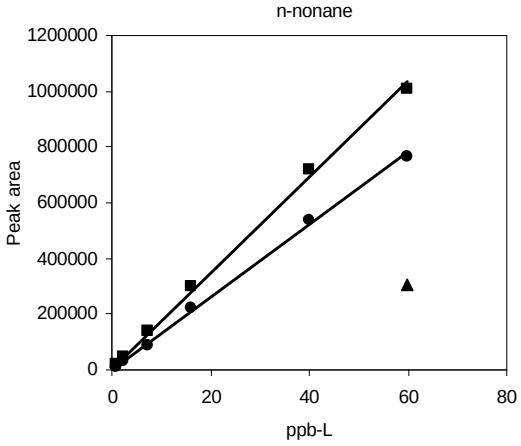
n-nonane
Peak area
ppb-L
1200000
1000000
800000
600000
400000
200000
0
0
20
40
60
80

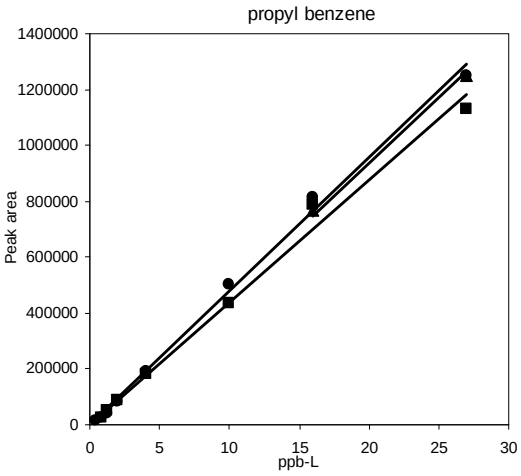
propyl benzene
Peak area
ppb-L
1400000
1200000
1000000
800000
600000
400000
200000
0
0
5
10
15
20
25
30

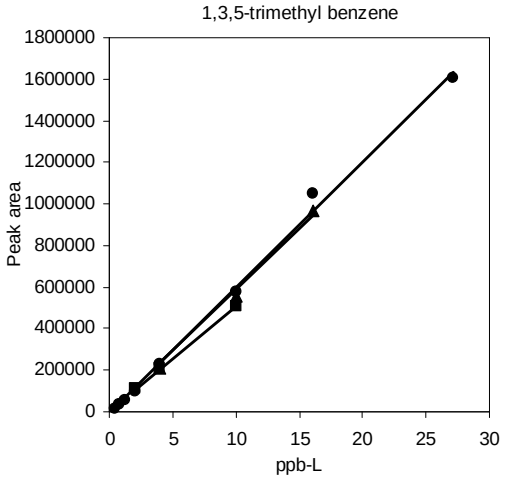
1,3,5-trimethyl benzene
Peak area
ppb-L
1800000
1600000
1400000
1200000
1000000
800000
600000
400000
200000
0
0
5
10
15
20
25
30

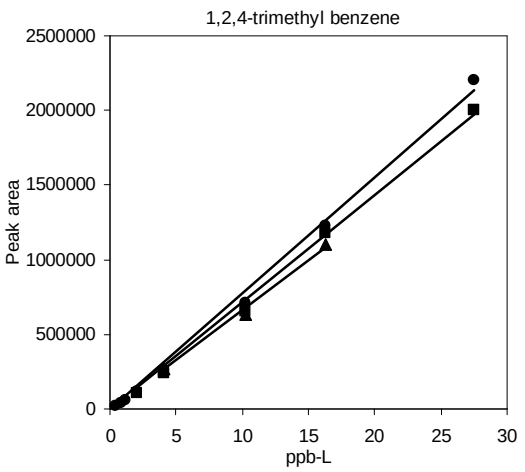
1,2,4-trimethyl benzene
Peak area
ppb-L
2500000
2000000
1500000
1000000
500000
0
0
5
10
15
20
25
30

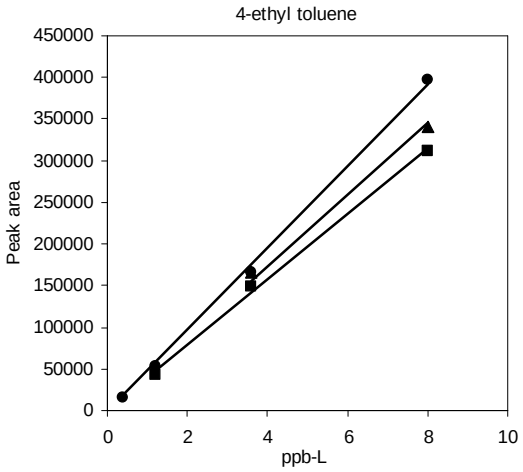
4-ethyl toluene
Peak area
ppb-L
450000
400000
350000
300000
250000
200000
150000
100000
50000
0
0
2
4
6
8
10

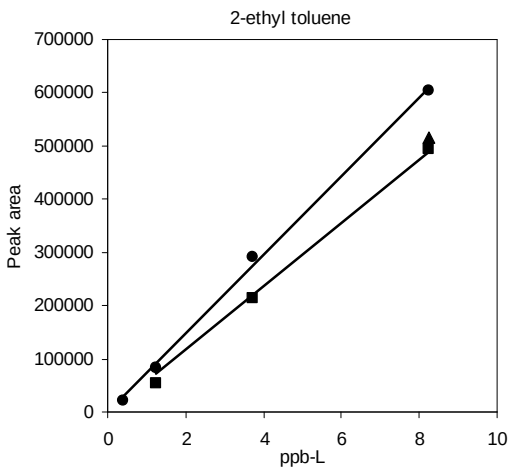
2-ethyl toluene
Peak area
ppb-L
700000
600000
500000
400000
300000
200000
100000
0
0
2
4
6
8
10

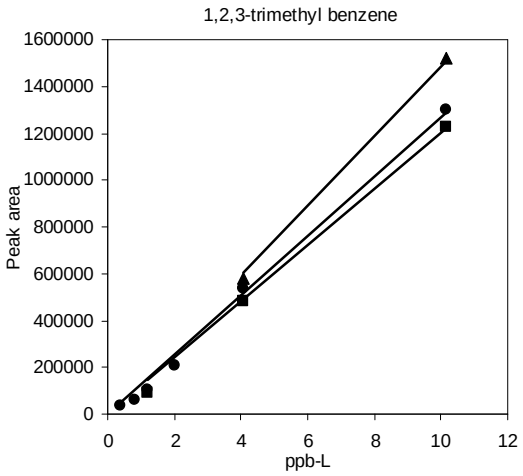
1,2,3-trimethyl benzene
Peak area
ppb-L
1600000
1400000
1200000
1000000
800000
600000
400000
200000
0
0
2
4
6
8
10
12

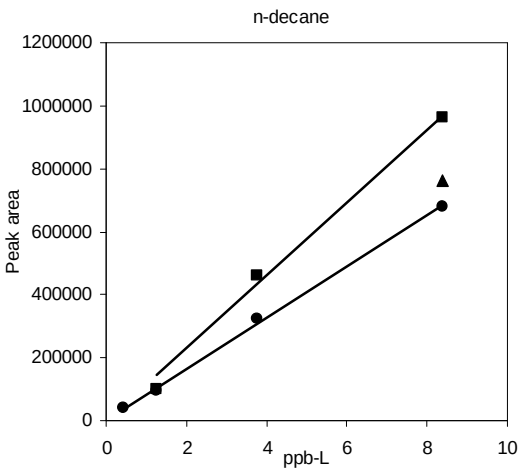
n-decane
Peak area
ppb-L
1200000
1000000
800000
600000
400000
200000
0
0
2
4
6
8
10

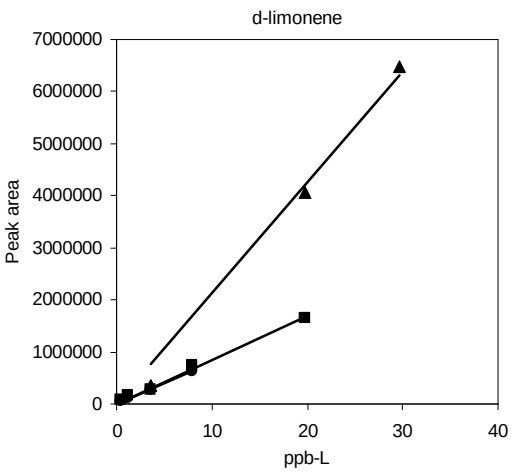
d-limonene
Peak area
ppb-L
7000000
6000000
5000000
4000000
3000000
2000000
1000000
0
0
10
20
30
40

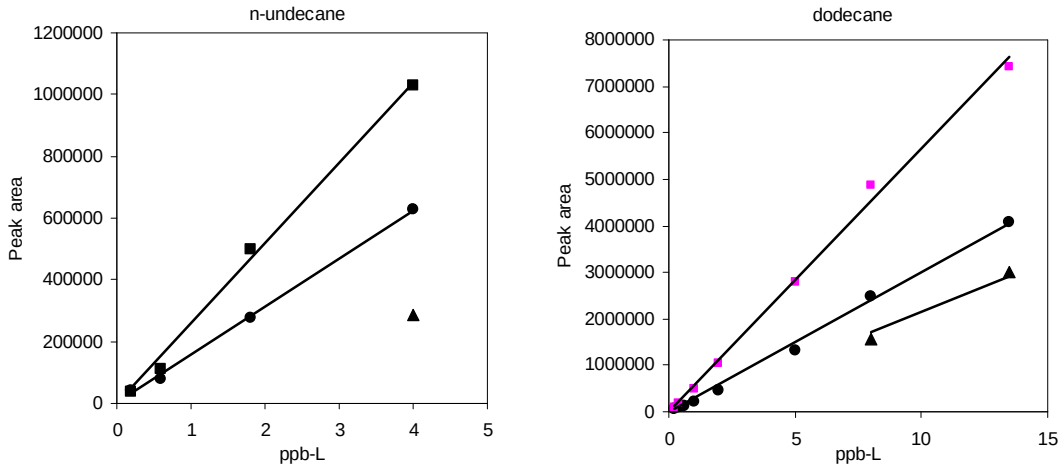

Response patterns (left: C8, middle: OPH, right: CCN)

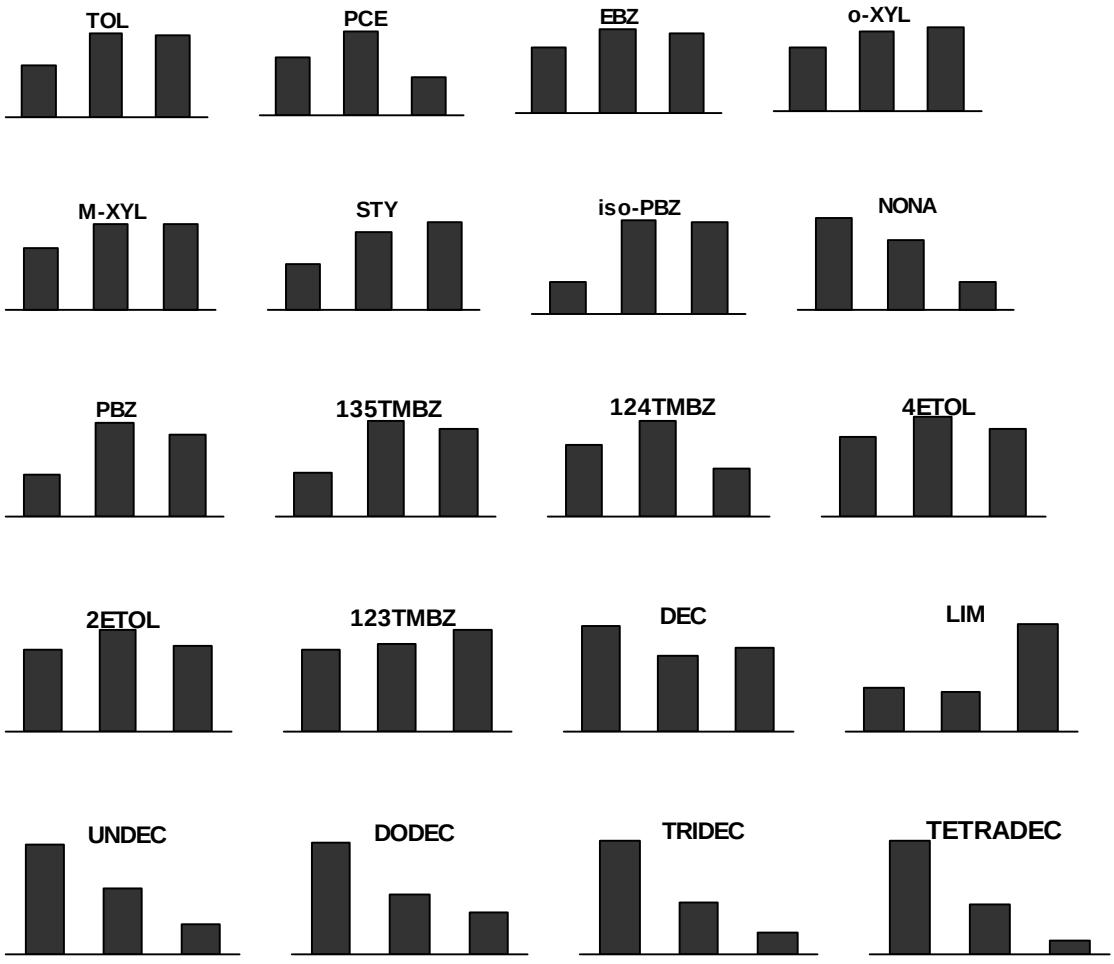

Vapor	Aabbreviation	Vapor	Aabbreviation
toluene	TOL	1,2,4-trimethyl benzene	124TMBZ
perchloroethylene	PCE	4-ethyl toluene	4ETOL
ethyl benzene	EBZ	2-ethyl toluene	2ETOL
o-xylene	o-XYL	1,2,3-trimethyl benzene	123TMBZ
m-xylene	M-XYL	n-decane	DEC
styrene	STY	d-limonene	LIM
isopropyl benzene	iso-PBZ	n-undecane	UNDEC
n-nonane	NONA	dodecane	DODEC
propyl benzene	PBZ	n-tridecane	TRIDEC
1,3,5-trimethyl benzene	135TMBZ	tetradecane	TETRADEC

Appendix 2. Calibration Data with the 2nd-Generation Instrument (Chapter 2)

Calibration Curves (Peak Area vs. Conc.)

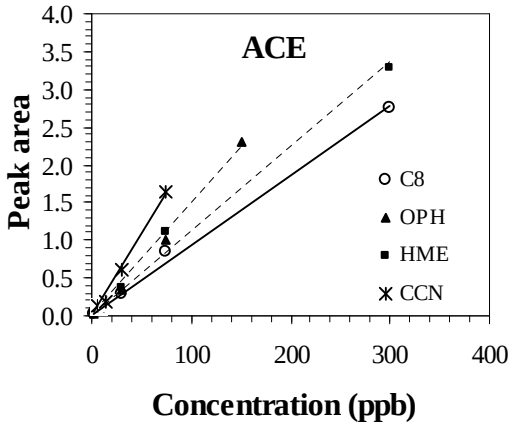

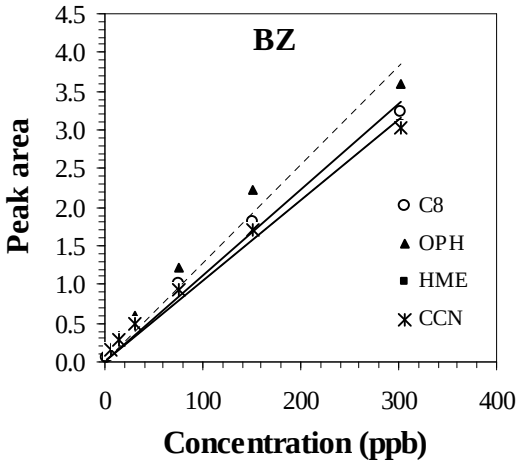

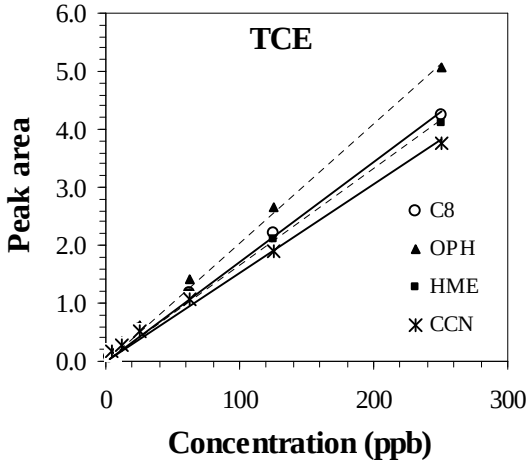

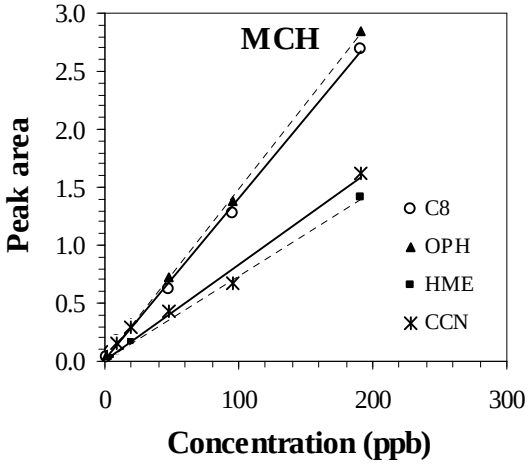

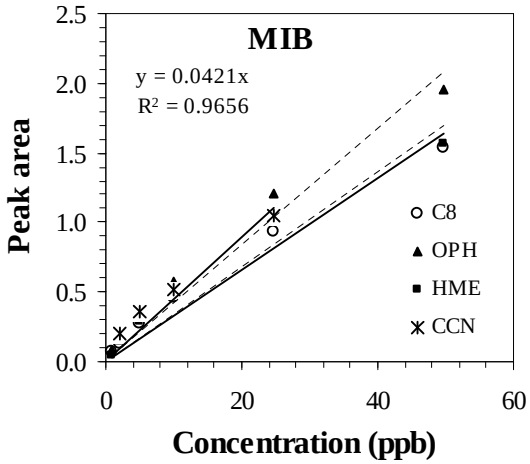

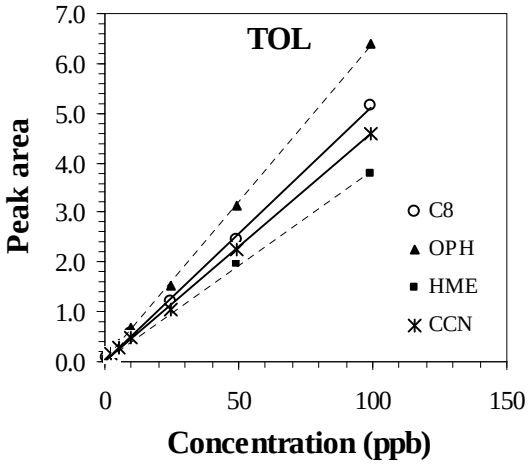

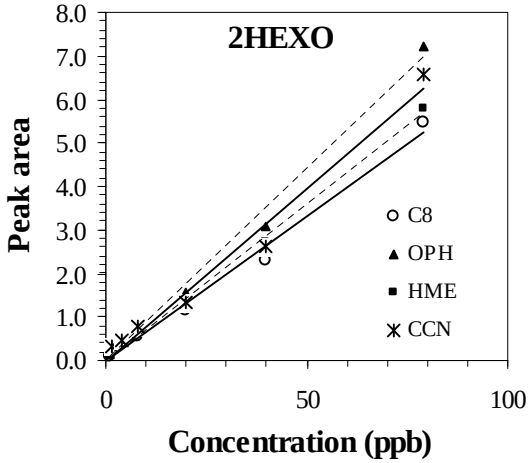
2HEXO
Peak area
Concentration (ppb)
C8
OPH
HME
CCN

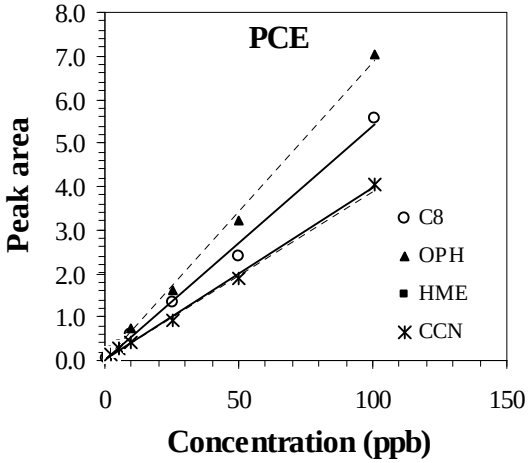
PCE
Peak area
Concentration (ppb)
C8
OPH
HME
CCN

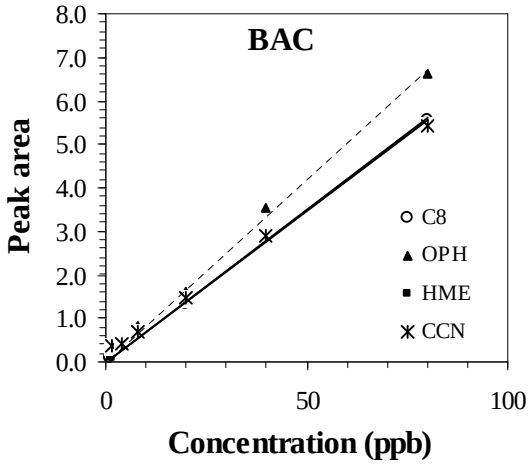
BAC
Peak area
Concentration (ppb)
C8
OPH
HME
CCN

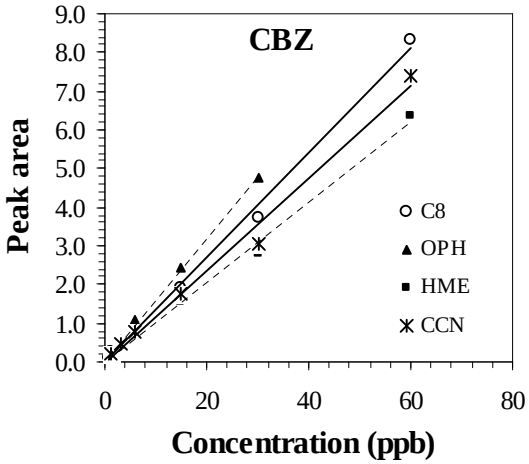
CBZ
Peak area
Concentration (ppb)
C8
OPH
HME
CCN

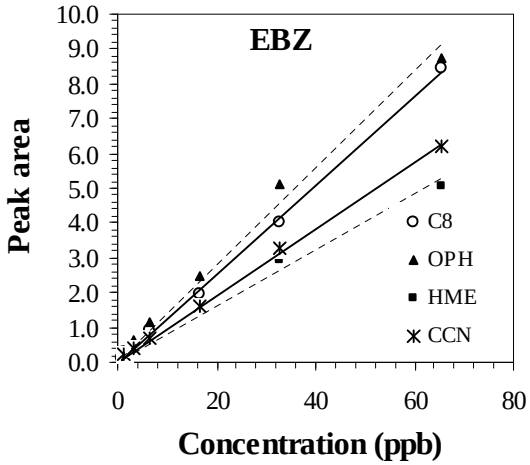
EBZ
Peak area
Concentration (ppb)
C8
OPH
HME
CCN

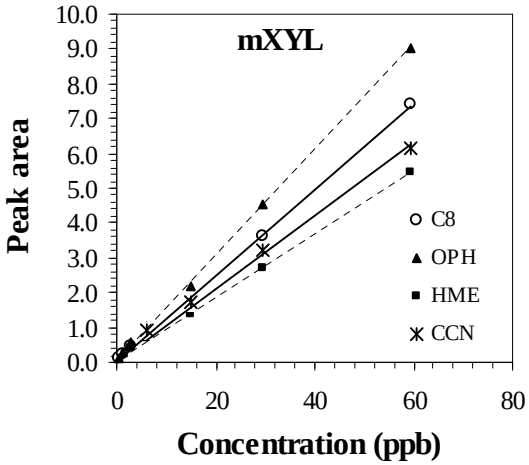
mXYL
Peak area
Concentration (ppb)
C8
OPH
HME
CCN

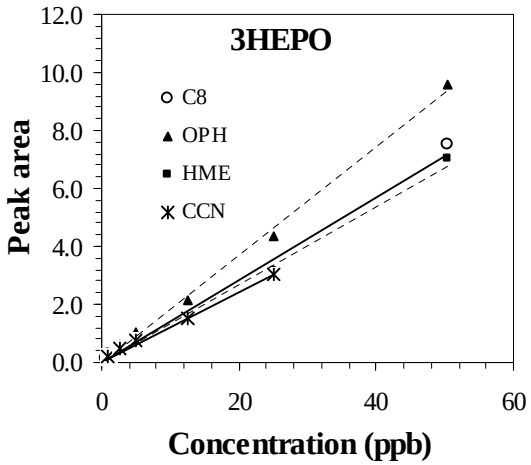
3HEPO
Peak area
Concentration (ppb)
C8
OPH
HME
CCN
0.0
2.0
4.0
6.0
8.0
10.0
12.0
0
20
40
60

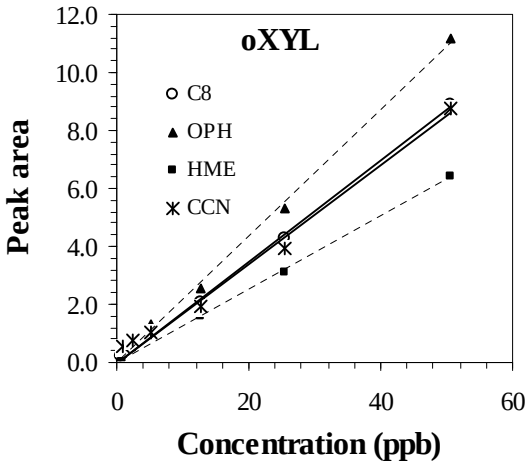
oXYL
Peak area
Concentration (ppb)
C8
OPH
HME
CCN
0.0
2.0
4.0
6.0
8.0
10.0
12.0
0
20
40
60

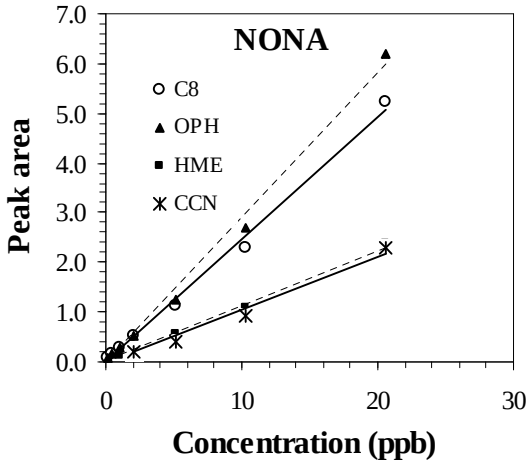
NONA
Peak area
Concentration (ppb)
C8
OPH
HME
CCN
0.0
1.0
2.0
3.0
4.0
5.0
6.0
7.0
0
10
20
30

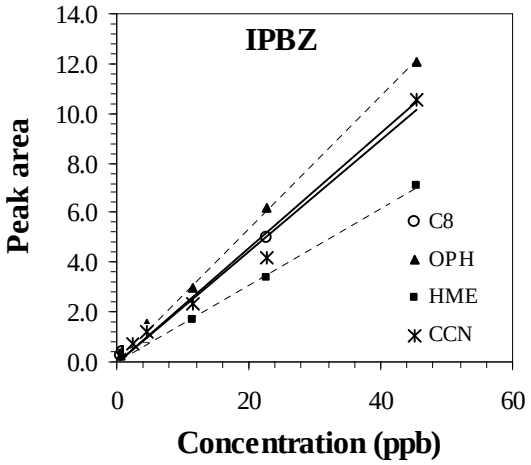
IPBZ
Peak area
Concentration (ppb)
C8
OPH
HME
CCN
0.0
2.0
4.0
6.0
8.0
10.0
12.0
14.0
0
20
40
60

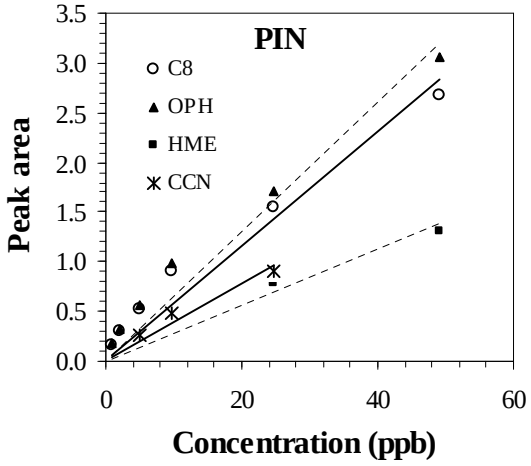
PIN
Peak area
Concentration (ppb)
C8
OPH
HME
CCN
0.0
0.5
1.0
1.5
2.0
2.5
3.0
3.5
0
20
40
60

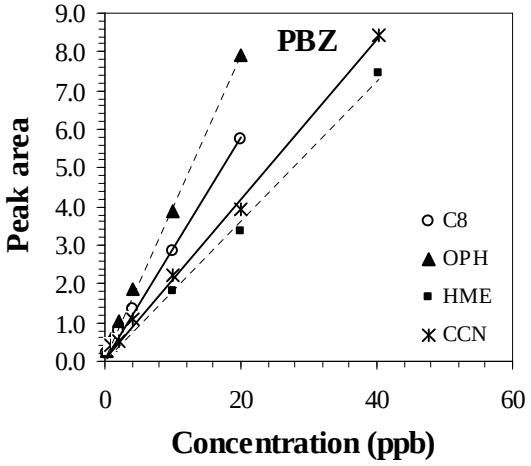
PBZ
Peak area
Concentration (ppb)
C8
OPH
HME
CCN
0.0
1.0
2.0
3.0
4.0
5.0
6.0
7.0
8.0
9.0
0
20
40
60

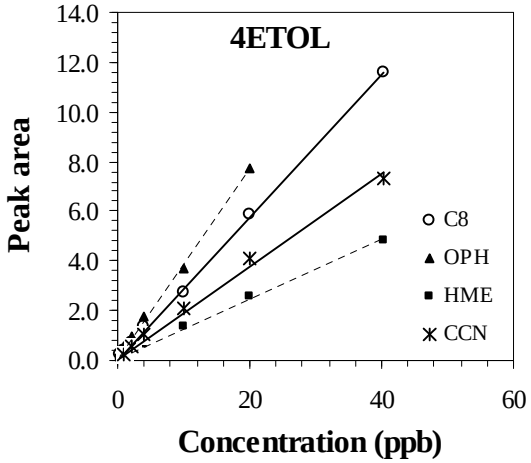
4ETOL
Peak area
Concentration (ppb)
C8
OPH
HME
CCN

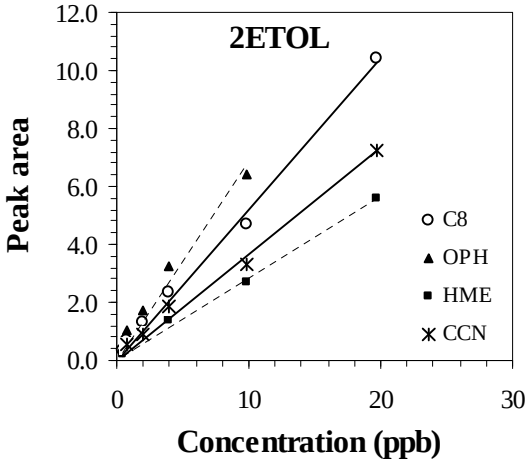
2ETOL
Peak area
Concentration (ppb)
C8
OPH
HME
CCN

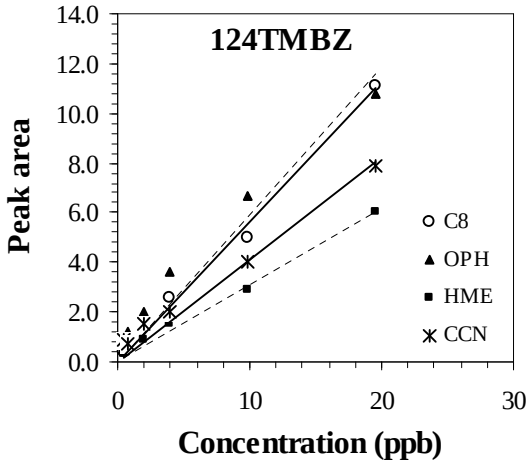
124TMBZ
Peak area
Concentration (ppb)
C8
OPH
HME
CCN

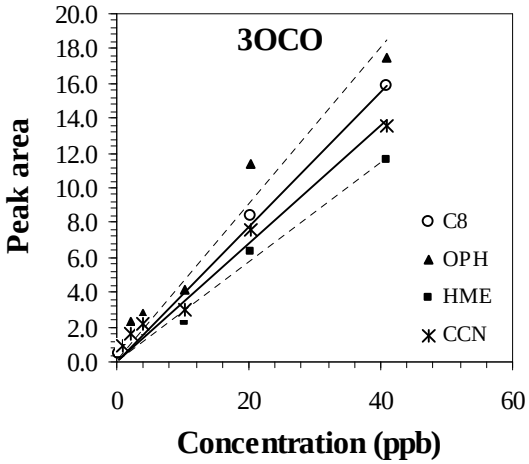
3OCO
Peak area
Concentration (ppb)
C8
OPH
HME
CCN

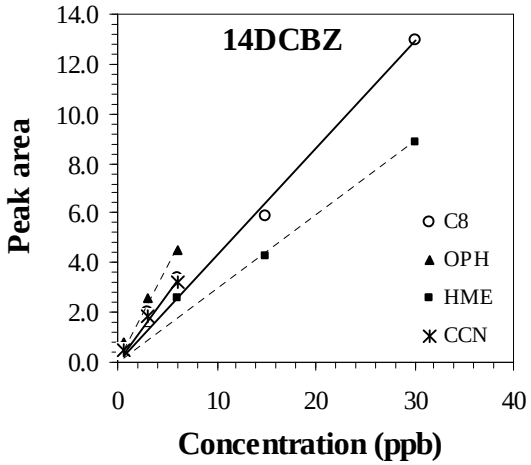
14DCBZ
Peak area
Concentration (ppb)
C8
OPH
HME
CCN

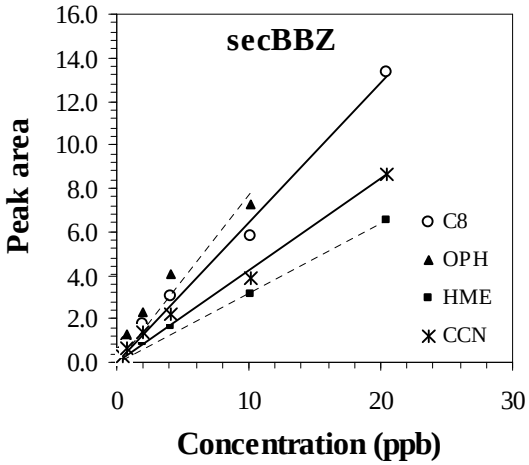
secBBZ
Peak area
Concentration (ppb)
C8
OPH
HME
CCN

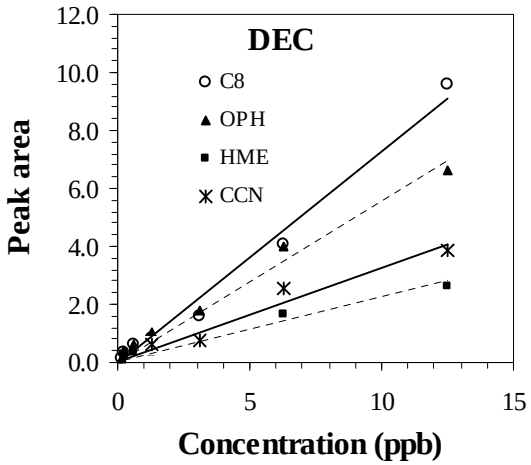
DEC
C8
OPH
HME
CCN
Peak area
Concentration (ppb)
0.0
2.0
4.0
6.0
8.0
10.0
12.0
0
5
10
15

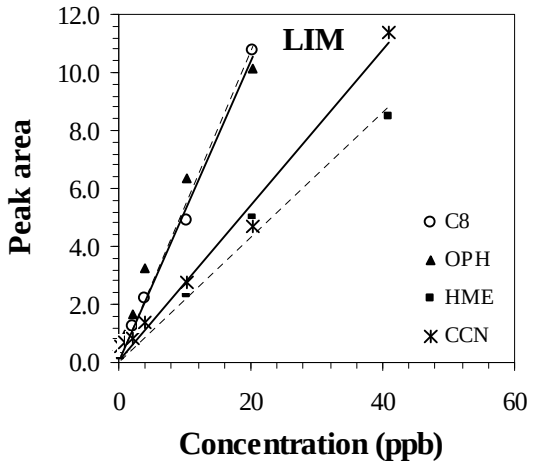
LIM
C8
OPH
HME
CCN
Peak area
Concentration (ppb)
0.0
2.0
4.0
6.0
8.0
10.0
12.0
0
20
40
60

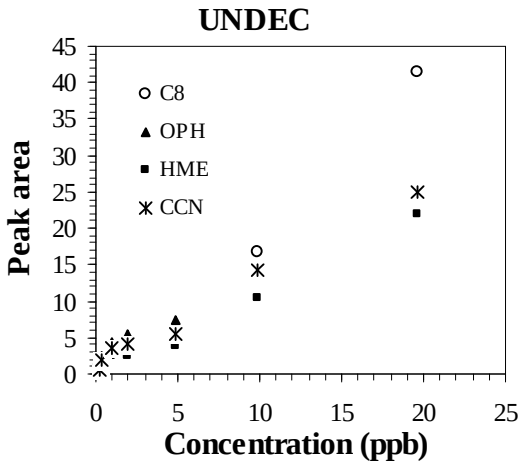
UNDEC
C8
OPH
HME
CCN
Peak area
Concentration (ppb)
0
5
10
15
20
25
30
35
40
45
0
5
10
15
20
25

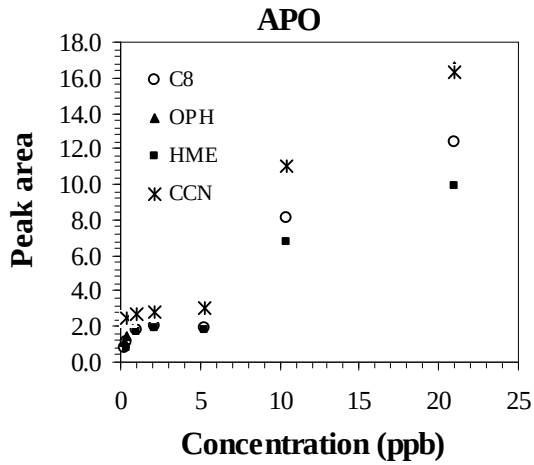
APO
C8
OPH
HME
CCN
Peak area
Concentration (ppb)
0.0
2.0
4.0
6.0
8.0
10.0
12.0
14.0
16.0
18.0
0
5
10
15
20
25

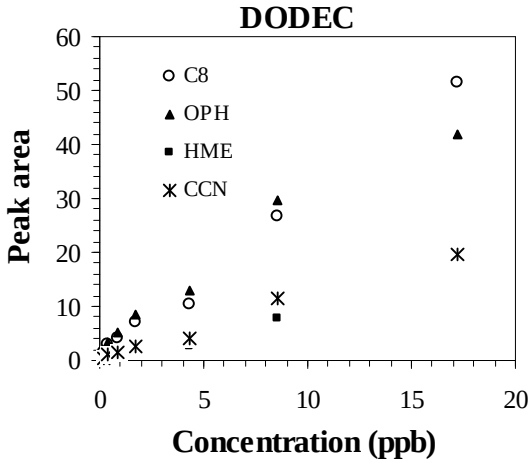
DODEC
C8
OPH
HME
CCN
Peak area
Concentration (ppb)
0
10
20
30
40
50
60
0
5
10
15
20

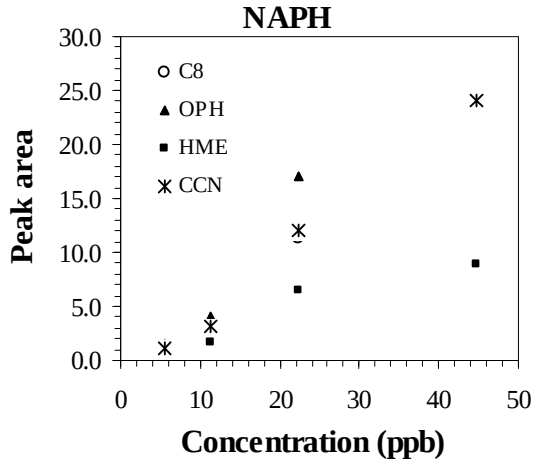
NAPH
C8
OPH
HME
CCN
Peak area
Concentration (ppb)
0.0
5.0
10.0
15.0
20.0
25.0
30.0
0
10
20
30
40
50

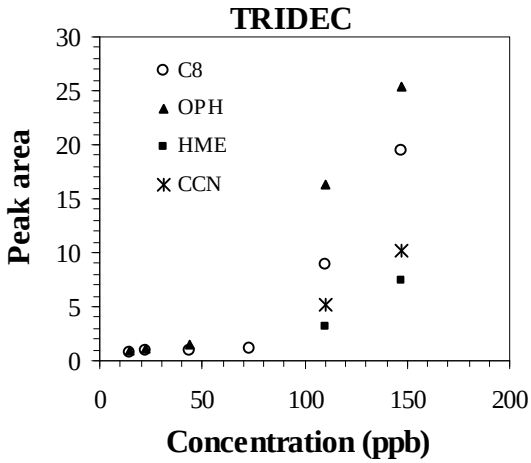
TRIDEC
Peak area
Concentration (ppb)
C8
OPH
HME
CCN
0
5
10
15
20
25
30
0
50
100
150
200

Calibration Curves (Peak Height vs. Conc.)

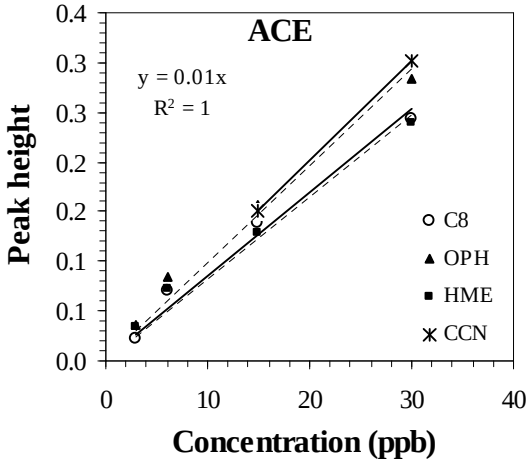

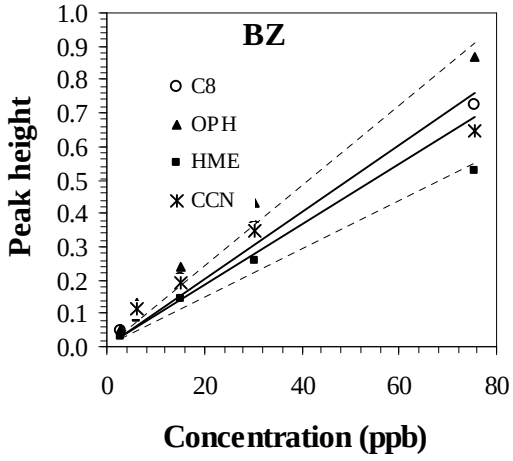

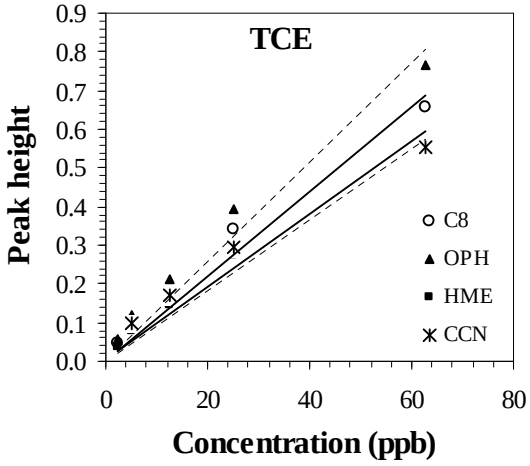

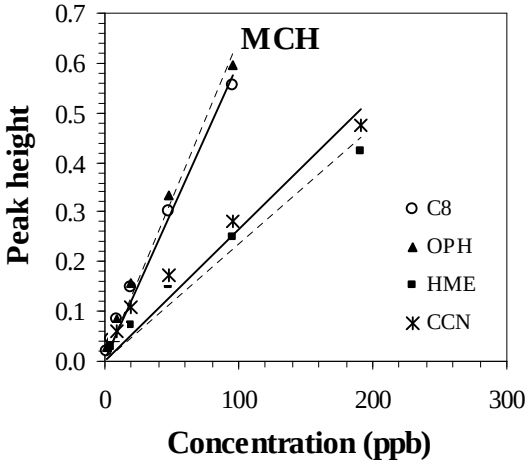

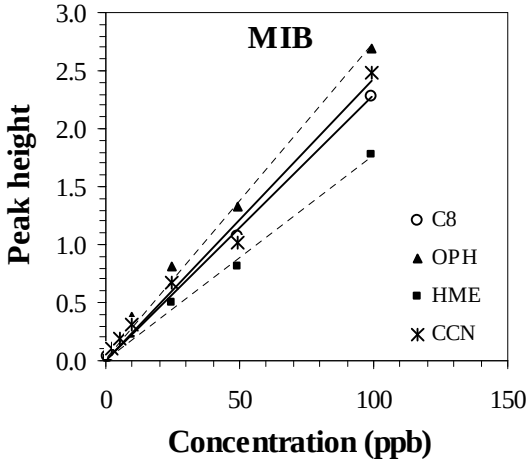

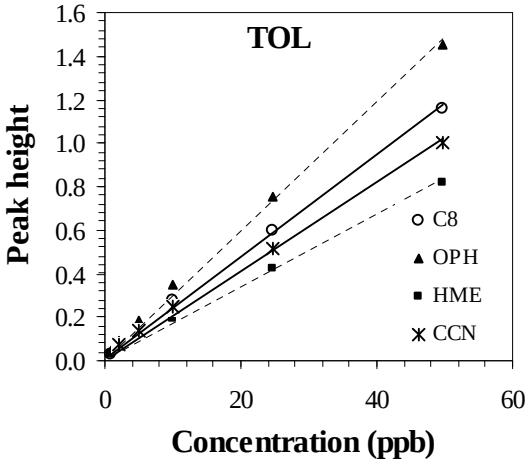

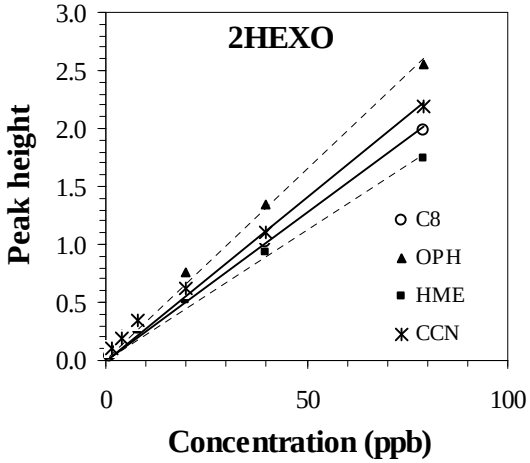
2HEXO
Peak height
Concentration (ppb)
C8
OPH
HME
CCN

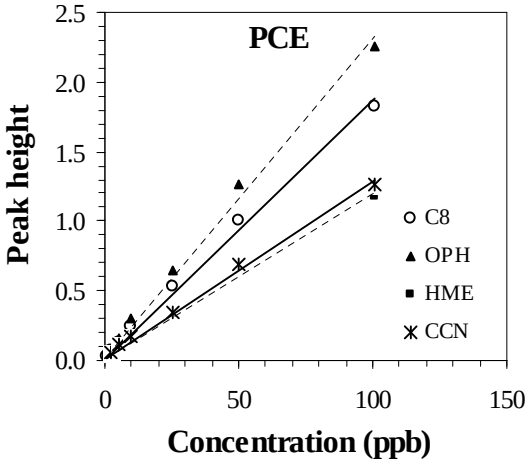
PCE
Peak height
Concentration (ppb)
C8
OPH
HME
CCN

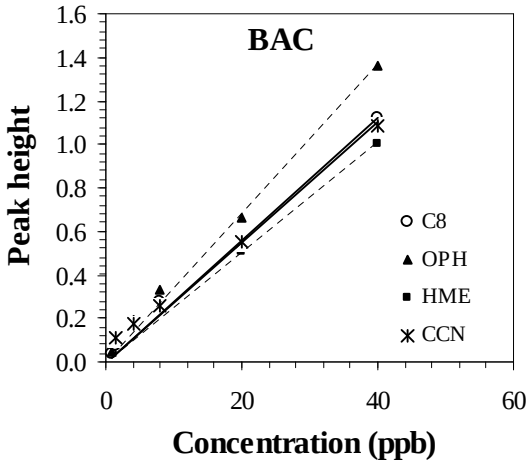
BAC
Peak height
Concentration (ppb)
C8
OPH
HME
CCN

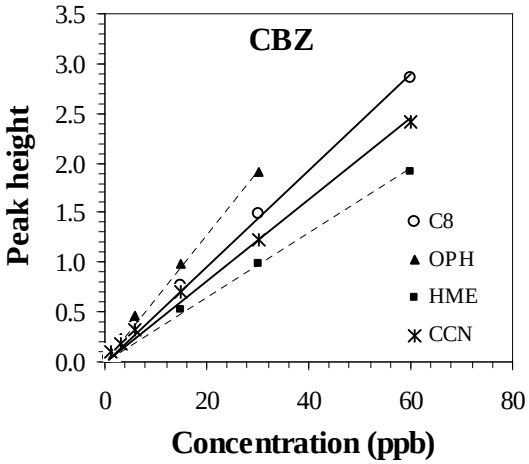
CBZ
Peak height
Concentration (ppb)
C8
OPH
HME
CCN

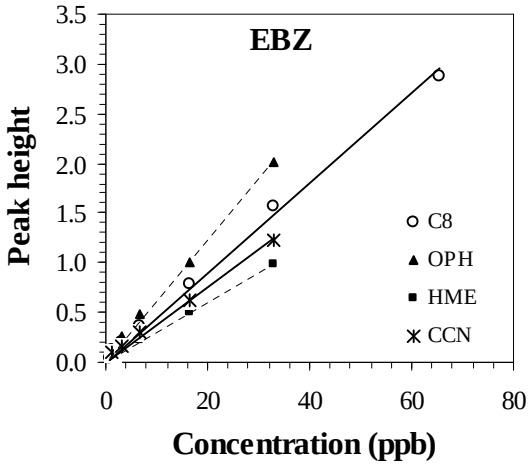
EBZ
Peak height
Concentration (ppb)
C8
OPH
HME
CCN

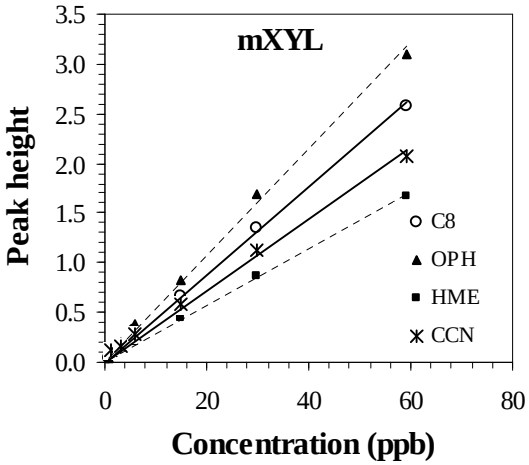
mXYL
Peak height
Concentration (ppb)
C8
OPH
HME
CCN

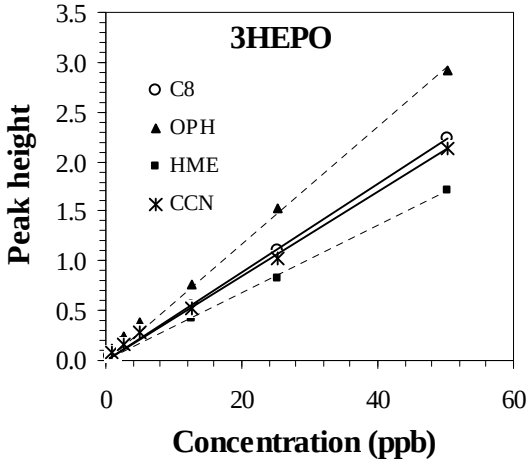
3HEPO
C8
OPH
HME
CCN
Peak height
Concentration (ppb)
0.0
0.5
1.0
1.5
2.0
2.5
3.0
3.5
0
20
40
60

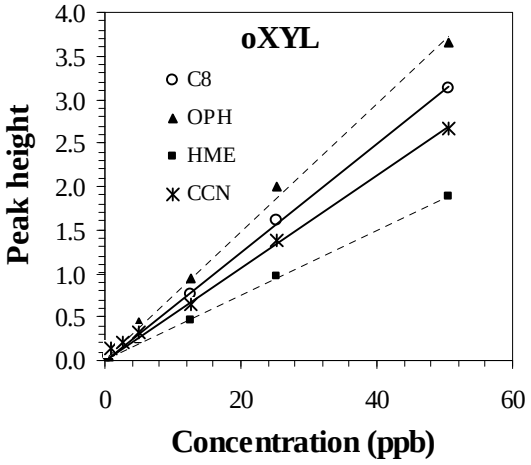
oXYL
C8
OPH
HME
CCN
Peak height
Concentration (ppb)
0.0
0.5
1.0
1.5
2.0
2.5
3.0
3.5
4.0
0
20
40
60

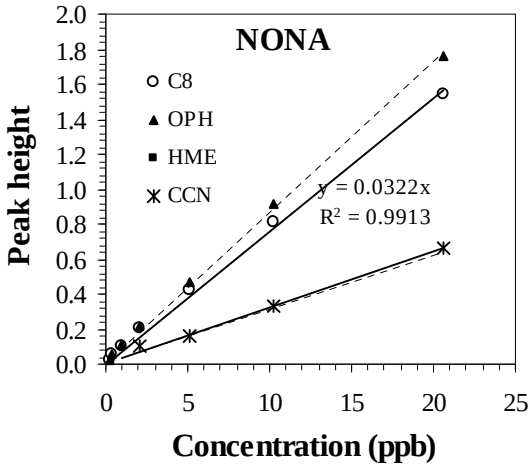
NONA
C8
OPH
HME
CCN
y = 0.0322x
R² = 0.9913
Peak height
Concentration (ppb)
0.0
0.2
0.4
0.6
0.8
1.0
1.2
1.4
1.6
1.8
2.0
0
5
10
15
20
25

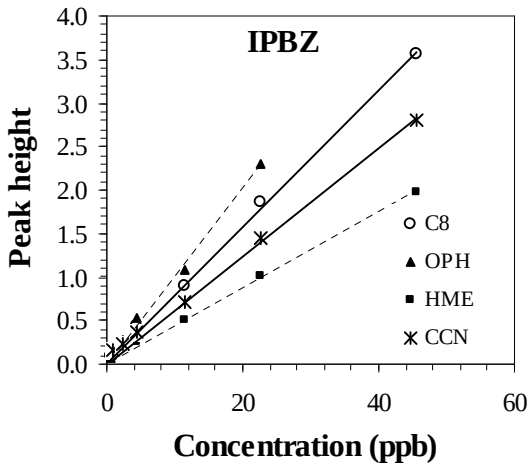
IPBZ
C8
OPH
HME
CCN
Peak height
Concentration (ppb)
0.0
0.5
1.0
1.5
2.0
2.5
3.0
3.5
4.0
0
20
40
60

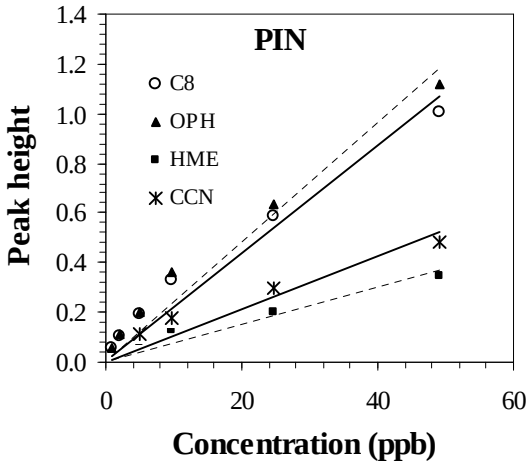
PIN
C8
OPH
HME
CCN
Peak height
Concentration (ppb)
0.0
0.2
0.4
0.6
0.8
1.0
1.2
1.4
0
20
40
60

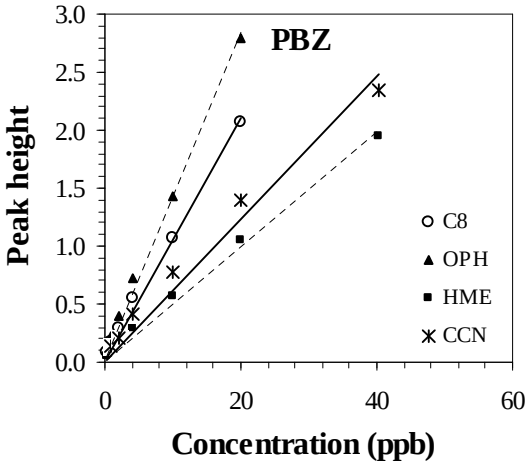
PBZ
C8
OPH
HME
CCN
Peak height
Concentration (ppb)
0.0
0.5
1.0
1.5
2.0
2.5
3.0
0
20
40
60

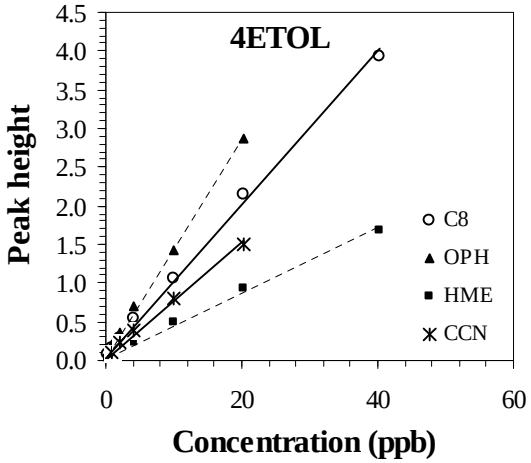
4ETOL
Peak height
Concentration (ppb)
C8
OPH
HME
CCN

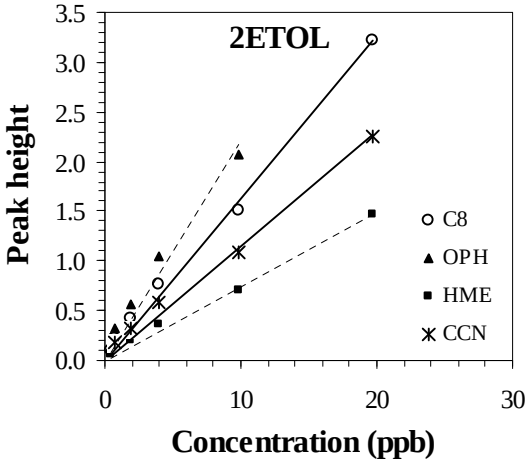
2ETOL
Peak height
Concentration (ppb)
C8
OPH
HME
CCN

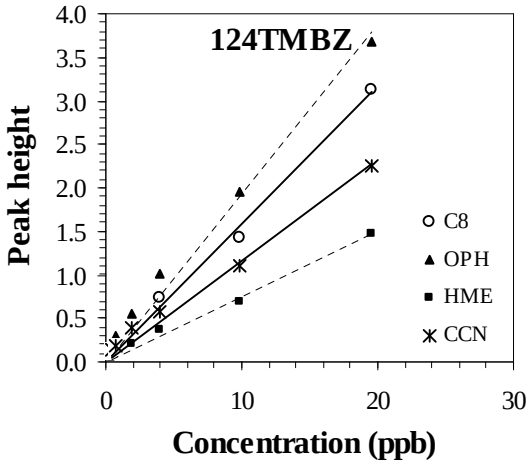
124TMBZ
Peak height
Concentration (ppb)
C8
OPH
HME
CCN

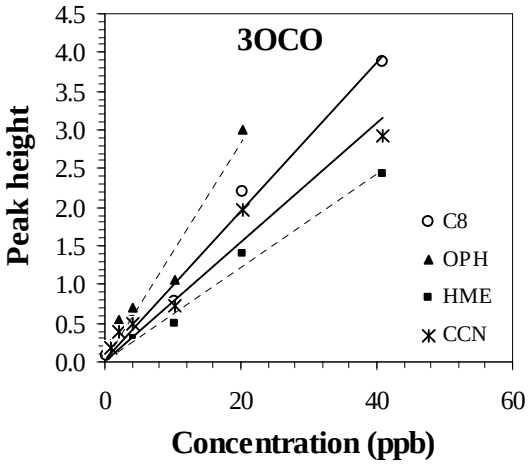
3OCO
Peak height
Concentration (ppb)
C8
OPH
HME
CCN

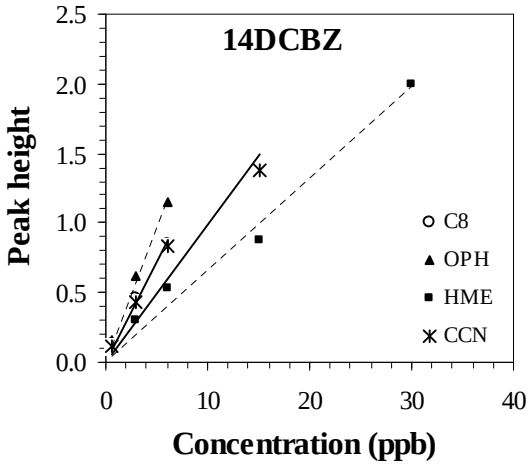
14DCBZ
Peak height
Concentration (ppb)
C8
OPH
HME
CCN

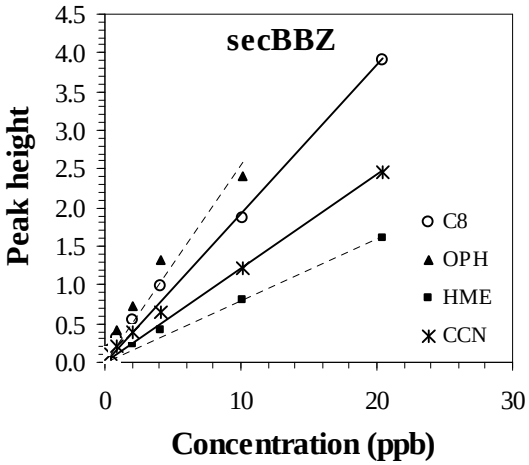
secBBZ
Peak height
Concentration (ppb)
C8
OPH
HME
CCN

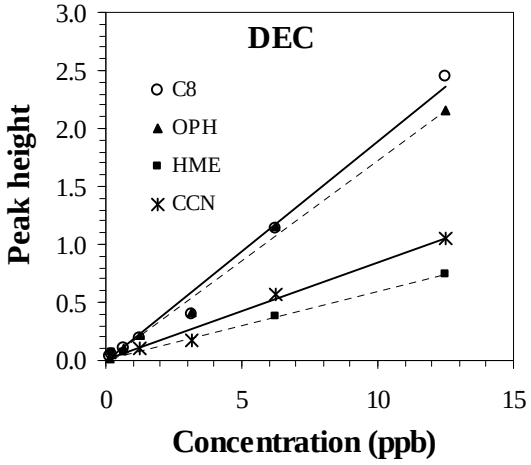
DEC
Peak height
Concentration (ppb)
C8
OPH
HME
CCN

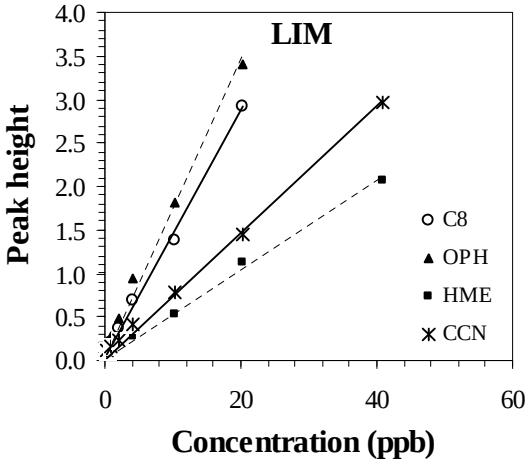
LIM
Peak height
Concentration (ppb)
C8
OPH
HME
CCN

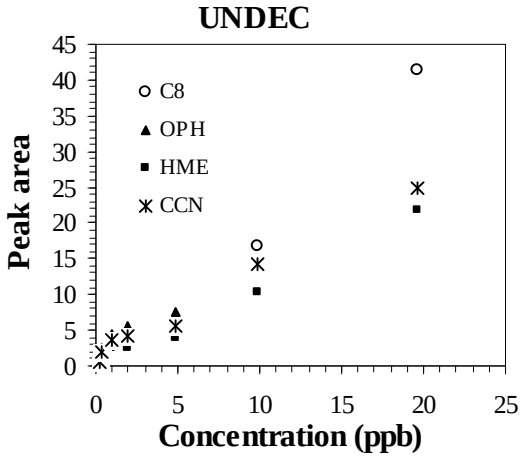
UNDEC
Peak area
Concentration (ppb)
C8
OPH
HME
CCN

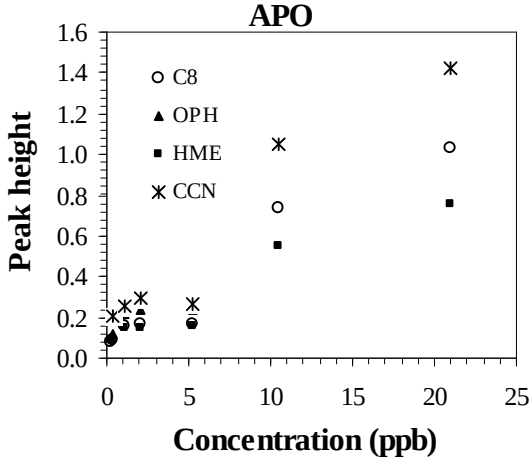
APO
Peak height
Concentration (ppb)
C8
OPH
HME
CCN

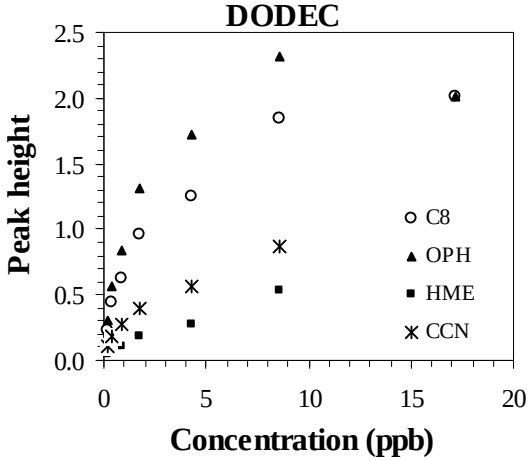
DODEC
Peak height
Concentration (ppb)
C8
OPH
HME
CCN

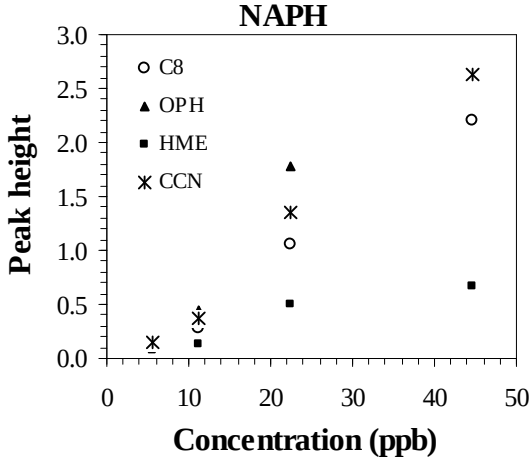
NAPH
Peak height
Concentration (ppb)
C8
OPH
HME
CCN

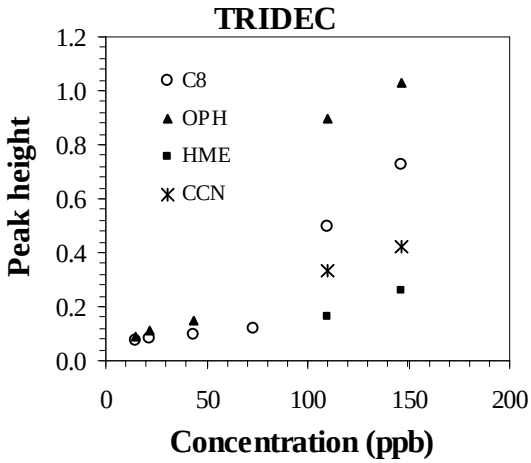
TRIDEC
Peak height
Concentration (ppb)
C8
OPH
HME
CCN
0.0
0.2
0.4
0.6
0.8
1.0
1.2
0
50
100
150
200

Appendix 3. Literature Review of the Determinations of 3-EP and VPN of ETS (Chapter 3)

1. Concentrations

3-EP of area samples

Ref.	Environment	N	Concentration Range (μg/m^3) Mean	SD	Median	Min.	Max.
	Smoking Offices						
1	Cubicles and offices in unrestricted smoking office building, USA (8-h TWA)	72	1.12	NA	0.91	NA	NA
	Smoking Homes						
2	Smoking homes in UK	32	0.8	1.4	0.3	ND	5.9
	Smoking Restaurants, etc.						
3	Smoking section of a restaurant, Canada	8	1.7	2.7	NA	NA	NA
4	Bar area in unrestricted smoking restaurant and tavern, USA	53	3.48	3.85	1.16	0.00	16.1
4	Non-bar area in unrestricted smoking restaurant and tavern, USA	32	1.44	2.13	0.580	0	8.83
5	Smoking-permitted medium-priced restaurant in France	15	3.08	2.20	2.40	0.00	7.80
5	Smoking-permitted medium-priced restaurant in Japan	16	2.67	1.54	3.06	0.44	4.86
5	Smoking-permitted medium-priced restaurant in Korea	47	1.66	0.85	0.10	1.80	3.50
5	Smoking-permitted medium-priced restaurant in Switzerland	35	2.54	2.57	1.59	0.16	10.5
5	Smoking-permitted medium-priced restaurant in UK	18	2.73	1.36	2.57	0.71	6.38
5	Smoking-permitted medium-priced restaurant in USA	20	1.27	1.22	0.87	0.11	3.72
6	Smoking permitted disco, nightclub in Finland	43	6.3	1.1	NA	0.30	37
6	Smoking permitted pub in Finland	12	1.6	0.3	NA	0.28	3.0
6	Smoking permitted dining restaurant in Finland	28	1.4	0.5	NA	0.30	6.0
	Nonsmoking Eenvironments						
3	Nonsmoking section of a restaurant, Canada	12	0.23	0.28	0.18	NA	NA
2	Nonsmoking home in UK	32	ND	ND	ND	ND	ND

NA = not abailable; ND = Not detected.

3-EP of personal exposure samples

Ref.	Environment	N	Concentration Range (µg/m^3)				
			Mean	SD	Median	Min.	Max.
1	Unrestricted smoking office building, USA (8-h TWA)	72	0.85	NA	0.80	NA	NA
9	Smoking and nonsmoking (not specified) Korean home	120	0.04	0.04	<MDL	<MDL	0.22
4	Bartender in unrestricted smoking restaurant and tavern, USA	80	3.31	4.12	1.17	0	23.6
4	Wait staff in unrestricted smoking restaurant and tavern, USA	83	1.73	2.84	0.59	0.00	14.9
9	Smoking away-from work and smoking work environment in 16 cities, USA (24-h TWA)	122	1.29	NA	0.839	NA	NA
9	Smoking away-from work and nonsmoking work environment in 16 cities, USA (24-h TWA)	149	0.708	NA	0.448	NA	NA
9	Nonsmoking away-from work and smoking work environment in 16 cities, USA (24-h TWA)	154	0.305	NA	0.131	NA	NA
9	Smoking away-from work and smoking work environment in 16 cities, USA (24-h TWA)	154	0.049	NA	0.022	NA	NA
10	Smoking environment in Germany, weekday winter (24-h TWA)	48	0.93	NA	0.63	NA	NA
10	Smoking environment in Germany, weekend winter (24-h TWA)	48	0.87	NA	0.53	NA	NA
10	Smoking environment in Germany, weekday summer (24-h TWA)	44	0.54	NA	0.29	NA	NA
10	Smoking environment in Germany, weekend summer (24-h TWA)	40	0.34	NA	0.11	NA	NA
10	Nonsmoking environment in Germany, weekday winter (24-h TWA)	50	0.21	NA	0.09	NA	NA
10	Nonsmoking environment in Germany, weekend winter (24-h TWA)	53	0.13	NA	0.03	NA	NA
10	Nonsmoking environment in Germany, weekday summer (24-h TWA)	43	0.12	NA	0.06	NA	NA

10	Nonsmoking environment in Germany, weekend summer (24-h TWA)	41	0.07	NA	0.03	NA	NA
11	Smoking household in Switzerland (24 h TWA)	26	0.39	NA	0.28	NA	NA
11	Nonsmoking household in Switzerland (24-h TWA)	56	0.11	NA	0.04	NA	NA
11	Smoking household and smoking workplace in Switzerland (24-h TWA)	23	0.70	NA	0.42	NA	NA
11	Smoking household and nonsmoking workplace in Switzerland (24-h TWA)	13	0.34	NA	0.12	NA	NA
11	Nonsmoking household and smoking workplace in Switzerland (24-h TWA)	42	0.26	NA	0.16	NA	NA
11	Nonsmoking household and nonsmoking workplace in Switzerland (24-h TWA)	27	0.13	NA	0.09	NA	NA

MDL =method detection limit.

VPN of area samples

			Concentration Range (µg/m^3)				
Ref.	**Environment**	**N**	**Mean**	**SD**	**Median**	**Min.**	**Max.**
	Smoking Offices						
1	Cubicles and offices in unrestricted smoking office building, USA (8-h TWA)	72	2.99	NA	1.83	NA	NA
	Smoking Restaurants, etc.						
3	Smoking section of a restaurant, Canada	8	12.2	19.3	NA	NA	NA
3	Smoking section of a restaurant, Canada	12	0.44	0.76	0.00	NA	NA
4	Bar area in unrestricted smoking restaurant and tavern, USA	53	14.4	16.9	5.80	0.00	61.3
4	Non-bar area in unrestricted smoking restaurant and tavern, USA	32	6.01	11.9	0.818	0	49.3
5	Smoking-permitted medium-priced restaurant in France	15	30.3	21.1	24.1	0.00	71.6
5	Smoking-permitted medium-priced restaurant in Japan	16	11.7	5.35	11.1	3.37	22.4
5	Smoking-permitted medium-priced restaurant in Korea	47	5.72	4.13	3.95	1.60	18.8
5	Smoking-permitted medium-priced	32	7.81	10.7	3.98	0.08	39.6

	restaurant in Switzerland						
	Smoking-permitted medium-priced						
5	restaurant in UK	20	9.78	6.92	10.1	0.80	27.6
	Smoking-permitted medium-priced						
5	restaurant in USA	18	3.03	3.36	1.52	0.04	9.43
	Smoking permitted disco, nightclub in						
6	Finland	43	42.2	6.3	NA	2.0	183
6	Smoking permitted pub in Finland	12	8.2	2.0	NA	1.0	25
	Smoking permitted dining restaurant in						
6	Finland	28	7.0	2.3	NA	0.40	46
7	Smoking billiard hall USA	NA	25.9	NA	NA	13.2	37.6
7	Smoking casino in USA	NA	11.8	NA	NA	8.2	18.6
7	Smoking gourmet restaurant in USA	NA	3.1	NA	NA	1.3	4.7
7	Smoking theme restaurant in USA	NA	4.5	NA	NA	1.6	7.1
	Nonsmoking Environments						
7	Nonsmoking gourmet restaurant in USA	NA	1.1	NA	NA	0.1	1.6
7	Nonsmoking theme restaurant in USA	NA	0.5	NA	NA	0.1	1.2

VPN of personal exposure samples

			Concentration Range (µg/m^3)				
Ref.	**Environment**	**N**	**Mean**	**SD**	**Median**	**Min.**	**Max.**
	Unrestricted smoking office building,						
1	USA (8-h TWA)	72	1.56		1.24		
	Smoking and nonsmoking (not specified)					<M	
8	Korean home	120	0.12	0.16	0.07	DL	0.82
	Bartender in unrestricted smoking					0.00	
4	restaurant and tavern, USA	80	14.1	20.9	4.45	0	116
	Wait staff in unrestricted smoking						
4	restaurant and tavern, USA	83	5.83	11.9	1.16	0.00	67.9
	Smoking away-from work and smoking work environment in 16 cities, USA (24-h						
9	TWA)	122	3.27	NA	1.72	NA	NA
	Smoking away-from work and nonsmoking work environment in 16						
9	cities, USA (24-h TWA)	149	1.40	NA	0.711	NA	NA
9	Nonsmoking away-from work and	154	0.686	NA	0.161	NA	NA

	smoking work environment in 16 cities, USA (24-h TWA)						
9	Smoking away-from work and smoking work environment in 16 cities, USA (24-h TWA)	154	0.055	NA	0.027	NA	NA
10	Smoking environment in Germany, weekday winter (24-h TWA)	48	2.8	NA	1.3	NA	NA
10	Smoking environment in Germany, weekend winter (24-h TWA)	48	2.3	NA	0.80	NA	NA
10	Smoking environment in Germany, weekday summer (24-h TWA)	44	1.2	NA	0.26	NA	NA
10	Smoking environment in Germany, weekend summer (24-h TWA)	40	0.73	NA	0.03	NA	NA
10	Nonsmoking environment in Germany, weekday winter (24-h TWA)	50	0.93	NA	0.12	NA	NA
10	Nonsmoking environment in Germany, weekend winter (24-h TWA)	53	0.20	NA	0.03	NA	NA
10	Nonsmoking environment in Germany, weekday summer (24-h TWA)	43	0.13	NA	0.06	NA	NA
10	Nonsmoking environment in Germany, weekend summer (24-h TWA)	41	0.07	NA	0.03	NA	NA
11	Smoking household in Switzerland (24 h TWA)	26	2.1	NA	1.0	NA	NA
11	Nonsmoking household in Switzerland (24-h TWA)	56	3.3	NA	0.50	NA	NA
11	Smoking household and smoking workplace in Switzerland (24-h TWA)	23	3.6	NA	2.5	NA	NA
11	Smoking household and nonsmoking workplace in Switzerland (24-h TWA)	13	2.2	NA	1.3	NA	NA
11	Nonsmoking household and smoking workplace in Switzerland (24-h TWA)	42	1.8	NA	0.84	NA	NA
11	Nonsmoking household and nonsmoking workplace in Switzerland (24-h TWA)	27	0.78	NA	0.50	NA	NA

2. Correlations of different markers

3-EP and nicotine concentrations were well correlated.[4-6,8,11-13] At lower smoke level, nicotine to 3-EP trends to be lower.[5] In one correlation analysis, 3-EP concentrations were less than half of those of nicotine.[11]

And also concentrations of the trace markers of ETS measured by area samples and personal exposure samples are in good agreement.[4]

3-EP has several advantages over nicotine when it is used an ETS marker, such as (1) Its concentration correlates better with ETS particle concentrations[11] and other gas-phase ETS components;[14-16] (2) It only exists in gas phase, while nicotine exists in both gas and particle phases;[8] (3) Nearly first-order kinetics can be applied to its decay;[17] (3) Its concentration increases linearly with the number of cigarettes smoked.[18]

3. Sampling methods

XAD-4 resin cartridge (SKC, Inc) is popularly for nicotine and 3-EP sampling.[1,3-5,7-11,19] With this method, sample is extracted with ethyl acetate which contains guinoline as internal standard and trimethylamine (TEA) to prevent adherence of the compounds. Other methods include using SS tubes packed with a single adsorbent, such as Tenax-TA 35/60 mesh,[6] or multi-adsorbent, such as Tenax-TA followed by Carbosieve S-III 60/80 mesh,[20] 300 mg of Tenax GR 60/80 mesh followed by 600 mg of Carbotrap 20/40 mesh,[2] 160 mg of Tenax TA 60/80 mesh followed by 160 mg of Carbotrap 20/40 mesh.[21] Thermal desorption is used if the vapors are collected with these adsorbent tubes. TEA was added to help the desorption.[22] 3M organic vapor samplers were used with a passive sampling method.[23]

4. Analysis methods

GC is used for separation. Detectors include nitrogen-selected detector,[1,3-5,8-11] NPD[12] and MS.[2,6,19-21,23]

5. Commercial availability of compounds

Nicotine is commercially available, while 3-EP is not. Instead of using 3-EP for calibration, 4-EP is use.[2,21,23]

References

1. Jenkins, R. A.; Maskarinec, M. P.; Counts, R. W.; Caton, J. E.; Tomkins, B. A.; Ilgner, R. H. *Journal of Exposure Analysis and Environmental Epidemiology* **2001,** *11*, 369-80.
2. Kim, Y. M.; Harrad, S.; Harrison, R. M. *Environ. Sci. Tech.* **2001,** *35*, 997-1004.
3. Jenkins, R. A.; Finn, D.; Tomkins, B. A.; Maskarinec, M. P. *Regulatory Toxicology and Pharmacology* **2001,** *34*, 213-20.
4. Maskarinec, M. P.; Jenkins, R. A.; Counts, R. W.; Dindal, A. B. *Journal of Exposure Analysis and Environmental Epidemiology* **2000,** *10*, 36-49.
5. Bohanan, H. R.; Piade, J. J.; Schorp, M. K.; Saint-Jalm, Y. *Journal of Exposure Analysis and Environmental Epidemiology* **2003,** *13*, 378-92.
6. Hyvarinen, M. J.; Rothberg, M.; Kahkonen, E.; Mielo, T.; Reijula, K. *Indoor Air-International Journal of Indoor Air Quality and Climate* **2000,** *10*, 121-25.
7. Moschandreas, D. J.; Vuilleumier, K. L. *Atmospheric Environment* **1999,** *33*, 4327-40.
8. Baek, S. O.; Jenkins, R. A. *Indoor and Built Environment* **2001,** *10*, 200-08.
9. Jenkins, R. A.; Palausky, A.; Counts, R. W.; Bayne, C. K.; Dindal, A. B.; Guerin, M. R. *Journal of Exposure Analysis and Environmental Epidemiology* **1996,** *6*, 473-502.
10. Phillips, K.; Bentley, M. C. *Environment International* **2001,** *27*, 69-85.
11. Phillips, K.; Howard, D. A.; Bentley, M. C.; Alvan, G. *Atmospheric Environment* **1999,** *33*, 1889-904.
12. Jenkins, R. A.; Counts, R. W. *Environmental Health Perspectives* **1999,** *107*, 341-48. Notes: Supplement: Suppl. 2.
13. Lourenco, M. G.; Matos, A. *International Journal of Environmental Analytical Chemistry* **2003,** *83*, 189-97.
14. Nelson, P. R.; Heavner, D. L.; Collie, B. B.; Maiolo, K. C.; Ogden, M. W. *Environmental Science & Technology* **1992,** *26*, 1909-15.
15. Ogden, M. W.; Heavner, D. L.; Foster, T. L.; Maiolo, K. C.; Cash, S. L.; Richardson, J. D.; Martin, P.; Simmons, P. S.; Conrad, F. W.; Nelson, P. R. *Environmental Technology* **1996,** *17*, 239-50.
16. Ogden, M. W.; Maiolo, K. C. *Environmental Science & Technology* **1989,** *23*, 1148-54.
17. Eatough, D. J.; Benner, C. L.; Bayona, J. M.; Richards, G.; Lamb, J. D.; Lee, M. L.; Lewis, E. A.; Hansen, L. D. *Environmental Science & Technology* **1989,** *23*, 679-87.
18. Heavner, D. L.; Morgan, W. T.; Ogden, M. W. *Environment International* **1995,** *21*, 3-21.
19. Xie, J. X.; Wang, X. M.; Fu, J. M.; Sheng, G. Y. *Chinese Journal of Analytical Chemistry* **2003,** *31*, 915-19.
20. Singer, B. C.; Hodgson, A. T.; Guevarra, K. S.; Hawley, E. L.; Nazaroff, W. W. *Environmental Science & Technology* **2002,** *36*, 846-53.
21. Heavner, D. L.; Ogden, M. W.; Nelson, P. R. *Environmental Science & Technology* **1992,** *26*, 1737-46.
22. Thompson C.V., Jenkins R.A., and Higgins C.E. *Environmental Science & Technology* **1989,** *23*, 429-435
23. Vainiotalo, S.; Vaaranrinta, R.; Tornaeus, J.; Aremo, N.; Hase, T.; Peltonen, K. *Environmental Science & Technology* **2001,** *35*, 1818-22.

Appendix 4. Calibration Data of 16 Compounds in Chapter 3

(diamond: C8, square:OPH, triangle: HME, open circle: CCN)

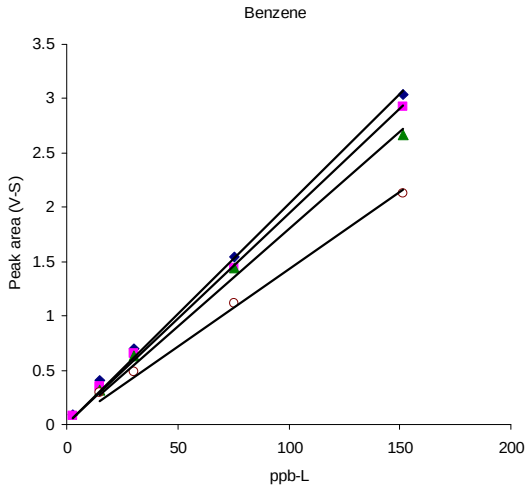

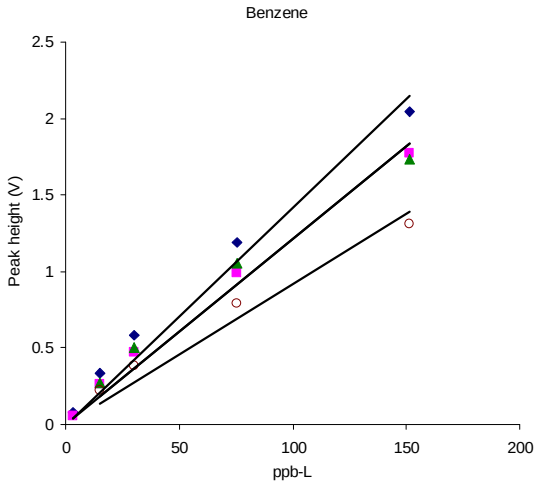

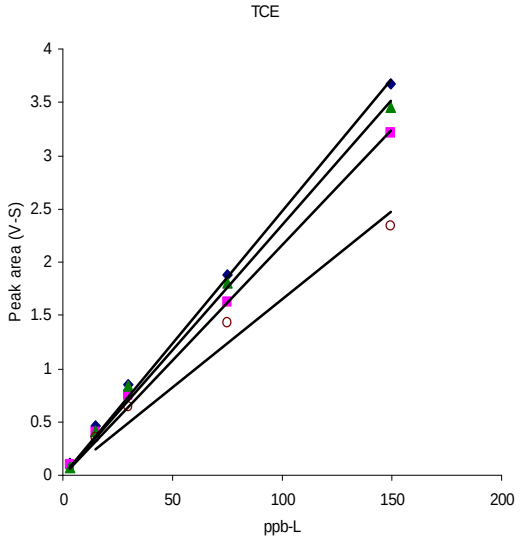

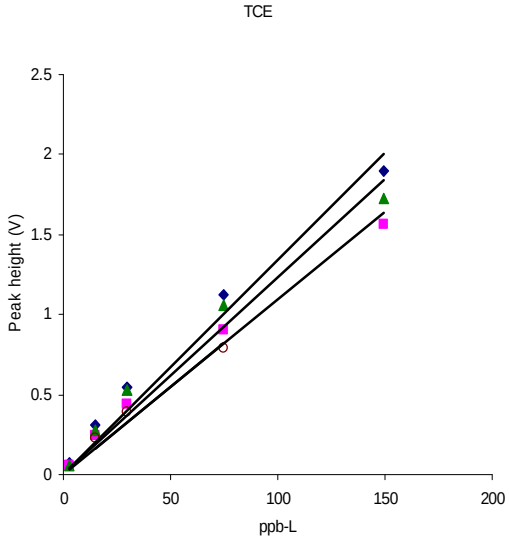

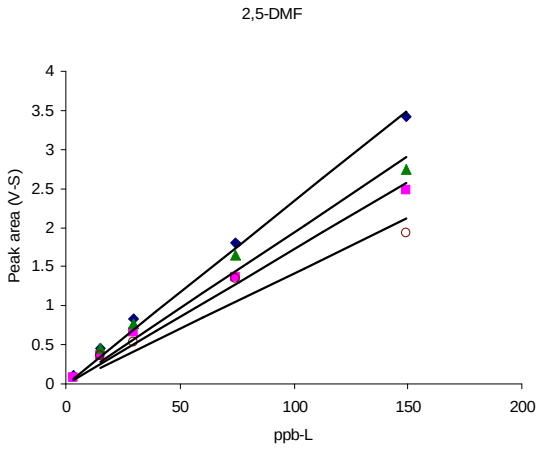

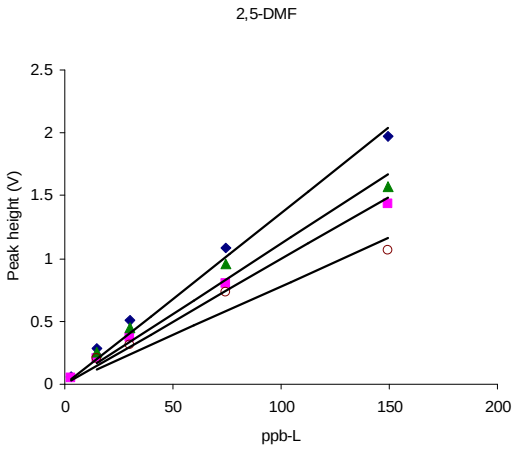

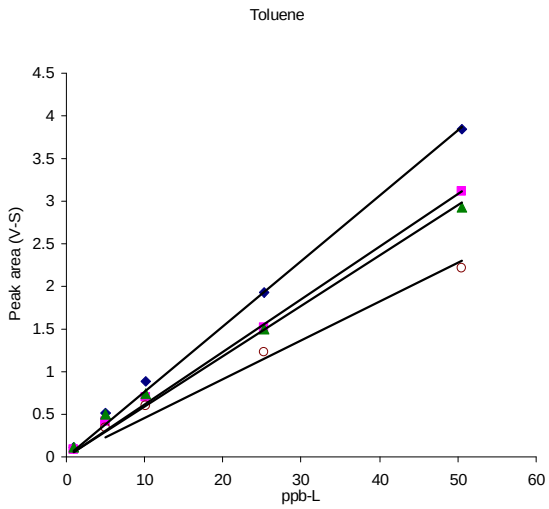
Toluene
Peak area (V-S)
ppb-L

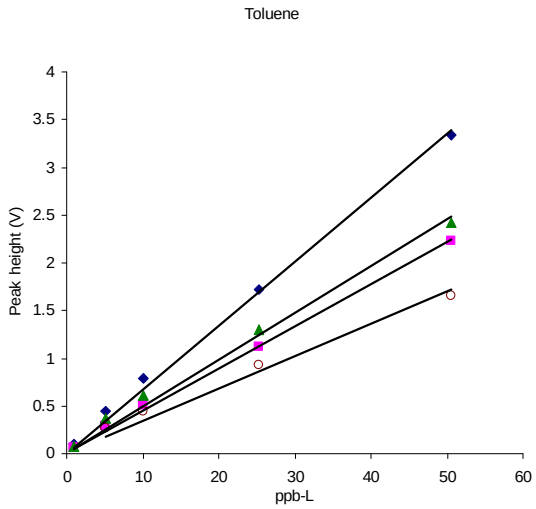
Toluene
Peak height (V)
ppb-L

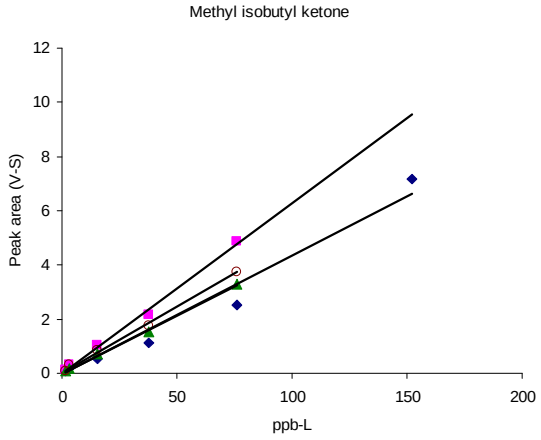
Methyl isobutyl ketone
Peak area (V-S)
ppb-L

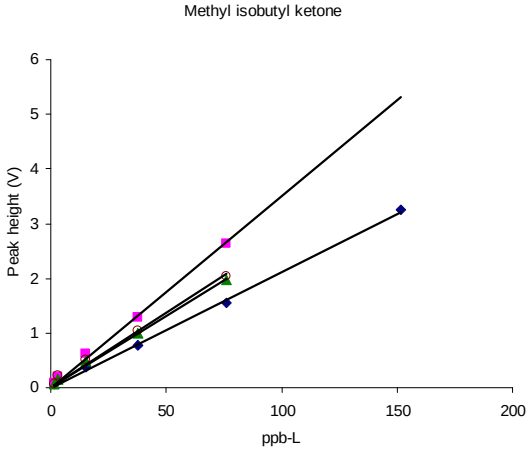
Methyl isobutyl ketone
Peak height (V)
ppb-L

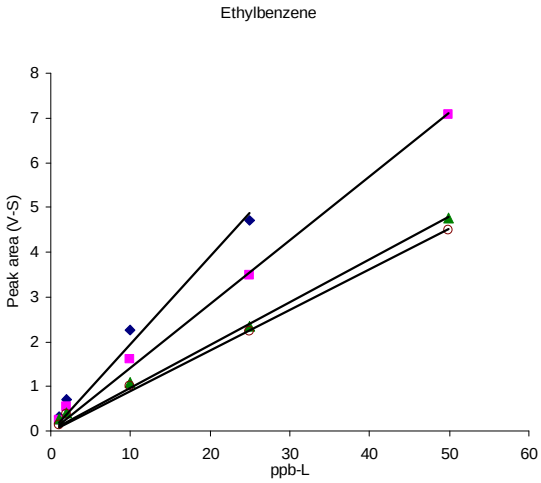
Ethylbenzene
Peak area (V-S)
ppb-L

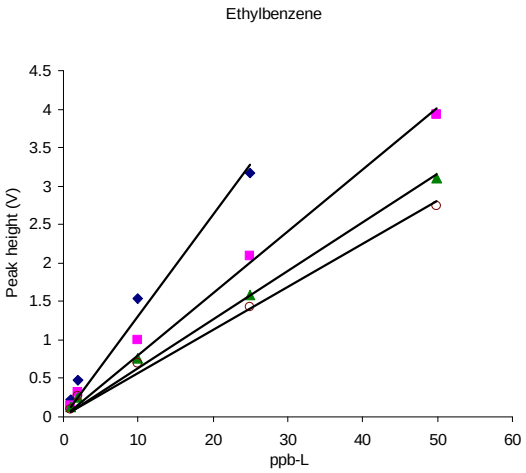
Ethylbenzene
Peak height (V)
ppb-L

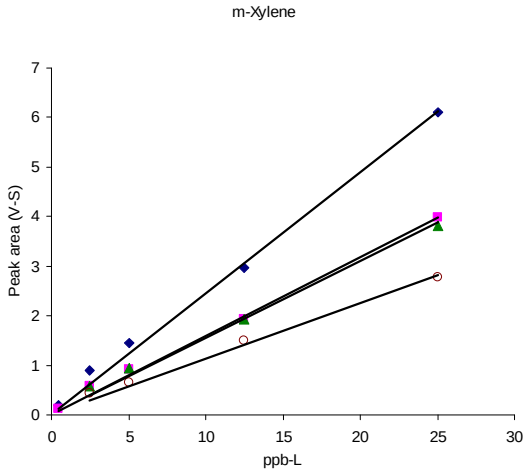
m-Xylene
Peak area (V-S)
ppb-L

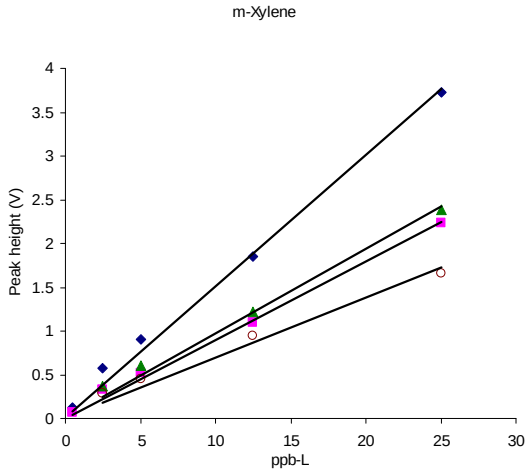
m-Xylene
Peak height (V)
ppb-L

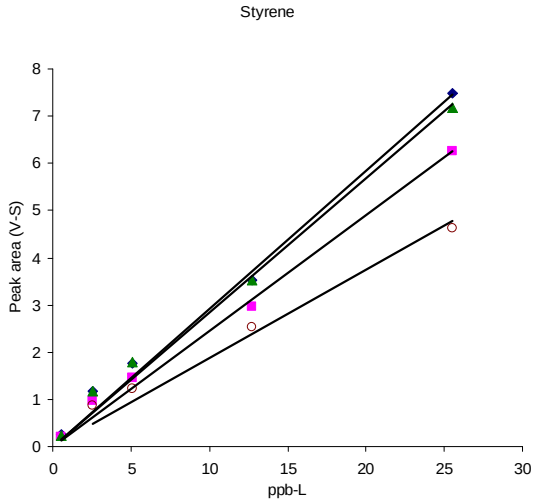
Styrene
Peak area (V-S)
ppb-L

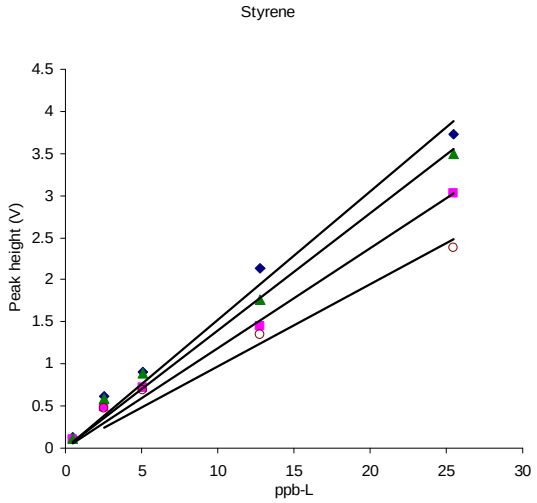
Styrene
Peak height (V)
ppb-L

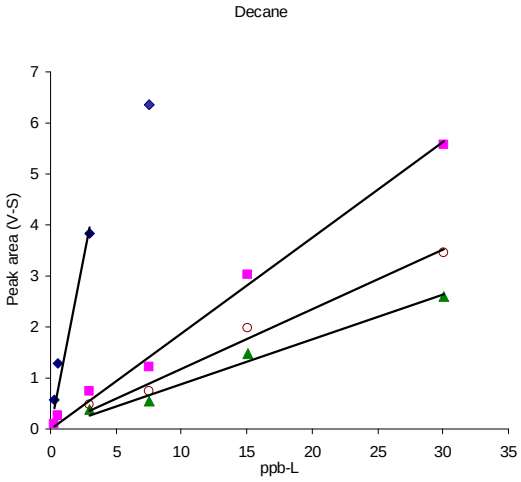
Decane
Peak area (V-S)
ppb-L

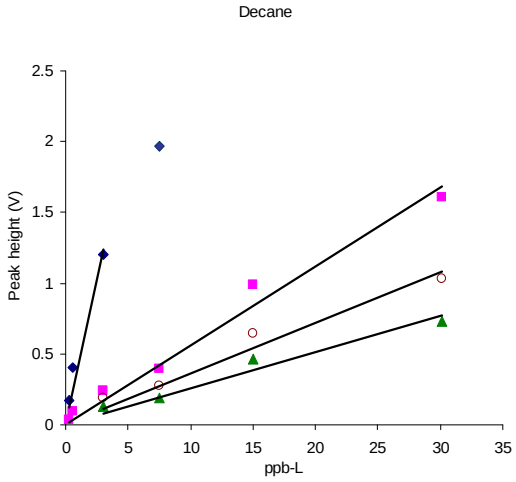
Decane
Peak height (V)
ppb-L

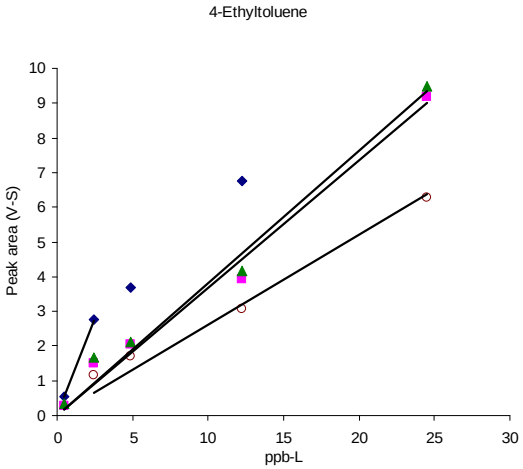
4-Ethyltoluene
Peak area (V-S)
ppb-L

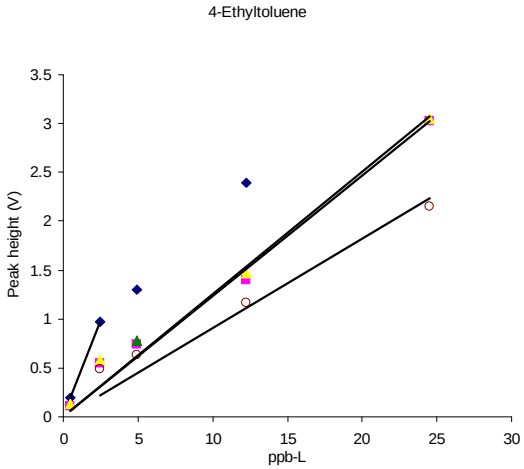
4-Ethyltoluene
Peak height (V)
ppb-L

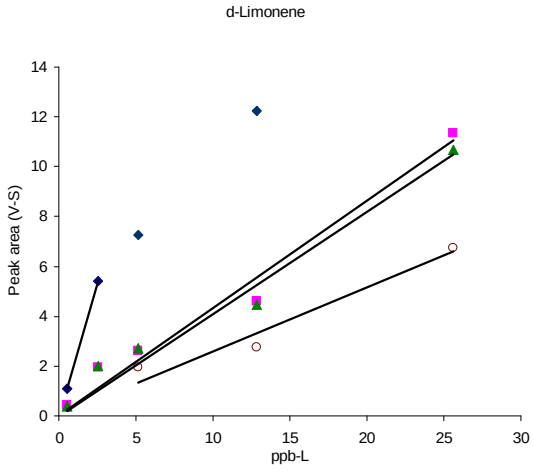
d-Limonene
Peak area (V-S)
ppb-L

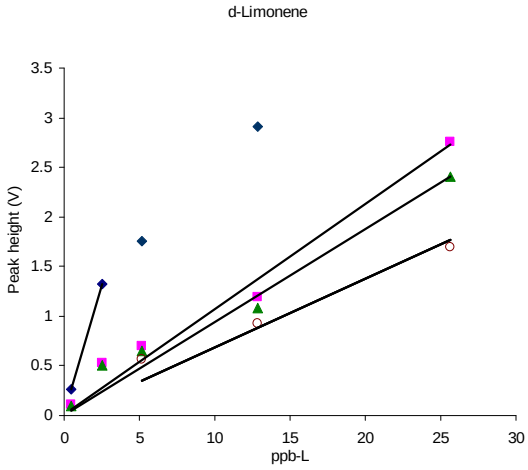
d-Limonene
Peak height (V)
ppb-L

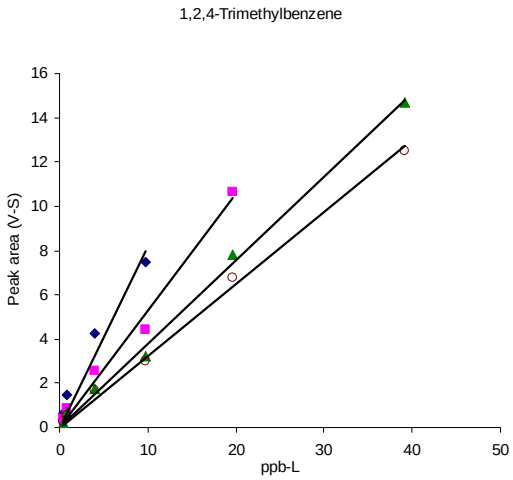
1,2,4-Trimethylbenzene
Peak area (V-S)
ppb-L

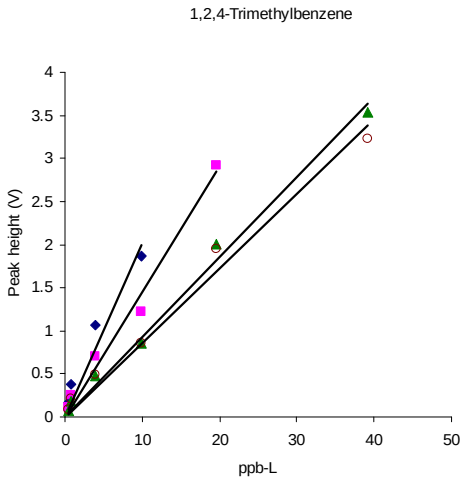
1,2,4-Trimethylbenzene
Peak height (V)
ppb-L

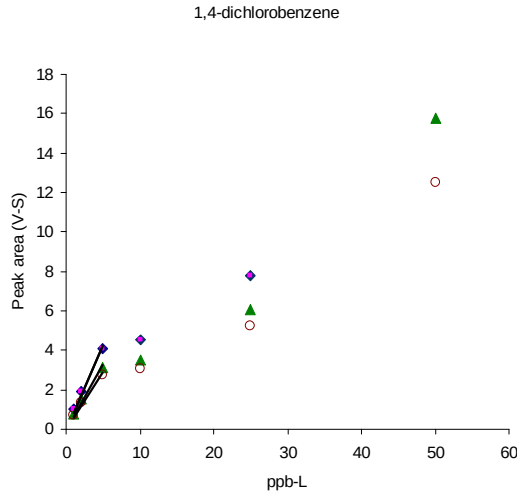
1,4-dichlorobenzene
Peak area (V-S)
ppb-L

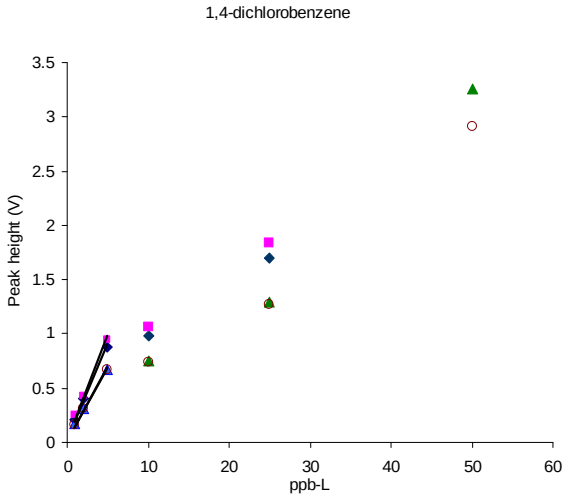
1,4-dichlorobenzene
Peak height (V)
ppb-L

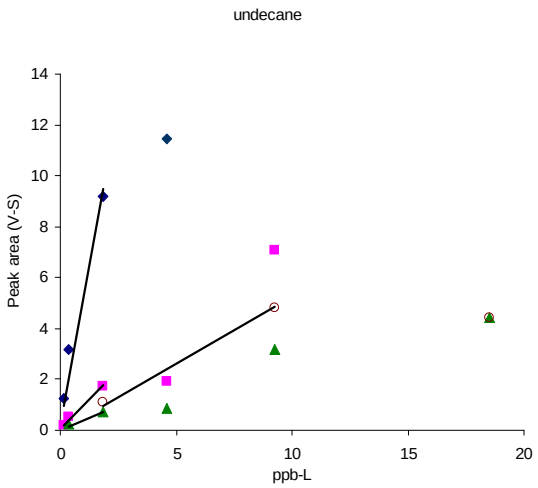
undecane
Peak area (V-S)
ppb-L

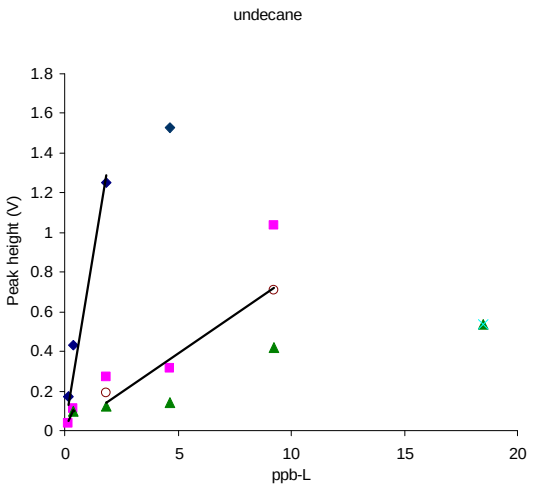
undecane
Peak height (V)
ppb-L

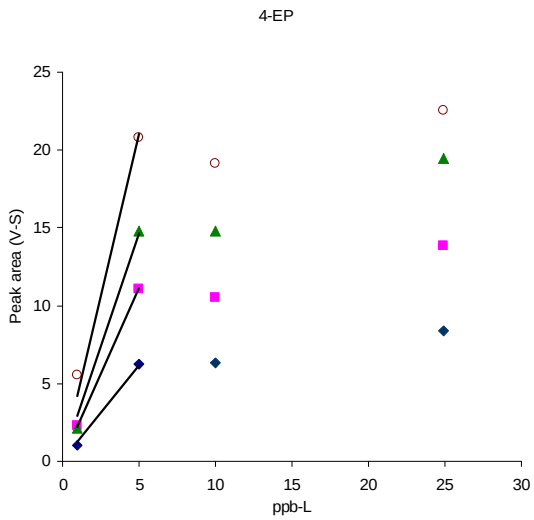
4-EP
Peak area (V-S)
ppb-L

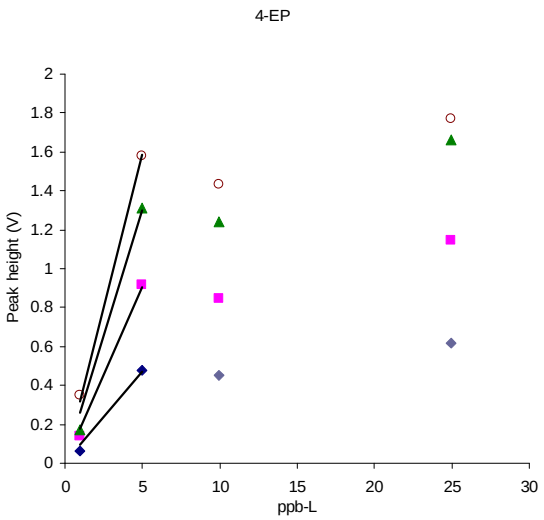
4-EP
Peak height (V)
ppb-L

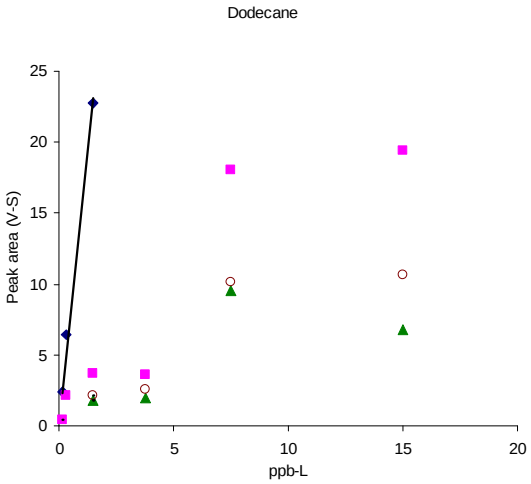
Dodecane
Peak area (V-S)
25
20
15
10
5
0
0
5
10
15
20
ppb-L

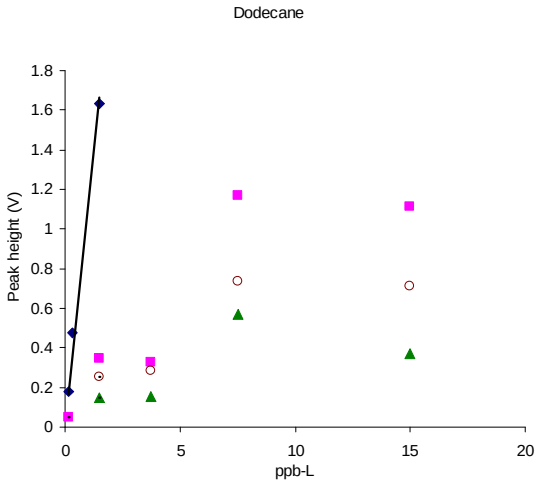
Dodecane
Peak height (V)
1.8
1.6
1.4
1.2
1
0.8
0.6
0.4
0.2
0
0
5
10
15
20
ppb-L

Appendix 5. Calibration Curves of Biomarkers of Lung Cancer in Chapter 4

The first sensor array

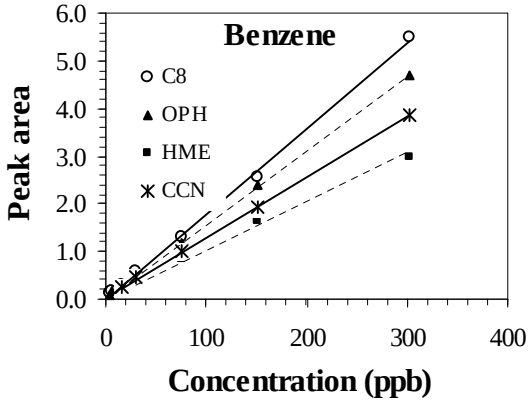

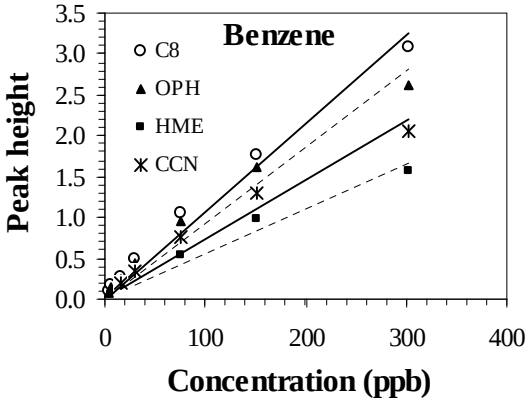

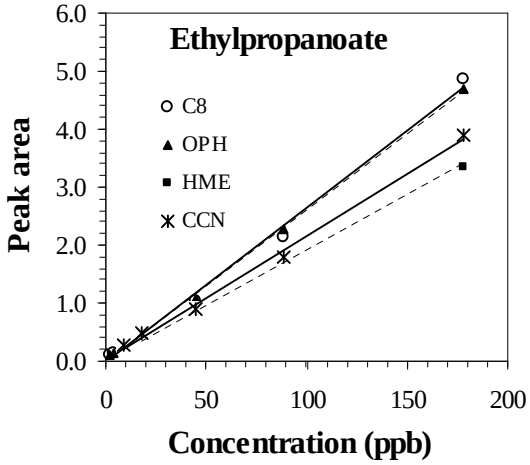

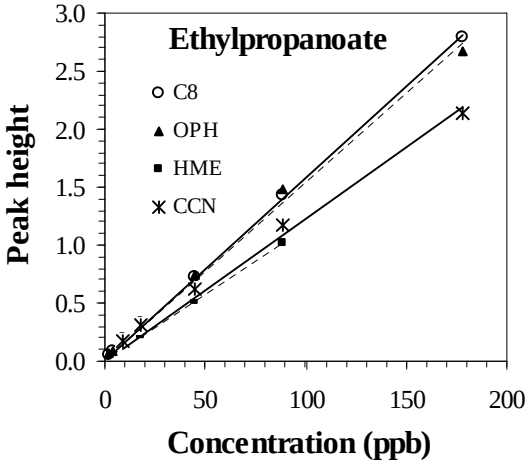

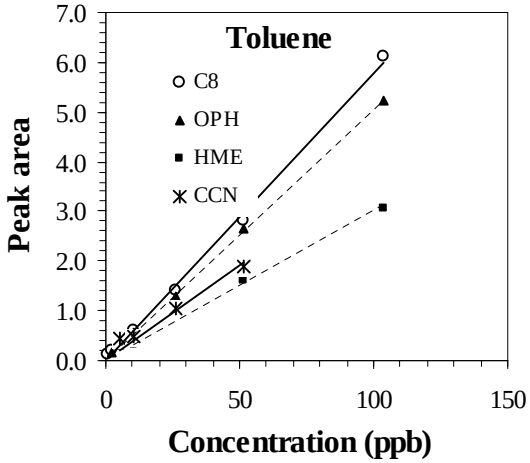

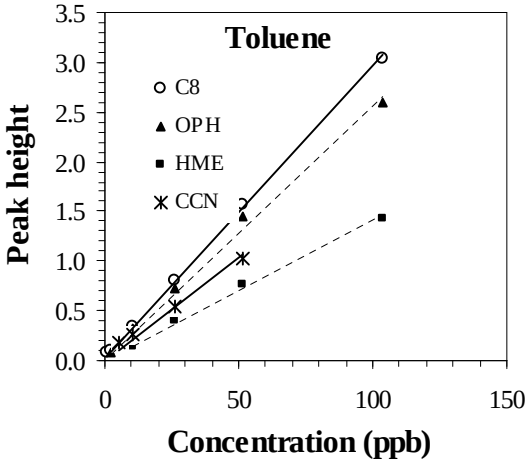

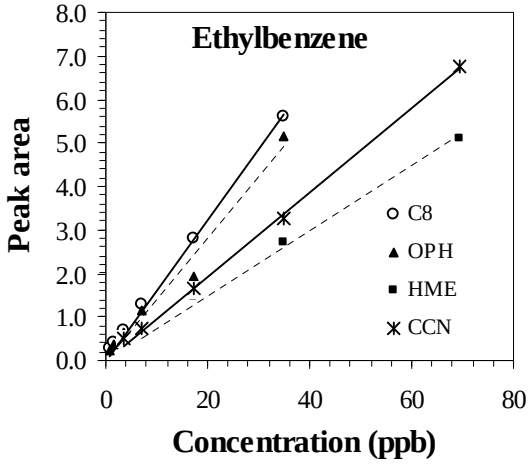

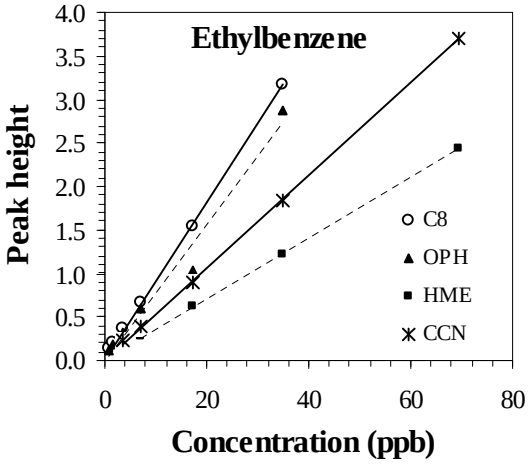

The second sensor array

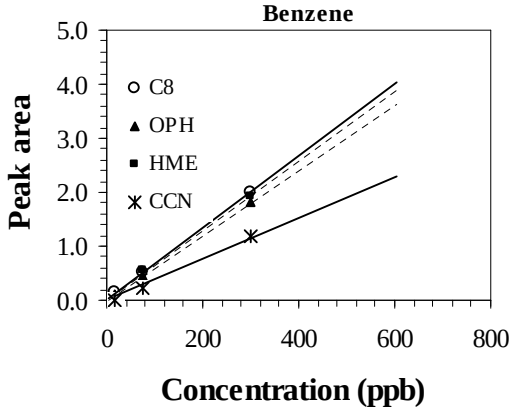

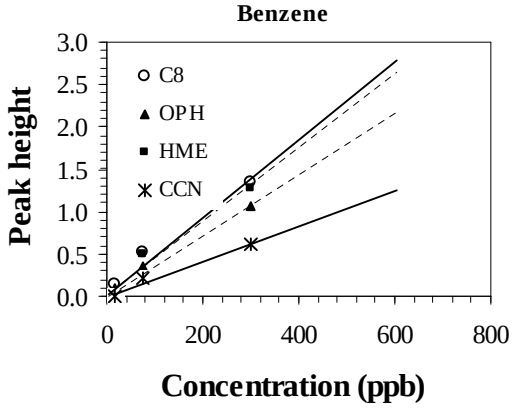

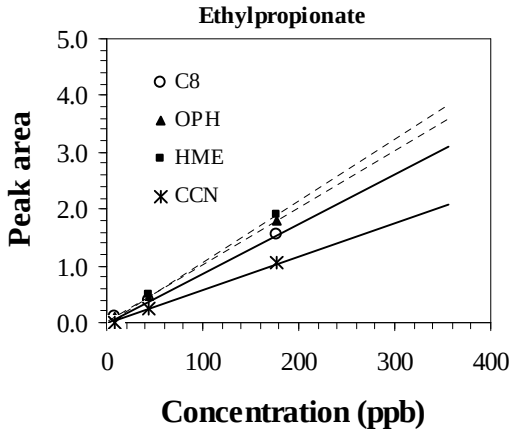

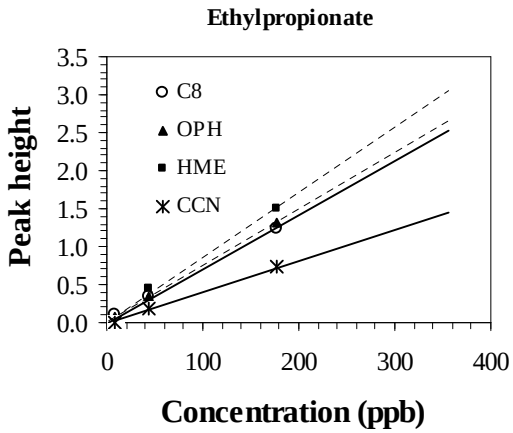

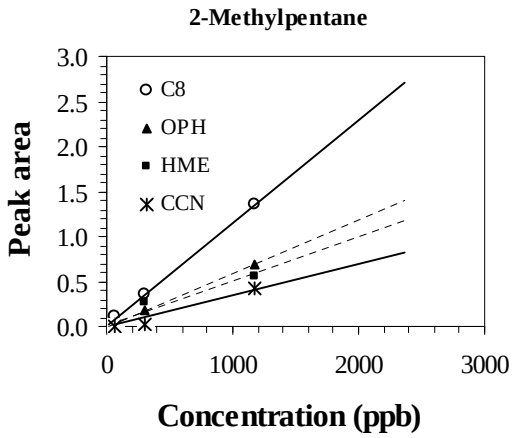
2-Methylpentane
Peak area
Concentration (ppb)
C8
OPH
HME
CCN
0.0
0.5
1.0
1.5
2.0
2.5
3.0
0
1000
2000
3000

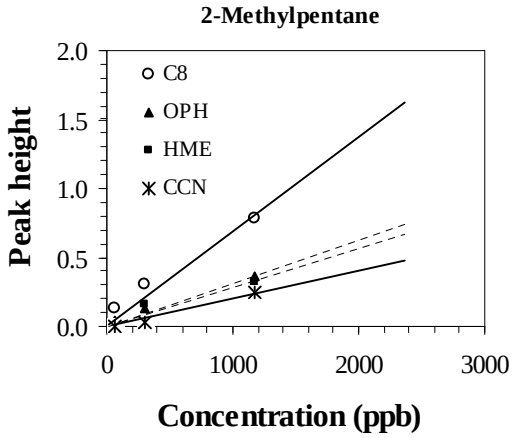
2-Methylpentane
Peak height
Concentration (ppb)
C8
OPH
HME
CCN
0.0
0.5
1.0
1.5
2.0
0
1000
2000
3000

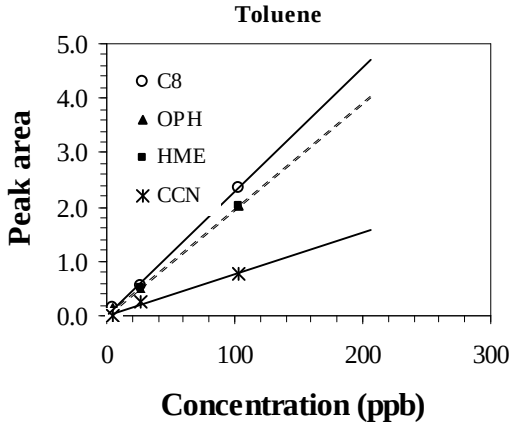
Toluene
Peak area
Concentration (ppb)
C8
OPH
HME
CCN
0.0
1.0
2.0
3.0
4.0
5.0
0
100
200
300

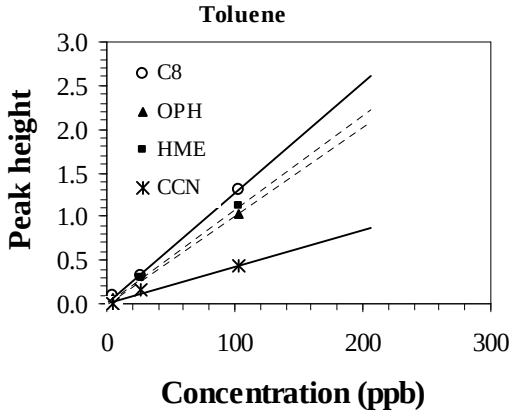
Toluene
Peak height
Concentration (ppb)
C8
OPH
HME
CCN
0.0
0.5
1.0
1.5
2.0
2.5
3.0
0
100
200
300

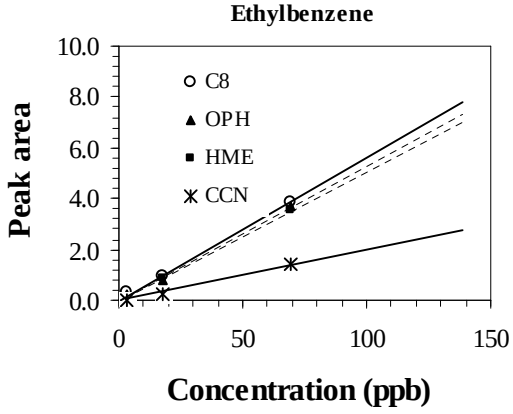
Ethylbenzene
Peak area
Concentration (ppb)
C8
OPH
HME
CCN
0.0
2.0
4.0
6.0
8.0
10.0
0
50
100
150

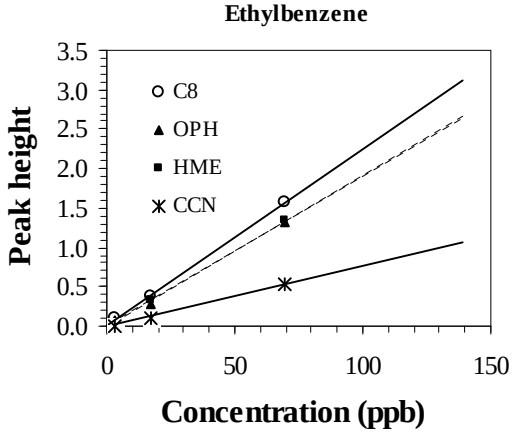
Ethylbenzene
Peak height
Concentration (ppb)
C8
OPH
HME
CCN
0.0
0.5
1.0
1.5
2.0
2.5
3.0
3.5
0
50
100
150